DOI:10.14753/SE.2016.1969

GENERAL AND DISEASE-SPECIFIC MECHANISTIC THERAPY APPROACHES FOR OPTIMIZATION OF LIVER TRANSPLANTATION

PhD thesis

Christian Dominik Fingas

Doctoral School of Pathological Sciences

Semmelweis University

Consultant: Zoltán Máthé, MD, Ph.D.

Official reviewers: Péter Igaz, MD, Ph.D.
Róbert Gáspár, Ph.D.

Head of the Final Examination Committee: Tibor Tihanyi, MD, Ph.D.

Members of the Final Examination Committee:
Klára Werling Marisné, MD, Ph.D.
Katalin Monostory, Ph.D.

Budapest
2016

DOI:10.14753/SE.2016.1969

DOI:10.14753/SE.2016.1969

TABLE OF CONTENTS

DOI:10.14753/SE.2016.1969

DOI:10.14753/SE.2016.1969

1 LIST OF ABBREVIATIONS IN ALPHABETICAL ORDER

α-SMA	α-smooth muscle actin
ALT	alanine transaminase
AP	alkaline phosphatase
AST	aspartate transaminase
Bcl-2	B-cell lymphoma
cAMP	cyclic adenosine monophosphate
CCA	cholangiocellular carcinoma
ChIP	chromatin immunoprecipitation
CIT	cold ischemic time
CK7	cytokeratin 7
DHH	desert hedgehog
DMEM	Dulbecco's modified Eagle Medium
ELISA	enzyme-linked immunosorbent assay
EPO	erythropoietin
ErbB-2	erythroblastic leukemia viral oncogene homolog
GFP	green fluorescent protein
GLDH	glutamate dehydrogenase
GLI	glioma-associated oncogene
HCC	hepatocellular carcinoma
Hh	hedgehog
HIP	hedgehog-interacting protein
HSC	hepatic stellate cells
HTK	histidine-tryptophan-ketoglutarate
IHH	indian hedgehog
INR	international normalized ratio
LBWR	liver body weight ratio
LDH	lactate dehydrogenase
LDLT	living donor liver transplantation
LTx	liver transplantation

MAPK	mitogen-activated protein kinase
MBF	myofibroblast
Mcl-1	myeloid cell leukemia-1
PDGF	platelet-derived growth factor
PDGFR	platelet-derived growth factor receptor
PH	partial hepatectomy
PKA	cAMP-dependent protein kinase
PLK	polo-like kinases
pLTx	30% partial liver transplantation
PT	prothrombin time
PTCH1	patched1
PTT	prothrombin time
RBC	red blood cells
RFU	relative fluorescence unit
RT	room temperature
RT-PCR	real time polymerase chain reaction
SHH	sonic hedgehog
shRNA	short hairpin RNA
sLTx	split liver transplantation
SMO	smoothened
TIRF	total internal reflection fluorescence
TRAIL	tumor necrosis factor-related apoptosis-inducing ligand
TUNEL	terminal deoxynucleotidyl transferase-mediated dUTP nick end labeling
VEGF	vascular endothelial growth factor
WIT	warm ischemic time

DOI:10.14753/SE.2016.1969

2 INTRODUCTION

Liver transplantation (LTx) is a viable treatment option for acute liver failure and various end-stage liver diseases including malignancies like hepatocellular carcinoma (HCC) and cholangiocellular carcinoma (CCA). The present work will focus on the development of accompanying mechanistic therapies that may be eligible for optimization of this lifesaving surgical procedure. The studies are divided into general optimization approaches of LTx and disease-specific mechanistic experiments aiming to identify suitable targets in order to improve LTx for unresectable CCA patients according to the multimodal therapy concept of the Mayo protocol.[1]

2.1 General Optimization Approaches For Liver Transplantation

In these experiments we sought to minimize liver preservation injury and improve microcirculation in implanted liver grafts by modification of a histidine-tryptophan-ketoglutarate (HTK)-based preservation solution. In addition, we tested the effect of the pleiotropic substance erythropoietin (EPO) on liver regeneration/donor liver growth and hepatocyte apoptosis (programmed cell death) in the setting of partial liver transplantation (pLTx).

2.1.1 Preservation solutions and the effect of chloride

Preservation injury is still a major concern in liver transplantation, especially for grafts obtained from "extended criteria donors".[2-4] Preservation injury can be regarded as a consequence of hypoxia,[5-8] injury triggered by hypothermia,[7, 9, 10] a certain toxicity of the preservation solutions,[11, 12] and at a later stage, inflammatory processes.[7, 13, 14] Taking into account new findings on the mechanisms of the initial processes already occurring during cold preservation, we developed a new preservation solution on the basis of HTK solution (for composition see Table 1), which, in a preliminary (chloride-poor) version, was already shown to reduce preservation injury to isolated perfused rat livers in comparison with HTK solution.[15]

	HTK Solution	Modified Solution Without Chloride	Modified Solution With Chloride
Cl^- (mmol/L)	50	0.04	34.04
α-Ketoglutarate (mmol/L)	1	3	2
Aspartate (mmol/L)	—	8	7
Lactobionate (mmol/L)	—	5	—
Na^+ (mmol/L)	15	16	16
K^+ (mmol/L)	10	10	10
Mg^{2+} (mmol/L)	4	8	8
Ca^{2+} (mmol/L)	0.015	0.02	0.02
Arginine (mmol/L)	—	5	5
Histidine (mmol/L)	198	103	139
N-Acetylhistidine (mmol/L)	—	104	52
Glycine (mmol/L)	—	10	10
Alanine (mmol/L)	—	5	5
Tryptophan (mmol/L)	2	2	2
Sucrose (mmol/L)	—	26	15
Mannitol (mmol/L)	30	—	—
pH	7.2	7.0	7.0
Osmolarity (mOsm/L)	310.02	305.06	305.06

Table 1. Compositions of HTK solution and the modified HTK solutions. To obtain a chloride-containing variant of the new solution, further but slight modifications became necessary for reasons of charge and osmolarity; these modifications mainly affected the concentrations of N-acetylhistidine (partly anionic), histidine (partly cationic), and sucrose.

In the course of the mechanistic studies that formed the basis for developing the new preservation solution, we have described the entity of cold-induced apoptosis, an injury that affects numerous mammalian cell types such as rat hepatocytes, rat liver endothelial cells, rat renal tubular cells, rat coronary endothelial cells, porcine aortic endothelial cells, porcine corneal endothelial cells, and human umbilical vein endothelial cells.[7, 9, 16-19] In all these cell types chelatable, ‘‘redox-active’’ iron plays the major role in the development of cold-induced apoptosis.[7, 9, 16-21]

However, hepatocytes appear to be slightly different since in these cells iron chelators only provide partial protection from cold-induced injury during rewarming after cold incubation in cell culture medium or Krebs-Henseleit buffer.[18, 19, 21] We further characterized this iron-*in*dependent weaker cold-induced injury to rat hepatocytes and found it to be dependent on extracellular chloride.[22]

In contrast to that, a another study on cold-induced injury to the endothelium of intact porcine aortic segments exhibited beneficial effects of chloride-containing preservation solutions on endothelial cell survival.[23] This is in line with other experiments in cultured porcine aortic endothelial cells revealing strong adverse effects of chloride-poor preservation solutions.[24]

As it was impossible to judge from these contradictory *in vitro* experiments which of the chloride-dependent effects has a higher biological relevance regarding the intact liver, we here tested a chloride-poor versus a chloride-containing variant of the new preservation solution in

an orthotopic rat liver transplantation model. Three different post-LTx survival series were performed since survival represents the study criterion with the highest medical relevance and since the clarification of the conflicting *in vitro* data is crucial for the further development of the preservation solution. The three series were designed to cover different balances of cold ischemic and warm ischemic injury as well as surgical trauma, thereby reflecting the broad range of potential clinical settings most closely. In addition, one LTx series (with intermediate cold and warm ischemic times [CIT/WIT]) was performed for assessment of intrahepatic microcirculation after reperfusion, laboratory data, bile production, and liver histology.

2.1.2 Erythropoietin and liver regeneration/apoptosis

After pLTx (or extended liver resection), efficient regeneration of the liver is essential for the clinical outcome. Especially after living donor liver transplantations (LDLT) and split liver transplantations (sLTx), which have been an important developments to overcome the growing problem of organ shortage,[25] an immediate regeneration is most desirable because of the graft's smaller size and its reduced functional liver mass. A small-for-size graft may not only be functionally insufficient for the recipient, but will also sustain injury characterized by rejection and ischemic insult, which results in an inadequate regeneration and leads to hepatic failure.[26] For the LDLT donor, an adequate regenerative response is of comparable importance. Unfortunately, more than 16% of all LDLT can not be performed, since the suggested graft/recipient- and remnant liver/donor-ratio of at least 0.8% can not be achieved.[27]

Therefore, improvement of the regenerative capacity is of fundamental importance and novel therapeutic approaches are needed to optimize liver regeneration in the setting of LDLT/sLTx. Previously, we were able to demonstrate the positive effects of vascular endothelial growth factor (VEGF) as well as tri-iodothyronine as stimulators of liver regeneration after partial hepatectomy (PH). However, none of the above mentioned treatment strategies have proven definitive.[28, 29]

EPO is a low molecular weight glycoprotein hormone stimulator of erythropoiesis produced in the fetal liver and subsequently in the adult kidney.[30, 31] Stimulation of erythropoiesis was considered to be the sole physiological action of EPO, but there is increasing evidence suggesting a wider biological role including angiogenesis and liver regeneration.[32, 33] Regarding the latter aspect it is known that not only the fetal but also the adult liver can be an extrarenal source of EPO.[34] Indeed, in liver regeneration an increased synthesis of EPO has been

described, whereas enhanced EPO serum levels correlate with the peak of liver regeneration after PH.[35] Here, the synthesis of EPO is mediated by erythropoietic hepatic factors [36, 37] and occurs in Kupffer cells [38-40] as well as erythroblastic islets within the liver lobules.[37, 41] EPO was also reported as a stimulator of liver regeneration after PH in rats and pigs.[32, 33]

2.2 Optimization Of Liver Transplantation For Cholangiocarcinoma

Sole LTx for unresectable CCA is often associated with early disease relapse and limited overall survival.[1] However, a small percentage of patients have achieved prolonged survival after LTx, suggesting that adjuvant approaches might improve the clinical outcome.[1] Thus, a multimodal therapy protocol was developed at the Mayo Clinic, Rochester, Minnesota, USA employing pre-LTx external-beam irradiation, chemotherapy, and iridium brachytherapy for patients with unresectable CCA above the cystic duct and without extrahepatic metastases.[1] After pretreatment and before LTx, patients undergo an exploratory laparotomy to exclude metastatic disease. The Mayo protocol has been proven to be quite successful for the treatment of patients with unresectable early-stage CCA.[1]

However, employing the conventional chemotherapeutic agents fluorouracil and capecitabine, this protocol does not consider new mechanistic findings on CCA tumor biology and, thus, might be improvable by the implementation of „targeted chemotherapy". The present CCA-specific LTx optimization experiments aim to identify mechanistic processes underlying the pronounced resistance to apoptotic cell death characteristic for CCA cells. Based on these findings, new mechanistic therapy approaches were tested.

2.2.1 The roles of myofibroblast derived growth factors and hedgehog signaling

CCA is a highly lethal malignancy with limited treatment options.[42-44] It is the most common biliary cancer and epidemiologic studies suggest that its incidence is increasing in several Western Countries.[45] Human CCA *in vivo* paradoxically expresses the death ligand tumor necrosis factor-related apoptosis-inducing ligand (TRAIL) and its cognate death receptors [46] suggesting that these cancers are reliant on potent survival signals for tumor maintenance and to circumvent apoptotic cell death by TRAIL. However, the mechanisms by which CCA evades apoptosis by TRAIL and other pro-apoptotic stimuli are incompletely understood.

CCAs are highly desmoplastic cancers suggesting cancer-associated fibroblasts within the tumor microenvironment contribute to their development and progression as has been proposed for other

cancers (e.g. breast cancer, prostate cancer, etc.).[47, 48] Cancer-associated fibroblasts are perpetually "activated" and express α-smooth muscle actin (α-SMA); cells exhibiting this activated phenotype are often referred to as myofibroblasts (MFBs).[49] In the liver, MFBs are derived from periportal fibroblasts, hepatic stellate cells (HSCs), and perhaps an epithelial-to-mesenchymal transition of cholangiocytes, hepatocytes, and/or the tumor itself.[50, 51] A role for MFBs in carcinogenesis and tumor biology receives increasing attention.[49, 52-54] Cross-talk between the cancer and MFBs appears to be exploited by cancer cells as a tumor promoting mechanism. For example, in CCA the number of MFBs correlates with tumor size and patient survival.[55, 56] MFBs also appear capable of providing survival signals as they reduce apoptosis of non-malignant cholangiocytes in co-culture experiments.[57] However, information regarding the nature of this cross-talk, and in particular the identity of the potential survival signals, remains obscure.

Growth factor and especially platelet-derived growth factor (PDGF) paracrine signaling between MFBs and cholangiocytes occurs in rodent models of biliary tract inflammation and fibrogenesis.[57, 58] Five different ligands of PDGF exist including PDGF-AA, -BB, -AB, -C and –D. However, PDGF-BB appears to be the predominant isoform secreted by liver MFBs.[59] Of the two cognate receptors, platelet-derived growth factor receptor (PDGFR)-α and –β, PDGFR-β is the cognate receptor for PDGF-BB. PDGFR-β is a receptor tyrosine kinase that is also known to alter plasma membrane dynamics associated with cell migration by a cyclic adenosine monophosphate (cAMP)-dependent kinase (PKA)-dependent process.[60] Thus, PDGF-BB effects on intracellular signaling cascades are pleiotropic. Given an emerging role for PDGF-BB in MFB-to-cholangiocyte cross-talk, a role for PDGF-BB as a survival factor for CCA warrants further investigation.

The Hedgehog (Hh) signaling pathway has been strongly implicated in gastrointestinal tumor biology including CCA.[61, 62] Hh signaling is initiated by any of the three ligands Sonic (SHH), Indian (IHH), and Desert (DHH) hedgehog. These ligands bind to the Hh receptor Patched1 (PTCH1) resulting in activation of Smoothened (SMO) and subsequently the transcription factors glioma-associated oncogene (GLI) 1, 2, and 3.[63] How PTCH1 modulates SMO was long enigmatic, as the two proteins do not physically associate. SMO trafficking from an intracellular compartment to the plasma membrane apparently results in its activation.[64] Hh ligand binding to PTCH1 increases the concentration of intracellular messengers (lipid phosphates), which in turn promote SMO trafficking to the plasma membrane.[65, 66] PKA affects SMO trafficking and activation, raising the unexplored possibility that cues from other ligand-receptor systems such

as PDGF-BB may also augment SMO activation by facilitating its trafficking to the plasma membrane.[64]

Interestingly, *SHH* mRNA expression is increased by PDGF-BB in immature cholangiocytes[58] providing an additional link between Hh signaling and PDGF. Hh signaling also is a master switch mediating resistance of CCA cells to TRAIL cytotoxicity. [67, 68] Taken together, these observations suggest MFB-derived PDGF-BB may modulate Hh survival signaling in CCA cells.

2.2.2 Interactions between hedgehog signaling and polo-like kinase 2

As mentioned above, Hh signaling was reported to be an important survival pathway in CCA.[67, 69, 70] Hh ligand SHH is abundantly expressed in CCA cells, [69, 71] and in a recent mRNA expression analysis employing CCA cells, Hh signaling was suggested to positively regulate the cell division modulating enzyme kinase polo-like kinase 2 (PLK2).[69]

PLK2 (or SNK) is one out of five mammalian PLK family members that orchestrate a wide range of critical cell cycle events.[72-74] Besides PLK2, PLK1 (or STPK13), PLK3 (or CNK, FNK and PRK), PLK4 (or SAK and STK18) and PLK5 have been identified.[73, 74] All PLK proteins share a similar structure with a canonical serine/threonine kinase domain at the N-terminus and a regulatory polo-box domain at the C-terminus [72]; however, PLK4 has a notably divergent structure as compared to other PLK proteins and PLK5 as it lacks kinase activity. [73, 74]

About 80% of human cancers express high levels of PLK transcripts in tumor cells (these PLK transcripts are mostly absent in surrounding healthy tissues) and PLK overexpression is often associated with poor prognosis and lower overall survival.[75] While PLK1 has been extensively studied and has become an attractive candidate for anti-cancer drug development, the roles of the other PLK proteins including PLK2 are less well understood.[74]

PLK inhibition in esophageal squamous cell carcinoma and osteosarcoma was reported to decrease protein levels of myeloid cell leukemia-1 (Mcl-1).[76, 77] This is of particular interest as Mcl-1, a potent anti-apoptotic member of the B-cell lymphoma (Bcl-2) protein family, has been identified as a survival factor in CCA.[78-80] Given the pivotal role of Mcl-1 in mediating CCA resistance to TRAIL-induced apoptosis, [78-80] PLK inhibition is another potential strategy for the targeted treatment of this devastating disease.

.

DOI:10.14753/SE.2016.1969

3 OBJECTIVES

The aims of the present studies were:

1. Optimization of a modified HTK-based preservation solution focusing on chloride-dependent effects on liver preservation injury and microcirculation after LTx.
2. Investigation of the impact of adjuvant administered EPO on liver regeneration/donor liver growth and hepatocyte apoptosis in the setting of pLTx.
3. Examination of the role of MFB-to-CCA cell paracrine signaling for CCA apoptosis resistance in the context of PDGF-BB/Hh co-activation networks
4. Exploration of anti-apoptotic effects mediated by Hh/PLK signaling crosstalk.
5. Based on the observations of 3) and 4), the objectives of subsequent studies were to test whether targeting PDGFR-β, Hh, or PLK signaling would be therapeutic in CCA and, thus, might be a suitable adjuvant therapy to optimize the Mayo LTx protocol for CCA patients.

4 METHODS

4.1 Materials

The chloride-poor (0.04 mmol/l) and chloride-containing (34.04 mmol/l, which is the highest possible chloride concentration within the confines given by all other compounds) preservation solutions were provided by Dr. Franz Köhler Chemie GmbH (Bensheim, Germany). EPO (EPREX®) was purchased from Ortho Biotech, Neuss, Germany.

rhTRAIL, rhPDGF-BB, rhSHH, anti-human PDGF-BB antiserum AB-220-NA (R&D Systems, Minneapolis, MN), PKA inhibitor H-89 (Cayman Chemical, Ann Arbor, MI), MG-132 (Merck, Rockland, MA), GDC-0449 (Selleck, Houston, TX), and cyclopamine (LC Laboratories, Woburn, MA) were prepared according to the suppliers protocols. Imatinib mesylate/STI-571, an inhibitor of the kinase activity of PDGFR(-β), was a generous gift from E. B. Leof (Div. of Pulmonary and Critical Care Medicine, Mayo Clinic, Rochester, MN). Imatinib was dissolved in sterile water (10 mmol/l stock solution) and subsequently diluted in cell culture medium. BI 6727/volasertib, a potent selective PLK inhibitor [81] was purchased from Active Biochem (Maplewood, NJ), dissolved in dimethyl sulfoxide (DMSO; Sigma, St. Louis, MO; 1 mmol/L stock solution) and subsequently diluted in cell culture medium for use in *in vitro* experiments. The SHH-neutralizing antibody 5E1 was obtained from the Developmental Studies Hybridoma Bank (DSHB, University of Iowa, IA). The construct encoding for S peptide-tagged human Mcl-1 mutant resistant to proteasomal degradation due to sequential mutagenesis of the established Mcl-1 ubiquitination sites (amino acids 5, 40, 136, 194, and 197) from lysine to arginine was generated as previously described. [82]

4.2 Cell lines/Culture/Co-Culture And Human Samples

The human CCA cell lines KMCH-1, KMBC, HuCCT-1, TFK-1, and Mz-ChA-1 and as well as the erythroblastic leukemia viral oncogene homolog (ErbB-2)/neu transformed malignant rat cholangiocyte cell line BDEneu (CCA *in vivo* experiments) and the LX-2 cells, an immortalized myofibroblast cell line derived from human HSCs, were cultured as previously described.[46, 83-86] The human primary myofibroblastic HSCs were kindly provided by V.H. Shah (Division of Gastroenterology and Hepatology, Mayo Clinic, Rochester, MN) and cultured in Dulbecco's modified Eagle Medium (DMEM) supplemented with 10% fetal bovine serum, penicillin G (100 U/mL), and streptomycin (100 μg/mL) under standard conditions.

CCA co-culture cell experiments were performed using a transwell insert co-culture system (24 wells) equipped with 0.4 μm pore size polyester (PET) inserts (Corning Coster, Acton, MA) for 6 days according to the manufacturer's recommendations. Briefly, KMCH-1 or KMBC cells were plated alone or together with myofibroblastic human primary HSCs or LX-2 cells in the transwell insert co-culture system (KMCH-1 or KMBC cells in the bottom and human primary HSCs or LX-2 cells in the top wells; 1:1 ratio). First, all cells were plated alone at a density of 2 x 10^3 cells/well overnight. The co-culture insert chambers with the human primary HSCs or LX-2 cells then were transferred the next day. Cells were treated as indicated whereas rhTRAIL was added at the end of the experiment (day 6) for 6 hrs and the anti-human PDGF-BB antiserum was added on day 5 for 24 hrs (anti-human PDGF-BB antiserum was added not longer than 24 hrs to minimize confounding effects on apoptosis measurement due to decreased cell proliferation). After rhTRAIL treatment, the KMCH-1 or KMBC cells in the bottom wells were analyzed for apoptosis by DAPI-staining and TUNEL assay as described in the "Quantitation of apoptosis" section (for the TUNEL assay, cells were plated on sterilized trimmed coverslips that were placed in the bottom wells prior to cell seeding).

Human samples (from patients with intrahepatic and extrahepatic CCA treated at Mayo Clinic, Rochester, MN, USA) for analysis by immunohistochemistry were collected with Institutional Review Board approval according to the principles embodied in the declaration of Helsinki.

4.3 In Vivo Microscopy

For assessment of microvascular liver perfusion and leukocyte-endothelial interaction (preservation solution study) *in vivo* microscopy was performed 30 min after reperfusion using a Leica DMLM epifluorescence microscope (Leica Microsystems Wetzlar GmbH, Wetzlar, Germany). The left lateral liver lobe was exteriorized on a specially designed stage. The abdominal cavity was kept moist and body temperature was maintained constant using a heated operation table. Sodium fluorescein (2.0 mmol/kg; Sigma, Deisenhofen, Germany) and rhodamin 6G (0.1 mmol/kg; Sigma) were injected intravenously for fluorescent staining of hepatocytes and leukocytes, respectively.[87] During the measurement, hemodynamic parameters (arterial blood pressure and heart rate) were monitored continuously via a polyethylene catheter placed in the right common iliac artery (Pressure measurement set IT2, Smiths Medical Int., Lancashire, UK; Dräger Infinity Delta XL monitor, Dräger Medical GmbH, Lübeck, Germany). Microcirculation was only assessed if the mean arterial pressure (MAP) was above 60 mmHg (in one case [chloride-poor preservation solution] the measurement was aborted after 40 min

due to systemic hypotension [technical reasons]). The following parameters were determined in 10 randomly selected acinar areas and postsinusoidal venules: *i*) diameters of sinusoids and postsinusoidal venules [μm]. *ii*) sinusoidal perfusion rate: ratio of perfused sinusoids to all sinusoids visible in a defined acinar area [%]. *iii*) red blood cell (RBC) velocity in sinusoids and postsinusoidal venules [μm/s]. *iv*) temporary leukocyte adherence in postsinusoidal venules (rollers): leukocytes moving along the wall of postsinusoidal venules with a velocity of less than 30 % of the central stream velocity (percentage of rollers of all free-moving leukocytes during the observation period of 20 sec [%]). *v*) permanent leukocyte adherence (sticker) in sinusoids and postsinusoidal venules: number of leukocytes adhering for at least 20 sec in sinusoids [n/lobule]; number of leukocytes attached for at least 20 sec to the venular surface of postsinusoidal venules ([n/mm^2]; calculation of the visible part of the vessel surface [approximately 50 %, since only the back wall or the front wall of the postsinusoidal venules could be observed]: $0.5 \cdot \pi \cdot d \cdot l$ [d = mean vessel diameter, l = vessel length]). Video tapes were analyzed by an examiner blinded to the experimental groups using the CapImage 7.3 analysis software (Image Analysis System, Dr. Zeintl, Heidelberg, Germany).

4.4 Light Microscopy

4.4.1 Histological evaluation after rat liver transplantation

Following *in vivo* microscopy (preservation solution study), specimens of the transplanted livers were taken. Histological evaluation was performed after formalin fixation, paraffin embedding, and hematoxylin/eosin as well as ASDCL (naphthol-AS-D-chloroacetate esterase; assessment of granulocyte invasion) staining by a pathologist, who also was blinded to the experimental groups. The severity of morphological/pathological changes was graded according to a numeric semiquantitative score (grade 1 = severe changes, grade 2 = moderate changes and grade 3 = minimal changes) evaluating the width of intrahepatic vessels, vacuolization in the cytoplasm of hepatocytes, prominence of Kupffer cells, necrosis/apoptosis as well as cholestasis.

4.4.2 Morphometric analysis of vessel area/perimeter

To assess dilatation of intrahepatic vessels (EPO study), hematoxylin-eosin stained slides were investigated by computed morphometry. Using an image analysis program (Zeiss KS 300, Oberkochen, Germany) the vessel area and perimeter was measured in central veins of the

hepatic parenchyma (10 randomly chosen visual fields). Results are given in μm² (area) and μm (perimeter), respectively.

4.4.3 Immunohistochemistry for Ki-67

Immunostaining for Ki-67, a marker for cell proliferation, was performed to evaluate the proliferation of hepatocytes (EPO study). The primary antibody was a rabbit monoclonal anti-rat/mouse/human Ki-67 antigen (DCS Diagnostics, Hamburg, Germany 1:1200 dilution). Immunohistochemistry was performed using a biotin-free enhanced polymer one-step staining technique (EPOS-method) with a peroxidase-conjugated polymer backbone coupled with a goat anti-rabbit secondary antibody (DAKO, Hamburg, Germany). "Proliferation index" was defined as the percentage of Ki-67 positive cells counted in 5 high-power-fields (x40) of a specimen.[29]

4.4.4 Immunohistochemistry for α-SMA, PDGFR-β, and PDGF-BB

Immunohistochemistry for CCA studies was performed using formalin-fixed, paraffin-embedded human and rat CCA samples (slides were also stained conventionally with hematoxylin/eosin). Slides were deparaffinized in xylene and rehydrated through sequential graded ethanol steps. For α-SMA-, PDGFR-β- and PDGF-BB-staining, the antigen retrieval was performed by permeabilizing the slides in 0.1% Triton X 100 for 2 min (α-SMA-staining) and incubation in sodium citrate (α-SMA- and PDGFR-β-staining; 0.01 M sodium citrate, 0.05% Tween 20; pH 6.0) or Tris-EDTA buffer (PDGF-BB-staining; 0.01M Tris base, 1 mM EDTA solution, 0.05% Tween 20, pH 9.0) using a vegetable steamer (30 min for α-SMA- and 60 min for PDGFR-β-/PDGF-BB-staining). After cooling, further steps were carried out according to the protocols of the EnVision+ System-HRP [DAB] detection kits (α-SMA: K4006 [anti-mouse]; PDGFR-β and PDGF-BB: K4010 [anti-rabbit]; Dako, Carpinteria, CA). The primary antiserum against α-SMA 1A4 (MS-113-R7, ready-to-use dilution; NeoMarkers, Fremont, CA) was applied for 60 min at RT (PDGFR-β: P-20, 1:25, applied overnight at 4°C, Santa Cruz, Santa Cruz, CA; PDGF-BB: ab21234, 1:10, applied overnight at 4°C, Abcam, Cambridge, MA). Finally, the slides were counterstained with Mayer's Hematoxylin Solution (Sigma, St. Louis, MO), mounted and examined by light microscopy.

4.4.5 Immunohistochemistry for PLK1, PLK2, and PLK3

Immunohistochemistry (CCA studies) was performed using formalin-fixed, paraffin-embedded human CCA samples. Slides were deparaffinized in xylene and rehydrated through sequential graded ethanol steps. The antigen retrieval was performed by permeabilizing the slides in 0.1% Triton X 100 for 2 min and incubation in sodium citrate (0.01 M sodium citrate, 0.05% Tween 20; pH 6.0) for 30 min using a vegetable steamer. After cooling, further steps were carried out according to the protocols of the EnVision+ System-HRP [DAB] detection kits (K4010 [anti-rabbit for PLK2 and PLK3], K4007 [anti-mouse for PLK1]; Dako, Carpinteria, CA). The primary antiserum against PLK1 (1:200; Merck Millipore, Darmstadt, Germany; CN: 05-844), PLK2 (1:100; Abcam, Cambridge, MA; ab34811) and PLK3 (1:200; Proteintech, Manchester, UK; CN: 10977-1-AP) was applied overnight at 4°C. The slides were counterstained with Mayer's Hematoxylin Solution (Sigma, St. Louis, MO), mounted and examined by light microscopy. PLK1/2/3 protein expression quantitation of intrahapatic and extrahepatic CCA samples was performed by histological grading according to the number of PLK1/2/3-positive cells and the intensity of PLK1/2/3 immunoreactivity (grade 0 = no protein expression, grade 4 = high protein expression).

4.5 Immunofluorescence Microscopy

4.5.1 Staining for cytokeratin 7/TUNEL assay

For cytokeratin 7 (CK7)-labeling (CCA studies), the antigen retrieval was performed incubating the slides in deionized water containing 5% urea using a vegetable steamer for 20 min (since some slides also were labeled for TUNEL-positive cells, an additional antigen retrieval step was performed with sodium citrate followed directly by cooling and application of the TUNEL reaction mix; the TUNEL assay is described in the "Quantitation of apoptosis" section). The primary antibody against CK7 (1:10; Abcam; ab9021) was applied for 30 min at RT. After being washed, the slides were incubated with Texas Red®-X goat anti-mouse IgG (1:1000; Invitrogen, Camarillo, CA; T6390) for 1 hr in the dark. The slides were then washed three times in PBS, one time in water and mounted using Prolong Antifade (also Invitrogen). The slides were analyzed by fluorescent confocal microscopy (LSM 510; Zeiss, Jena, Germany).

4.5.2 Staining for PLK2 and Mcl-1

Immunohistochemistry was performed using formalin-fixed, paraffin-embedded (cyclopamine CCA study) or frozen (BI 627 CCA study) rat CCA samples. Paraffin slides were deparaffinized

in xylene and rehydrated through sequential graded ethanol steps Antigen retrieval for the paraffin slides was performed by permeabilizing the slides in 0.1% Triton X 100 for 2 min and incubation in deionized water containing 5% urea using a vegetable steamer for 20 min with subsequent cooling for 20 min. Frozen slides were fixed with 4 % paraformaldehyde in PBS for 10 min at RT and tissue permeabilization was performed with 0.1% Triton X 100 for 15 min at RT. After a blocking step with 5% BSA in PBS for 1 hr at RT the primary antisera/antibodies against PLK2 (1:50; Abcam, Cambridge, MA; ab34811) and Mcl-1 (1:100; Santa Cruz, Santa Cruz, CA; sc-819) were applied overnight at 4 °C. After washing, the slides were incubated with Alexa Fluor® 488 chicken anti-rabbit IgG (for PLK2 and Mcl-1; 1:1000; Invitrogen, Camarillo, CA; A21441) for 1 hr in the dark at RT. The slides were then washed three times in PBS, one time in water and mounted using Prolong Antifade with DAPI (Invitrogen). The slides were analyzed by fluorescent confocal microscopy (LSM 510; Zeiss, Jena, Germany) and PLK2 as well as Mcl-1 immunoreactivity was quantitated using the software ImageJ 1.44o (Wayne Rasband, NIH, Bethesda, MD).

4.6 Microscopy For Smoothened (SMO) Trafficking

HuCCT-1 CCA cells were cultured on coverslips, treated as indicated, and fixed with PBS containing 4% paraformaldehyde for 20 min at 37°C. After being washed with PBS, cells were incubated with 0.5% Triton X-100 in PBS for 15 min at RT and then blocked with PBS containing 5% BSA for 60 min at 37°C. Cells were subsequently incubated with anti-SMO antiserum (1:250; Santa Cruz, Santa Cruz, CA; H-300) at 4°C overnight. After being washed, coverslips were incubated with Texas Red®-X goat anti-rabbit IgG (1:1000; Invitrogen, Camarillo, CA; T6391) for 1 hr in the dark. Cells were then washed three times in PBS, one time in water and mounted using Prolong Antifade (Invitrogen). The slides were analyzed by fluorescent confocal microscopy (LSM 510; Zeiss, Jena, Germany). In additional experiments, SMO trafficking was examined by total internal reflection microscopy (TIRF).[88] KMCH-1 cells cultured on coverslips were transfected with GFP-SMO plasmid 48 hours prior to study. Cells were treated as indicated, and fixed with ddH_2O containing 2.5% formaldehyde, 0.1 M PIPES, 1.0mM EGTA, and 3.0 mM $MgSO_4$ for 20 min at 37°C. Cells were then washed three times in PBS, one time in water and mounted using Prolong Antifade (Invitrogen). The slides were analyzed with a TIRF microscop (Zeiss AxioObserver.Z1, Munich, Germany). GFP-SMO localized to the plasma membrane was quantified using image analysis software (Carl Zeiss

AxioVision 4.8.2.0, Munich, Germany). Data were expressed as the average fluorescence intensity in the cell multiplied by the number of pixels above the background.

4.7 Quantitation Of Apoptosis

Apoptosis in CCA cells was quantified by assessing the characteristic nuclear changes of apoptosis after staining with 4',6-diamidino-2-phenylindole dihydrochloride (DAPI; Sigma, St. Louis, MO) using fluorescence microscopy.[89] Terminal deoxynucleotidyl transferase-mediated dUTP nick end labeling (TUNEL) assays (cell co-culture and rat liver samples in the EPO and CCA studies) were carried out using the In situ Cell Death Detection kit (Roche, Indianapolis, IN) according to the supplier's protocol and as previously described.[84] Caspase 3/7-activity in the CCA studies was quantitated using the ApoONE Homogenous Caspase-3/7 Assay (Promega, Madison, WI) according to manufacturer's recommendations.[89]

4.8 Real-Time Polymerase Chain Reaction (RT-PCR)

Total RNA was extracted from cells and liver tissue (EPO and CCA studies) using the RNeasy Plus Mini Kit (Qiagen, Hilden, Germany), and was reverse-transcribed with Moloney leukemia virus reverse transcriptase and random primers (Invitrogen, Camarillo, CA). Quantitation of the complementary DNA template was performed with real-time polymerase chain reaction (PCR; LightCycler, Roche, Indianapolis, IN) using SYBR green (Roche) as a fluorophore.[78] Oligonucleotide sequences and expected product sizes for primer pairs used for quantitative RT-PCR analysis are shown in Table 2. Primer pairs for *c-jun*, Bcl-X_L, and the EPO-receptor (EPO study) were purchased from Invitrogen, Mississauga, Ontario, Canada. As an internal control, primers for 18S rRNA (Ambion, Austin, TX) were employed. Using gel purified amplicons, a standard curve was generated to calculate the copy number/µL. The target mRNA expression level of each sample was calculated as the copy ratio of target mRNA to 18S rRNA and then normalized to the target mRNA expression of controls.

Gene	**Primer sequence**	**Product length**
SHH	forward 5'-GATGTCTGCTGCTAGTCCTCG-3'	300 bp
	reverse 5'-CACCTCTGAGTCATCAGCCTG-3'	
IHH	forward 5'-TGGCATGCATTGGTACTCTC-3'	350 bp
	reverse 5'-GCTTGCAGCTCTATGACTAC-3'	
DHH	forward 5'-GAGACTCTTTCACAGCTTGG-3'	250 bp

	reverse 5’-TATCACCTCCTCTCAGTACG-3’	
PTCH1	forward 5’-CCACCAGACGCTGTTTAGTCA-3’	72 bp
	reverse 5’-CGATGGAGTCCTTGCCTACAA-3’	
SMO	forward 5’-GTTCTCCATCAAGAGCAACCAC-3’	250 bp
	reverse 5’-CGATTCTTGATCTCACAGTCAGG-3’	
Gli1	forward 5’-TGCAGTAAAGCCTTCAGCAATG-3’	132 bp
	reverse 5’-TTTTCGCAGCGAGCTAGGAT-3’	
Gli2	forward 5’-TGGCCGCTTCAGATGACAGATGTTG-3’	200 bp
	reverse 5’-CGTTAGCCGAATGTCAGCCGTGAAG-3’	
Gli3	forward 5’-AAACCCCAATCATGGACTCAAC-3’	98 bp
	reverse 5’-TACGTGCTCCATCCATTTGGT-3’	
PDGFR-β	forward 5’-AATGTCTCCAGCACCTTCGT-3’	688 bp
	reverse 5’-AGCGGATGTGGTAAGGCATA-3’	
PLK1	forward 5’-CACAGTGTCAATGCCTCCAA-3’	95 bp
	reverse 5’-TTGCTGACCCAGAAGATGG-3’	
PLK2	forward 5’-TCAGCAACCCAGCAAACACAGG-3’	230 bp
	reverse 5’-TTTCCAGACATCCCCGAAGAACC-3’	
PLK3	forward 5’-GAAGGTGGGGGATTTTGG-3’	74 bp
	reverse 5’-GGGTGCCACAGATGGTCT-3’	
Mcl-1	forward 5’-AAGCCAATGGGCAGGTCT-3’	121 bp
	reverse 5’-TGTCCAGTTTCCGAAGCAT-3’	
*Shh**	forward 5’-CTGGCCAGATGTTTTCTGGT-3’	117 bp
	reverse 5’-TAAAGGGGTCAGCTTTTTGG-3’	
*Ihh**	forward 5’-ACCCCACCTTCAGCGATGT-3’	78 bp
	reverse 5’-GAGTCTCGATGACCTGGAAAGC-3’	
*Dhh**	forward 5’-CGTTACGTGCGCAAGCAA-3’	69 bp
	reverse 5’-GGTCCGCTCGGGCATACT-3’	
*Ptch1**	forward 5’-GCAGAGGACTTACGTGGAGG-3’	245 bp
	reverse 5’-CTGACAGTGCAACCAACAGG-3’	
*Smo**	forward 5’-GGGAGGCTACTTCCTCATCC-3’	226 bp
	reverse 5’-TAGCACATAGTCCCGGAAGC-3’	
*Gli1**	forward 5’-TGGAAGGGGACATGTCTAGC-3’	195 bp
	reverse 5’-GCTCACTGTTGATGTGGTGC-3’	
*Gli2**	forward 5’-CCATCCATAAGCGGAGCAAG-3’	105 bp
	reverse 5’-CCAGATCTTCCTTGAGATCAG-3’	
*Gli3**	forward 5’-CATAGCTTCGACCTTCAGACC-3’	211 bp

	reverse 5'-AACCTAAGCTCTGCTGTCGG-3'	
PDGF-B*	forward 5'-TTGTGAGAAAGAAGCCAGTC-3'	213 bp
	reverse 5'-TGTGCTTAAACTTTCGGTGC-3'	
PDGFR-β*	forward 5'-CGAGCACCTTTGTTCTGACA-3'	352 bp
	reverse 5'-TTCTTCTCATGCAGCGTCAC-3'	
PLK1*	forward 5'-TTGAGGACAGCGACTTTGTG-3'	84 bp
	reverse 5'-GCGCCTTCCTCCTTTTGT-3'	
PLK2*	forward 5'-CACCACCATCATCACCATTC-3'	125 bp
	reverse 5'-TCGTAACACTTTGCAAATCCA-3'	
PLK3*	forward 5'-CTGGCAGCTCGGCTAGAG-3'	69 bp
	reverse 5'-GGCCACATAGTTGGGAGTACC-3'	
Mcl-1*	forward 5'-CTACTGGAGCGCGTGAGC-3'	100 bp
	reverse 5'-GGTACAGCTCGTCGTCTTCC-3'	

Table 2. Primer sequences and expected product sizes of human and rat primer pairs used for quantitative RT-PCR analysis. All primers were designed to have an optimum annealing temperature between 50 and 60 °C. * = rat primer pairs (all others are complementary to human targets).

4.9 Immunoblot Analysis

For CCA studies, whole cell lysates were obtained as previously described.[90] For the examination of GLI2 activation, nuclear protein extracts were obtained using the NE-PER Nuclear and Cytoplasmatic Extraction Kit (Thermo Scientific , Barrington , IL; Product no.: 78833). Primary antisera/antibodies used were: Actin (1:2000; Santa Cruz, Santa Cruz, CA; C-11), Lamin B (1:1000; Santa Cruz, Santa Cruz, CA; M-20), PDGFR-β (1:1000; Santa Cruz, Santa Cruz, CA; P-20), phospho-PDGFR-β (Tyr^{857}; 1:1000; Cell Signaling, Danvers, MA; #3170), GLI2 (R&D Systems, Minneapolis, MN; Antibody Part 965887 from the GLI2 ExactaChIP Kit Catalog no.: ECP3526), PLK1 (1μg/ml; Merck Millipore, Darmstadt, Germany; CN: 05-844), PLK2 (1 μg/ml; Abcam, Cambridge, MA; ab34811), PLK3 (1:1000; Cell Signaling Danvers, MA; CN: D14F12), Mcl-1 (1:1000; Santa Cruz, Santa Cruz, CA; sc-819), and Bcl-2 (1:1000; Santa Cruz, Santa Cruz, CA; sc-492). The mouse anti-S peptide antibody was a generous gift from S. H. Kaufmann (Oncology Research, Mayo Clinic, Rochester, MN). Horseradish peroxidase-conjugated secondary antibodies for rabbit (Santa Cruz; sc-2004), goat (Santa Cruz; sc-2020), mouse (Santa Cruz; sc-2031), and sheep (Santa Cruz; sc-2770) were incubated at a dilution of 1:2000 for 1 hr at RT. Proteins were visualized using enhanced chemiluminescence reagents (ECL, Amersham Biosciences, Buckinghamshire, UK) and Kodak X-OMAT films.

4.10 Chromatin Immunoprecipitation (ChIP Assay)

ChIP was performed from KMCH-1 CCA cells treated with rhSHH (500 ng/ml, 5 hrs) plusminus cyclopamine (10 μM, 5 hrs) using total cellular DNA sheared to ≈ 500 bp fragments employing an automated cooled sonication device (Bioruptor XL; Diagenode, Denville, NJ; 20 cycles with 30 seconds sonication/30 second intervals). ExactaCHIP chromatin immunoprecipitation kits for GL1, GLI2 and GL3 (R&D Systems, Minneapolis, MN; GLI1: ECP3324, GLI2: ECP3526, GLI3: ECP3690) and streptavidin agarose beads (Merck, Rockland, MA; #69203), were used following the manufacturer's instructions. Samples were pre-cleared using agarose beads plus salmon sperm slurry (Upstate, Lake Placid, NY) prior to immunoprecipitation (also performed with agarose beads). Primers for RT-PCR were forward 5'-TCA TGT CTC CCC GTT CCA ACT-3', reverse 5'-TGC AAA GCC ACC CTG AAA GGA-3' (PLK pomotor site I, 277 bp) and forward 5'-CAT TTG GGT CAG CTC CAA GT-3', reverse 5'-TCT CAC GCC AGT TAA AAT GGC G-3' (PLK pomotor site II, 297bp). Positive control primers supplied by the manufacturer were for the Bcl-2 promoter (bound by GLI1 and GLI2, 147 bp) and the GLI1 promoter (bound by GLI3, 211 bp).

4.11 Assessment Of Laboratory Parameters

Subsequent to *in vivo* microscopy (approximately 90 min after reperfusion; preservation solution study) blood samples were drawn (vena cava puncture) for analysis of liver enzymes (aspartate transaminase [AST], alanine transaminase [ALT], lactate dehydrogenase [LDH] and alkaline phosphatase [AP]) and prothrombin time. The samples were processed using standard blood analysis tests. In addition, blood samples from n=8 untreated Lewis rats were drawn as reference. In the EPO experiments, glutamate dehydrogenase (GLDH), total bilirubin, prothrombin time (PTT), international normalized ratio (INR), and hematocrit were additionally assessed as described before.[29] Furthermore, EPO serum concentrations were measured by means of an immunoluminometric assay (Limbach, Heidelberg, Germany)

4.12 Enzyme-Linked Immunosorbent Assay (ELISA) for PDGF-BB

Levels of secreted human PDGF-BB in CCA and MFB cell experiments were determined by an enzyme-linked immunosorbent assay using a commercially available kit (RayBiotech, Norcross, GA) according to the suppliers protocol.

4.13 Assessment Of Bile Production

As an indicator of liver function, postoperative bile production was measured (preservation solution study). The amount of bile draining from the bile duct via a polyethylene tube (prepared from a 22G IV Catheter, Medex Medical GmbH, Germany) over a period of 90 min was collected, weighed and given in mg per g of liver wet weight.

4.14 cDNA Array

A customized cDNA array consisting of 183 rat genes was established as previously described (EPO study).[28] As a control, 13 GAPDH and ß-actin gene probes were added. Subsequently, the gene products were spotted on Hybond N^+ nylon membranes (Amersham Pharmacia, Freiburg, Germany) and hybridized overnight at 65°C with P^{32} labeled cDNA prepared from 10µg total RNA of each rat liver sample. The membranes were stored in a Phosphoimager Cassette (Amersham Biosciences, Freiburg, Germany), exposed for 2-3 days and scanned on the STORM Phosphoimager (Amersham Biosciences, Freiburg, Germany). The data were analyzed using Image Quant software (Amersham Biosciences, Freiburg, Germany) as described bevore.[91]

4.15 Genome-Wide mRNA Expression Analysis

For the CCA studies, KMCH-1 cells were treated with vehicle, PDGF-BB (200 ng/ml, 8hrs), or SHH (500 ng/ml, 8hrs) in the presence or absence of cyclopamine (10 µM, 8hrs). After total mRNA extraction (see section real time polymerase chain reaction) and confirmation of the sample quality by Agilent bioanalysis, 150-500 ng of total RNA per sample were analyzed for 33617 target genes (after MAS5 noise filtering) employing an Affymetrix GeneChip Platform with the Affymetrix Human U133 Plus 2.0 labeling method. Specifically, biotin-labeled cRNA, produced by in vitro transcription, was hybridized to the Affymetrix Human Genome U133 Plus 2.0 GeneChips. These experiments were conducted in collaboration with the Advanced Genomics Technology Center Core Mayo Clinic, Rochester, MN.

4.16 Generation Of A Transfectant Expressing SMO Short Hairpin RNA

Short hairpin RNA (shRNA) lentiviral plasmid for SMO was from Thermo Fisher Scientific (Hunsville, AL; Oligo ID: V2LHS_56569; GenBank accession no.: NM_005631). KMCH-1 CCA cells were transfected using OptiMEM I (Gibco-Invitrogen, Carlsbad, CA) containing 6 μL/mL Lipofectamine (Invitrogen),1 μg/mL plasmid DNA, and 6 μL/mL Plus reagent (Invitrogen). Forty-eight hours after transfection, fresh DMEM containing 0.5 μg/mL puromycin was added. Surviving clones were separated using cloning rings and individually cultured. A clone with a scrambled shRNA was employed as a control (stable scrambled KMCH-1 cells). The expression/knockdown of SMO in the clones was assessed by immunoblot analysis.

4.17 Generation Of A Transfectant Expressing PLK1, 2, or 3 Short Hairpin RNA.

Short hairpin RNA (shRNA) lentiviral plasmids for PLK1 and PLK3 were obtained from Thermo Fisher Scientific/Open Biosystems (Hunsville, AL; Oligo ID: V2LHS_241437, Gen Bank accession no.: NM_005030 and Oligo ID: V2LHS_172853, Gen Bank accession no.: NM_004073, resp.). PLK2 shRNA lentiviral plasmids were obtained from Sigma-Aldrich (St. Louis, MO; Gen Bank accession no.: NM_006622.2). KMCH-1 cells were transfected using OptiMEM I (Gibco-Invitrogen, Carlsbad, CA) containing 6 μl/ml Lipofectamine (Invitrogen), 1 μg/ml plasmid DNA and 6 μl/ml Plus reagent (Invitrogen). Forty-eight hours after transfection, fresh DMEM containing 0.5 μg/ml puromycin was added. Surviving clones were separated using cloning rings and individually cultured. A clone with a scrambled shRNA was employed as a control (stable scrambled KMCH-1 cells). The expression/knockdown of PLK1, PLK2 or PLK3 in the clones was assessed by immunoblot analysis.

4.18 Generation Of AN Enhanced Green Fuorescent Protein (GFP)–Tagged SMO

A pRK7 plasmid containing the human SMO sequence (GenBank accession no.: NM_005631) for the CCA studies was a generous gift from M. Fernandez-Zapico (Division of Oncology Research, Mayo Clinic, Rochester, MN). The pRK7-SMO plasmid was modified to accept the green fluorescent protein (GFP) tag first by inserting recognition sites for EcoRI and NotI at the C-terminus of SMO, replacing the stop codon. For this, a PCR-generated EcoRI/NotI modified SMO C-terminal coding sequence was inserted into pRK7-SMO. Next, GFP from the pEGFP-N1 protein fusion vector (Clontech Laboratories, Inc., Mountain View, CA; Catalog no.: 6085-1; GenBank accession no.: U55762) was digested and inserted into the modified pRK7-SMO plasmid to generate a SMO construct fused to GFP at the C-terminal cytoplasmic domain. The GFP-SMO plasmid was sequenced to confirm that the construct was in frame and no polymerase chain reaction artifacts were introduced.

4.19 GLI Reporter Construct And Promoter-Reporter Assay

To determine GLI activity in the CCA studies, a reporter containing eight directly repeated copies of a consensus GLI-binding site (8x-GLI) downstream of the luciferase gene was employed (pδ51*Luc*II plasmid; δ-crystalline promoter). [92] The 8x-GLI reporter was kindly provided by M. Fernandez-Zapico (Division of Oncology Research, Mayo Clinic, Rochester, MN). The plasmid was transfected into normal, stable scrambled, or shSMO KMCH-1 cells (0.5 μg/well) using FuGene HD (Roche Diagnosis, Basel, Switzerland). Cells were co-transfected with 50 ng of a plasmid expressing Renilla luciferase (pRL-CMV; Promega, Madison, WI). 24 hours after transfection, cells were treated as indicated, cell lysates prepared, and both firefly and Renilla luciferase activities quantified using the Dual-Luciferase Reporter Assay System (Promega) according to the manufacturer's instructions. Firefly luciferase activity was normalized to Renilla luciferase activity to control for transfection efficiency and cell numbers. Data (firefly/Renilla luciferase activity) are expressed as fold increase over vehicle-treated cells transfected with the 8x-GLI/pRL-CMV reporter constructs.

4.20 Animal Experiments

4.20.1 Orthotopic full size rat liver transplantation

Male Lewis and Wistar rats (240–300 g) were obtained from the Central Animal Facility of the University Hospital Essen (preservation solution studie). Animals were kept under standard conditions with free access to food (recipient rats were fastened for 2 h preoperatively) and water. All operations and handling procedures were conducted in accordance with the German Animal Welfare Law and with approval of the district administrative authorities (Regierungspräsidium Düsseldorf and Landesamt für Natur, Umwelt und Verbraucherschutz Recklinghausen). Surgical procedures and interventions were performed under volatile anesthesia (O_2 with up to 2.5 % isoflurane) with maintained spontaneous ventilation. The study was subdivided into two parts in order to compare the effects of the new HTK solutions (for composition see Table 1) on *i*) overall survival under different conditions and *ii*) microcirculation as well as laboratory and histological parameters.

Three different microsurgeons performed orthotopic LTx in male Lewis and Wistar rats (donors and recipients: 240–300 g) according to the cuff technique described by Kamada and Calne without hepatic artery reconstruction.[93] Perfusion (approx. 50 ml) and storage (150 ml) of the livers at 4°C were done using the same preservation solution (chloride-poor vs. chloride-containing new solution). The following three protocols were carried out for comparison of overall survival. *Protocol 1:* CIT: 24 h; WIT (during implantation): 17.1 ± 1.6 min; Wistar to Wistar; n=7 recipient rats each group; randomized; sacrifice after 7 days. *Protocol 2:* CIT: 12 h; WIT: 19.7 ± 3.2 min; Wistar to Wistar; n=8 recipient rats each group; randomized; blinded; sacrifice after 7 days. *Protocol 3:* CIT: 3 h; WIT: 25.0 ± 0.0 min (fixed to 25.0 min; no standard deviation); Lewis to Lewis; n=8 recipient rats each group; randomized; blinded; sacrifice after 28 days. LTx prior to assessment of microcirculatory parameters was performed according to the following protocol with average CIT and WIT: CIT: 18 h; WIT: 18.0 ± 1.1 min; n=7/8 Lewis rats each group; randomized; blinded (one rat [chloride-containing preservation solution] died of unknown reasons 30 min after beginning of *in vivo* microscopy); sacrifice directly after *in vivo* microscopy. Analgesia in all rats was achieved by preoperative subcutaneous injections of 5 mg/kg BW carprofen (Rimadyl®, Pfizer, Karlsruhe, Germany). Recipient rats participating in survival experiments additionally obtained 100 mg/kg BW mezlocillin (Baypen®, Bayer AG, Leverkusen, Germany) intramuscularly after LTx as antibiotic prophylaxis.

4.20.2 Orthotopic partial (30%) rat liver transplantation

Male Lewis rats (Charles River Laboratories, Sulzfeld, Germany) weighing 250-300g were maintained on a commercial pelleted diet and water ad libidum under normal laboratory lighting conditions (EPO studie). All animal study protocols were approved by the German Animal Welfare Law and with approval of the district administrative authorities (Regierungspräsidium Düsseldorf and Landesamt für Natur, Umwelt und Verbraucherschutz Recklinghausen).

For transplantation, donor and recipient rats underwent isoflurane anesthesia. Liver reduction was achieved by resecting the left lateral and median lobe, which resulted in a 70% reduction of the liver mass. The graft was flushed and stored in cold HTK solution with a CIT of 180 minutes (sacrifice after 24 h) and 360 min. (sacrifice after 28 days = survival experiments), respectively. pLTx was performed according to the cuff technique of Kamada and Calne without hepatic artery reconstruction.[93] The transplantation procedure required less than 60 min. The portal vein was clamped for 16 to 19 min. After the observation period (see protocols below), the remnant, regenerated liver was resected, weighed and total body weight was measured. The acquired data were expressed as percentage of the ratio between remnant liver weight (A), divided by the total body weight (B) times 100 (Liver body weight ratio [LBWR] in (%) = A/B x 100).

Preconditioning experiments (protocol 1) were carried out to establish optimal EPO-doses for donor animals. Controls were treated with heat-inactivated EPO in the same vehicle volume. The following protocols were employed. *Protocol 1:* In two preconditioning experiments rats (n=8 in each group) were injected once or thrice with several doses of EPO i.p. The animals were sacrificed 4, 8 and 12 days after the first injection. *Protocol 2***:** Donor rats (n=8 in each group) were injected thrice with 1 I.U. EPO/g BW i.p. or vehicle 9 days prior to partial liver transplantation (pLTx). Recipient rats were injected thrice with 5 I.U. EPO/g BW or vehicle i.v. perioperatively. The animals were sacrificed after 24 h and 28 days (survival experiments) postoperatively.

4.20.3 Syngeneic, orthotopic rat modell of cholangiocarcinoma

All CCA animal studies were performed in accordance with and approved by the Institutional Animal Care and Use Committee. *In vivo* intrahepatic cell implantation was carried out in male adult Fischer 344 rats (Harlan, Indianapolis, IN) with initial body weights between 190 and 230 g as previously described.[84-86] In the experiments targeting PDGF siganaling, imatinib mesylate (30 mg/kg BW; approx. 0.5 mL) or vehicle (normal saline) was given intraperitoneally every

day for one week (1st injection: 7th post-operative day; 7th injection: 13th post-operative day). In the experiments targeting Hh siganaling, cyclopamine (2.5 mg/kg BW; 0.5 mL) complexed with 2-hydroxypropyl-β-cyclodextrin (Tocris, Ellisville, MO) as previously described [94, 95] or vehicle was given intraperitoneally every day for one week (1st injection: 7th post-operative day; 7th injection: 13th post-operative day). In the experiments targeting PLK siganaling, BI 6727 (3 injections of 10 mg/kg body weight [0.5 mL] intraperitoneally every other day; the first injection was given on postoperative day 7,and the third injection was given on postoperative day11) formulated in hydrochloric acid (0.1 N) diluted with 0.9% NaCl.[81] Twenty-four hours (forty-eight hours in the BI 6727 study) after receiving the last injection, the rats were euthanized and the livers removed for further analysis including histopathology and mRNA extraction. To assess the numbers of metastases-free and metastases-bearing rats, the abdominal cavities, the retroperitoneal spaces and the thoracic cavities were thoroughly examined as previously described.[85]

4.21 Statistical Analysis

4.21.1 Preservation solution/erythropoietin studies

All data are expressed as mean ± SD unless indicated otherwise and represent at least three independent experiments. Comparison between experimental groups was performed using the two-tailed Student's *t*-test for quantitative continuous variables. Overall survival curves were estimated with the Kaplan-Meier method and statistical analysis was performed using the logrank test for each single series and Fishers-combination rule to calculate an overall one-sided p-value that combines the results from all three independent survival experiments. Further statistical analyses (EPO study) were performed by one-way Anova or Wilcoxon´s test. Differences were considered as significant at levels of $p < 0.05$. Statistical analysis was performed using GraphPad Prism v4.00 (GraphPad Software Inc., La Jolla, CA) and SPSS v12.0 (SPSS Inc., Chicago, IL).

4.21.2 Cholangiocarcinoma studies

Data are expressed as the mean ± s.e.m. unless indicated otherwise and represent at least three independent experiments. Box-and-whisker plots depict minimum, 25th percentile, median, 75th percentile, maximum, and outliers. Differences in experiments with two groups were compared using the two-tailed Student *t*-test or the Chi-square test (χ^2, analysis of metastasis) as well as

Mann Whitney's test (analysis of PLK1/2/3 expression in human CCA samples). Differences in experiments with more than two groups were compared using ANOVA with Bonferroni post hoc correction. Differences were considered as significant at levels of $p < 0.05$. Statistical analysis was performed using GraphPad Prism v4.00 (GraphPad Software Inc., La Jolla, CA).

DOI:10.14753/SE.2016.1969

5 RESULTS

5.1 General Optimization Approaches For Liver Transplantation

5.1.1 Chloride improves survival due to beneficial effects on microcirculation

Postoperative survival. Each of the three experimental series performed to assess postoperative survival showed a (strong) tendency towards a prolonged survival using the chloride-containing new solution. In the first series (n=7 Wistar rats/group) a long CIT (24 h) was combined with a short WIT (17.1 ± 1.6 min). Here the survival rates 7 days after LTx were 100 % vs. 71.4 % (χ^2 = 2.16 [p>0.05 by logrank test]) for the chloride-containing vs. the chloride-poor solution, respectively (Figure 1A). The second series (n=8 Wistar rats/group) was carried out with intermediate CITs and WITs (12 h/19.7 ± 3.2 min). Figure 1B depicts the Kaplan-Meier 7d-survival plot with 75 % of the rats surviving after LTx with the chloride-containing solution in comparison with 37.5 % of the rats still living 7 days after LTx with the chloride-poor solution (χ^2 = 1.70 [p>0.05 by logrank test]). While follow-up time in the first two series utilizing Wistar rats was limited to 7 days in order to avoid influences due to rejection reactions (the Wistar rats are not inbred), Lewis rats (a syngeneic strain) in the third series (n=8 Lewis rats/group) with a short CIT (3 h) and long a WIT (fixed to 25.0 min; no standard deviation) were observed over a period of 28 days (Figure 1C). In this series with a median survival of 23.5 vs. 9.5 days, for the third time the survival rates between animals receiving grafts preserved with the chloride-containing new solution vs. animals receiving grafts preserved with the chloride-poor new solution suggested a better outcome with chloride (50 % vs. 12.5 %, χ^2 = 3.06 [p=0.07 by logrank test]). After combining the results from the three independent experimental series using Fishers-combination rule, an overall one-sided p-value of 0.012 was obtained, underlining the results shown in Figure 1A-C by a statistical summary.

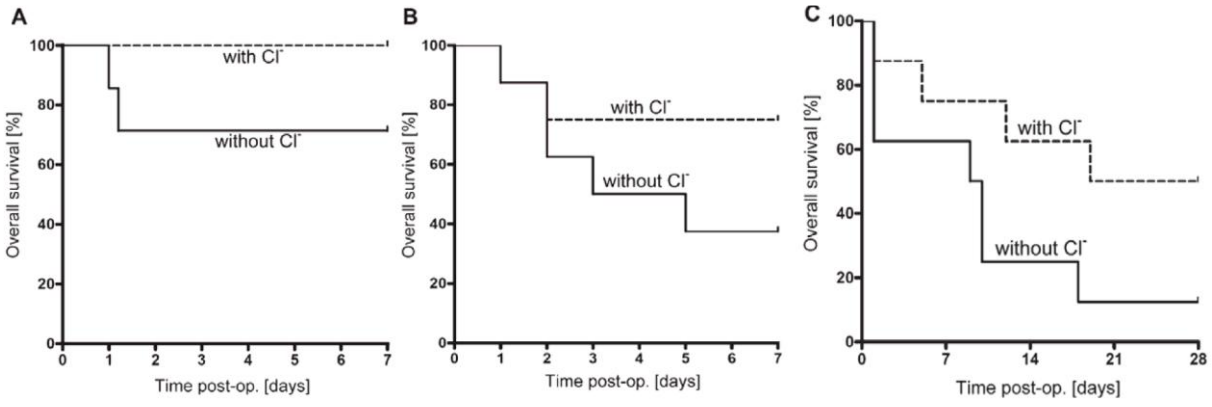

Figure 1. Overall survival of different rat strains after LTx by 3 different microsurgeons with the chloride-poor and chloride-containing solutions. (A) Kaplan-Meier 7-day survival plot (CIT = 24 hours, WIT = 17.1 ± 1.6 minutes, 7 Wistar rats in each group, P = 0.14), (B) Kaplan-Meier 7-day survival plot (CIT = 12 hours, WIT = 19.7 ± 3.2 minutes, 8 Wistar rats in each group, P = 0.19), and (C) Kaplan-Meier 28-day survival plot (CIT = 3 hours, WIT = 25.0 ± 0.0 minutes, 8 Lewis rats in each group, P = 0.07). A combination of the results from all 3 experimental series with Fisher's method yielded an overall 1-sided P value of 0.012.

Microcirculation. Assessment of microcirculation and leukocyte-endothelial interaction was performed in an additional series with an intermediate CIT (18 h) and an intermediate WIT (18.0 ± 1.1 min; Table 3). In this series systemic hemodynamic parameters, i.e. arterial blood pressure and heart rate were also measured since these systemic parameters have a relevant impact on hepatic microcirculation. There were no significant differences between the rats of both test groups in regard to systemic hemodynamics, body weight, and liver wet weight (Table 3).

	Modified Solution Without Chloride	Modified Solution With Chloride	*P* Value
Recipient body weight (g)	284.5 ± 13.3	283.9 ± 16.2	0.96
Donor liver wet weight (g)	9.8 ± 0.9	9.9 ± 1.0	0.88
Arterial blood pressure (mm Hg)*	76.5 ± 2.8	74.1 ± 7.0	0.46
Heart rate (min^{-1})*	251.3 ± 20.8	257.4 ± 15.2	0.78
CIT (hours)	18.0 ± 0.1	18.0 ± 0.1	0.84
WIT (minutes)	18.1 ± 1.2	17.9 ± 1.0	0.88

Table 3. General, physiological, and LTx data for the test groups participating in the *in vivo* microscopy experiments. The experiments were performed with 7 or 8 Lewis rats in each group. *At the beginning of the *in vivo* microscopy analysis.

In vivo microscopy starting 30 min after reperfusion exhibited obvious pathological alterations such as intraparenchymal hemorrhages, areas with reduced RBC velocities, and stasis of blood flow in both test groups. These disturbances of microcirculation were observed in both sinusoids and postsinusoidal venules. However, number and size of malperfused areas were clearly decreased in rats that underwent LTx with grafts preserved with the chloride-containing preservation solution. This impression was confirmed by quantitative analysis (carried out in a blinded fashion) exhibiting clearly higher sinusoidal perfusion rates in liver grafts preserved with the chloride-containing new solution at start point, end point, and during 60 min (mean) of *in vivo* microscopy (Figure 2A). In addition, mean RBC velocities in sinusoids and postsinusoidal venules were clearly higher with the chloride-containing new solution (Figure 2B). The most significant RBC velocity difference was observed at the end point of *in vivo* microscopy (90 min after reperfusion) in postsinusoidal venules (339.0 ± 95.9 µm/s vs. 182.1 ± 41.1 µm/s; p = 0.001). While sinusoidal perfusion rates and RBC velocities remained

relatively constant in both test groups during the whole period of the measurement, diameters of postsinusoidal venules (not sinusoids) showed differences over time (Table 4). Interestingly, diameters of postsinusoidal venules in liver grafts preserved

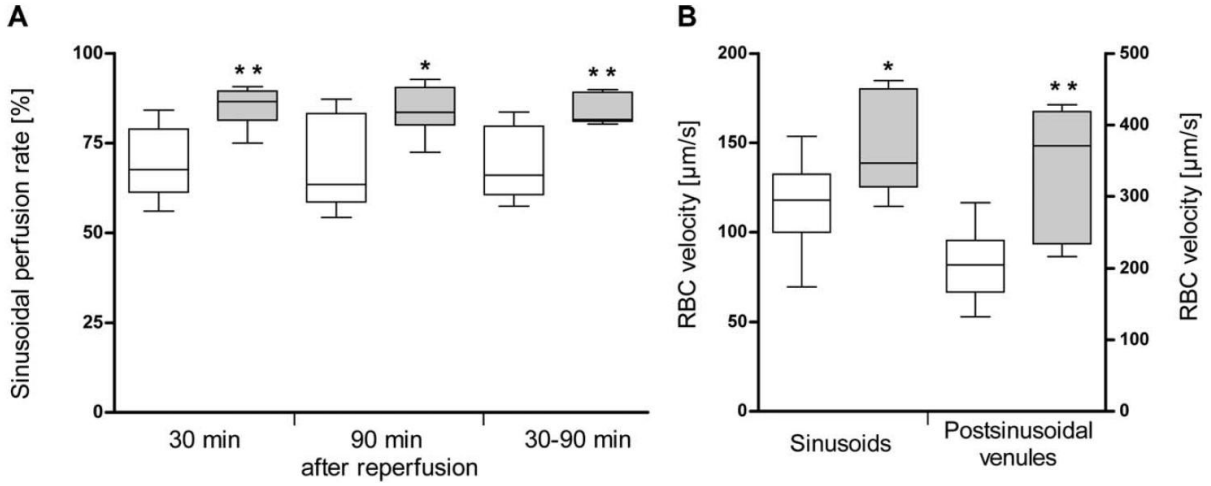

Figure 2. Microcirculation 30 to 90 minutes after reperfusion with the chloride-poor solution (white boxes) and the chloridecontaining solution (gray boxes). (A) sinusoidal perfusion rates at the beginning and end of the in vivo microscopy analysis (30 and 90 minutes after reperfusion, respectively) and during 60 minutes of the analysis (mean rates from 30 to 90 minutes after reperfusion). (B) RBC velocities in sinusoids and postsinusoidal venules. The LTx protocol was as follows: CIT =18 hours, WIT = 18.0 ± 1.1 minutes, and there were 7 or 8 Lewis rats in each group. Box and whisker plots depict the distributions of the measurements (the box limits are the 25th and 75th percentiles, the medians are marked between them, and the whiskers depict the minima and maxima). *P < 0.05 and **P < 0.01.

with the chloride-containing solution increased over the 60 min observation period, while preservation with the chloride-poor solution led to a decrease in postsinusoidal venule diameters within the same time. At the end of *in vivo* microscopy these reverse developments resulted in significantly wider postsinusoidal venule diameters within liver grafts that were preserved with the chloride-containing preservation solution (Table 4).

Leukocyte-endothelial interaction. Although the number of stickers per surface postsinusoidal venule increased with time in both test groups there were no significant differences concerning any parameter of leukocyte-endothelial interaction comparing the chloride-containing vs. the chloride-poor preservation solution (Table 4).

	Modified Solution Without Chloride	Modified Solution With Chloride	*P* Value
Diameter of sinusoids (μm)	6.3 ± 0.5	6.2 ± 0.2	0.96
Diameter of postsinusoidal venules (μm)			
Starting point of measurement	28.9 ± 13.8	22.8 ± 7.0	0.51
Endpoint of measurement	24.3 ± 7.2	31.9 ± 5.0	0.02
Rollers in postsinusoidal venules (%)	7.6 ± 2.3	7.8 ± 4.5	0.87
Sinusoidal stickers (n/lobule)	54.3 ± 21.3	47.5 ± 18.2	0.87
Stickers in postsinusoidal venules (n/mm^2)			
Starting point of measurement	310.0 ± 270.7	265.0 ± 349.4	0.57
Endpoint of measurement	494.0 ± 293.2	505.6 ± 180.2	0.78

Table 4. Vessel diameters and leukocyte-endothelium interactions. The LTx protocol was as follows: CIT = 18 hours, WIT = 18.0 ± 1.1 minutes, 7 or 8 Lewis rats in each group. Only 2 parameters (diameter of postsinusoidal venules and stickers in postsinusoidal venules) showed notable differences between the starting points and endpoints of the *in vivo* microscopy analysis.

Liver histology. No signs of necrosis/apoptosis or cholestasis were observed in either test groups 90 min after reperfusion. In addition, no granulocyte invasion occurred with exception of minimal cell counts of neutrophilic granulocytes in a few periportal tracts. Comparing the chloride-containing vs. the chloride-poor preservation solution, there were no significant differences with regard to postmortal width of intrahepatic vessels (severity score of morphological/pathological parameters [semiquantitative score; 1-3 = high-grade to low-grade]: 1.4 ± 0.5 vs. 1.6 ± 0.7), vacuolization in the cytoplasm of hepatocytes (1.4 ± 0.7 vs. 2.0 ± 0.9) as well as prominence of Kupffer cells (2.0 ± 0.5 vs. 2.0 ± 0.5).

Laboratory parameters. In both test groups postoperative serum transaminase and LDH activities were clearly increased 90 min after reperfusion in comparison with non-treated animals (reference). However, rats that underwent LTx with the chloride-containing preservation solution exhibited lower serum transaminase (AST, ALT) and LDH activities than rats after LTx with the chloride-poor preservation solution (Figure 3A). Statistical significance was barely missed (p = 0.087; p = 0.118; p = 0.052). AP activity was not notably increased compared to non-treated animals in both test groups. Prothrombin time was slightly elevated possibly due to consumption of clotting factors at this early time point, but also did not show any difference when comparing the chloride-containing vs. the chloride-poor preservation solution (Figure 3B).

Bile production. As a parameter of hepatocellular function bile flow was significantly less impaired in rats that underwent LTx with the chloride-containing new solution (Figure 3C).

DOI:10.14753/SE.2016.1969

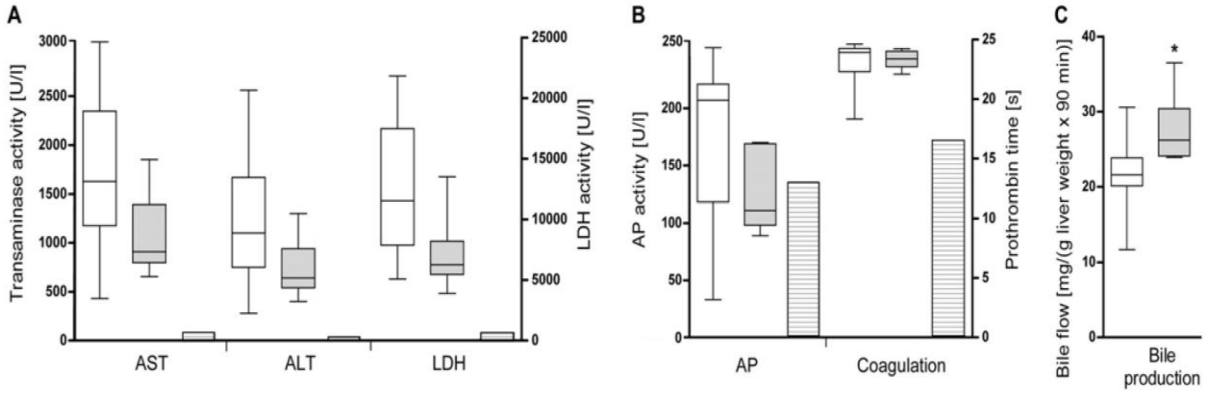

Figure 3. Serum liver enzyme activities and prothrombin time 90 min after reperfusion as well as bile production during a period of 90 min after reperfusion comparing the chloride-poor (□) vs. the chloride-containing (■) solution. (A) Aspartate transaminase (AST), alanine transaminase (ALT) and lactate dehydrogenase (LDH). B: Alkaline phosphatase (AP) and prothrombin time (PT). C: Bile production given in mg per g of liver wet weight. Grey hatched bars = references consisting of mean values collected from blood samples of n=8 untreated Lewis rats. LTx protocol: CIT = 18 h; WIT = 18.0 ± 1.1 min; n=7/8 Lewis rats each group. Box-and-whisker plots depicting the distribution of measurements (limits of the box are the minimum, 25th and 75th percentile with the median marking in between; ○ = outliners). *P < 0.05.

5.1.2 Erythropoietin increases liver growth and inhibits apoptosis

Systemic effects of EPO. To demonstrate correct application and efficacy of EPO, we measured EPO serum concentrations and hematocrit in the rats after three successive intravenous injections of 5 I.U. EPO/g BW. There were no changes of the hematocrit within the first 48 h. 96 h after the first of three EPO-injections, however, the hematocrit rose from 42% ± 2% to 49% ± 3% (p=0.028; n=8). The EPO serum concentrations in treated rats (n=8) reached levels that were 569 times higher than in control animals (796 mU/ml ± 214 mU/ml vs. 1.4 mU/ml ± 0.3 mU/ml; p<0.001; n=8).

EPO effects on growth of unresected (donor) livers. EPO treatment resulted in a steady increase of cellular mass of the liver after the first EPO injection, as indicated by an elevated LBWR compared to control animals. The highest LBWR was achieved by applying 1 I.U. EPO/g BW i.p. thrice on three successive days (3.80% ± 0.12% vs. 3.56% ± 0.15%; p=0.016). Applying 1 I.U. EPO/g BW i.p. once led to a higher LBWR compared to control animals, but was lower than in animals, which had received EPO three times. There was nu further increase of the LBWR upon doubling the amount of EPO (2 I.U. EPO/g BW i.p. thrice). In contrast, reducing the dosage to 0.5 I.U. led to a smaller increase of the LBWR.

EPO effects on hepatocyte proliferation in unresected (donor) livers. The increase of liver mass was accompanied by an increase in Ki-67 proliferation index. EPO-treated rats showed the most significant increase of hepatocyte proliferation 12 days after EPO application with 4.6% ± 1.3% vs. 1.1% ± 0.5% in control rats when receiving 1 I.U. EPO/g BW i.p. thrice on three successive days compared to controls ($p<0.001$).

EPO effects on growth of partial liver grafts (donor and recipient). In these experiments, we investigated the impact of preconditioning (donor rats) and perioperative treatment with EPO after pLTx (recipient rats). To assess liver regeneration, LBWR was measured (Figure 4A). After 24 h, recipients of the EPO-group showed a higher absolute liver weight-increase in comparison with control rats (0.58g ± 0.23g vs. 0.37g ± 0.13g; $p=0.046$). The relative increase in liver weight was significantly higher 15.7% ± 6.74% in EPO-treated compared to control animals (9.9% ± 2.68%, $p=0.040$).

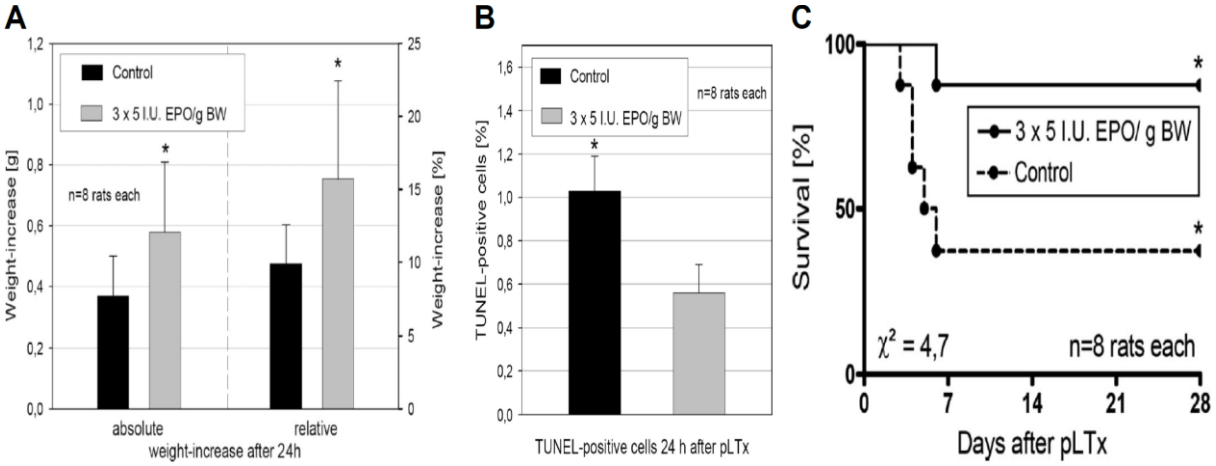

Figure 4. EPO effects in the setting of partial liver transplantation (pLTx). (A) Absolute and relative liver-to-body weight ratio (LBWR) after pLTx. Animals were treated with EPO or heat-inactivated EPO in the same vehicle volume. LBWR increased 24 h and 5 days after pLTx regarding absolute and relative LBWR. (B) Hepatocyte apoptosis (TUNEL index) after pLTx. Hepatocyte apoptosis was assessed in rat livers 24 h after pLTx. There was a significantly lower proportion of hepatocytes undergoing apoptosis 24 h after pLTx (0.56% vs. 1.03%, P=0.04) compared with control rats. (C) Twenty-eight-day survival after pLTx. Sixteen rats were investigated for overall survival after undergoing 30% pLTx. EPO-treated animals showed an improved overall survival after pLTx. Only one animal died within the EPO group, whereas five rats died in the control arm (*$P < 0.05$.; χ^2=Chi-square value).

EPO effects on hepatocyte proliferation in partial liver grafts. Twent-four hours after pLTx the increase of liver mass in the EPO-group was accompanied by a trend towards a higher Ki-67-

proliferation index. However, due to a high standard deviation, no statistical significance was obtained (12.7% ± 12.7% vs. 4.74% ± 2.2%; p=0.1).

EPO effects on laboratory parameters after pLTx. Twenty-four hours after pLTx there were no significant differences concerning postoperative raises of AST (3852 U/l ± 2221 U/l vs. 4097 U/l ± 1208 U/l), ALT (1981 U/l ± 655 U/l vs. 2145 U/l ± 1234 U/l), GLDH (2345 U/l ± 1343 U/l vs. 2546 U/l ± 1622 U/l) and total bilirubin (0,9 mg/dl ± 1,23 mg/dl vs. 0,83 mg/dl ± 0,76 mg/dl) in EPO vs. control rats. However, there was a trend towards an improved postoperative coagulation in the EPO group (INR: 1.27 ± 0.14 vs. 1.41 ± 0.05; p=0.06; PTT: 18.96s ± 4.83s vs. 23.48s ± 1.28s; p=0.08).

EPO effects on hepatocyte apoptosis in partial liver grafts. For hepatocyte apoptosis analysis, TUNEL staining was performed in rats after pLTx. There was a significantly lower proportion of hepatocytes undergoing apoptosis 24 h after pLTx (0.56% vs. 1.03%; p<0.04) as compared to control rats (Figure 4B).

EPO effects on gene expression in partial liver grafts. In order to examine the mechanistic processes underlying our prior observations, the expression of 183 genes involved in liver regeneration and apoptosis were measured by a customized cDNA array. Relevant results were confirmed by quantitative RT-PCR. Finally, the immediate-early gene *c-jun* as well as the anti-apoptotic gene Bcl-X_L were confirmed to be significantly upregulated in the EPO-group. In contrast, the gene expression of the EPO-receptor was not altered (Table 5).

EPO effects on angiogenesis in partial liver grafts. The morphometric parameters vessel perimeter (346 µm² ± 50 µm² vs. 324 µm² ± 104 µm²; p>0.05) and vessel area (8653 µm² ± 2951 tµm² vs. 7532 µm² ± 4766 µm²; p>0.05) did not reveal differences in early angiogenesis 24 h after surgery.

Gene	EPO	Control	*P*
c-jun	2.89±0.62	1.51±1.07	0.049
Bcl-X_L	21.31±21.47	6.05±2.14	0.048
EPO-receptor	0.98±0.08	1.19±0.15	NS

Table 5. Gene expression analysis by RT-PCR. Twent-four hours after pLTx, mRNA level alterations of relevant genes were assessed (mRNA fold changes within 24 h in EPO-treated versus control rats; n=8 each).

Impact of treatment with EPO on 28-day survival after pLTx. Finally, twenty-eight-day survival was assessed in additional 16 rats (Figure 4C). We observed an overall survival of 88% (7/8) in rats receiving EPO as compared to only 38% (3/8) in control rats at the end of the observation period as demonstrated by the Kaplan-Meier survival curve (p=0.03; Chi-square [χ^2] = 4.7). All animal deaths occurred within the first week after transplantation.

5.2 Optimization Of Liver Transplantation For Cholangiocarcinoma

5.2.1 Myofibroblast-derived PDGF-BB promotes hedgehog survival signaling

Expression of PDGF-BB by MFBs and PDGFR-β by CCA cells. Initially, we assessed basal PDGF-BB secretion by two human CCA cell lines, KMCH-1 and KMBC, primary HSC cells, and the human MFB cell line LX-2 by ELISA (monoculture conditiones, Figure 5A). The MFB cells secreted significantly higher levels of PDGF-BB than the CCA cell lines. Because many cancer cells do not express PDGF receptors, [96] we next examined KMCH-1 cells for the presence of PDGFR-β and its activating phosphorylation by PDGF-BB (Figure 5B). Immunoblot analysis confirmed protein expression of PDGFR-β in KMCH-1 cells (Figure 5B, lower), while PDGFR-α was not detectable (data not shown). PDGFR-β also displayed receptor phosphorylation (Tyr^{857}) upon PDGF-BB treatment (Figure 5B, upper). In addition, we confirmed mRNA expression of PDGFR-β in KMCH-1 cells and 4 other human CCA cell lines (KMBC, HuCCT-1, TFK-1, and MzChA-1) as well as in the ErbB-2/neu transformed malignant rat cholangiocyte cell line BDEneu (employed in the *in vivo* CCA model; Figure 6)

DOI:10.14753/SE.2016.1969

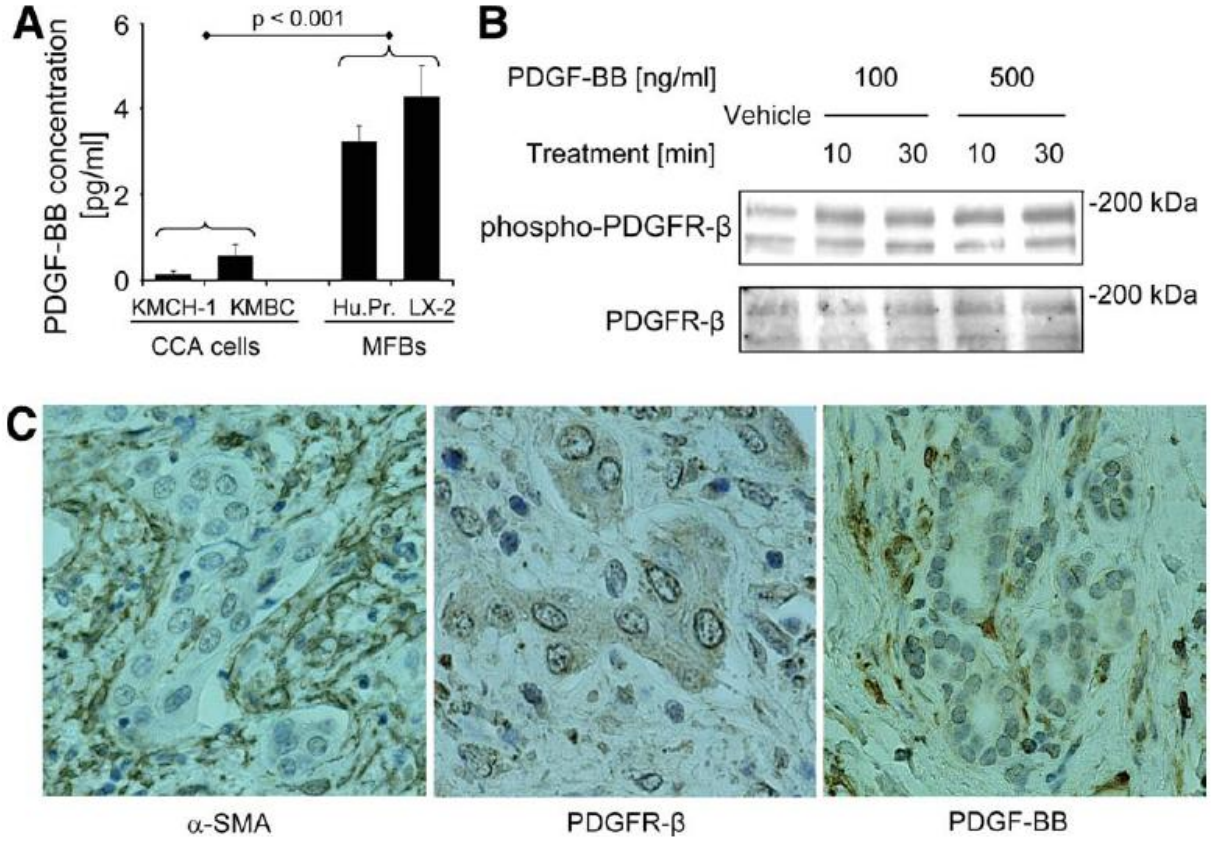

Figure 5. Cellular expression of PDGF-BB, PDGFR-β, and α-SMA in CCA. (A, B) PDGF-BB is secreted by MFBs and phosphorylates PDGFR-β in CCA cells *in vitro* (A) Basal PDGF-BB secretion (24 hours; corrected for total protein expression) by two human CCA cell lines, KMCH-1 and KMBC, a human myofibroblast (MFB) cell line, LX-2, and myofibroblastic human primary HSC cells (Hu.Pr.) was assessed in the serum-free supernatant by ELISA (monoculture conditiones). Mean ± s.e.m. (n=3). (B) KMCH-1 cells (serum-starved for 2 days) were treated with vehicle or PDGF-BB at the concentrations and time intervals indicated. Cell treatment was followed by immunoblot analysis for PDGFR-β and phospho-PDGFR-β (Tyr^{857}).Upper bands show the N-linked glycosylated and lower bands the unglycosylated forms of PDGFR-β. (C) α-SMA (MFB marker; left), PDGFR-β (middle), and PDGF-BB (right) protein expression (brown) was examined by immunohistochemistry (counterstaining with Mayers' Hematoxylin; photomicrographs were taken in 600x magnification) in human CCA specimens.

To characterize the expression of α-SMA, PDGFR-β, and PDGF-BB *in vivo*, we performed immunohistochemistry for these proteins in human CCA specimens (Figure 5C). Numerous α-SMA-positive MFBs were present in the stromal tumor microenvironment in all human CCA samples examined (Figure 5C, left). Moreover, PDGFR-β immunoreactivity was confirmed in CCA cell glands in approximately half of the samples (Figure 5C, middle), whereas PDGF-BB was expressed in MFBs in two-thirds of the samples (Figure 5C, right). Thus, PDGF-BB was shown to be secreted by MFBs and its receptor expressed by CCA cells.

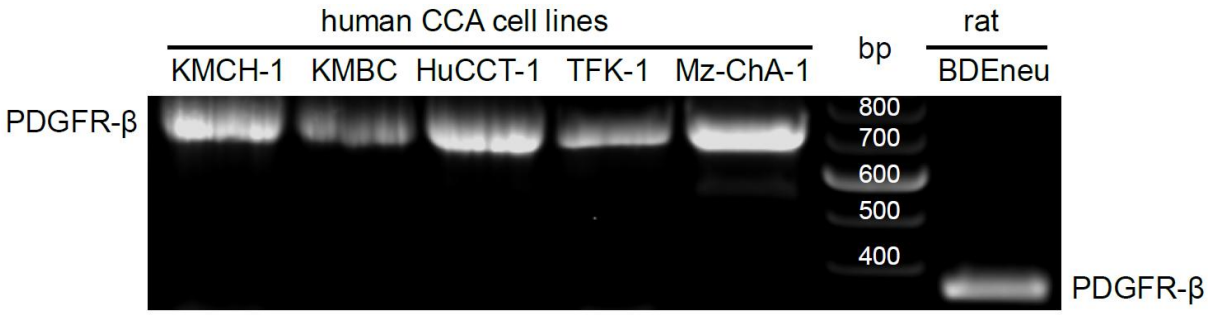

Figure 6. PDGFR-β expression in 6 CCA cell lines. mRNA expression levels of PDGFR-β was assessed by qualitative RT-PCR analysis in the 5 human CCA cell lines KMCH-1, KMBC, HuCCT-1, TFK-1, and MzChA-1 (left of the 100bp-DNA ladder) as well as in the ErbB-2/neu transformed malignant rat cholangiocyte cell line BDEneu (employed in the *in vivo* CCA model; right of the 100bp-DNA ladder).

MFB-derived PDGF-BB promotes resistance to TRAIL cytotoxicity. Next, we examined the effect of co-culturing KMCH-1 cells with PDGF-BB-secreting myofibroblastic human primary HSCs (Figure 7A and C) or LX-2 cells (Figure 7B and D) on TRAIL-induced CCA cell apoptosis. As assessed by either nuclear morphology (Figure 7A and B) or the TUNEL assay (Figure 7C and D), KMCH-1 cells were more resistant to TRAIL-induced apoptosis when co-cultured with human primary HSCs or LX-2 cells as compared to monoculture conditions. Interestingly, the KMCH-1 cells were resensitized to TRAIL (10 ng/mL) when co-cultured in the presence of neutralizing anti-human PDGF-BB antiserum (Figure 7A-D). Thus, PDGF-BB secreted by co-cultured MFB cells, reduces the susceptibility of CCA cells to TRAIL-induced apoptosis.

PDGF-BB cytoprotection is dependent on Hh signaling. Given that PDGF-BB modulates anti-apoptotic Hh signaling in immature cholangiocytes [58] and Hh signaling appears to be a potent survival signal for CCA cells, [67, 68] we explored the effect of Hh signaling inhibition on PDGF-BB-mediated cytoprotection against TRAIL cytotoxicity. Apoptosis was assessed morphologically following DAPI-staining (Figure 8A upper and B) and biochemically

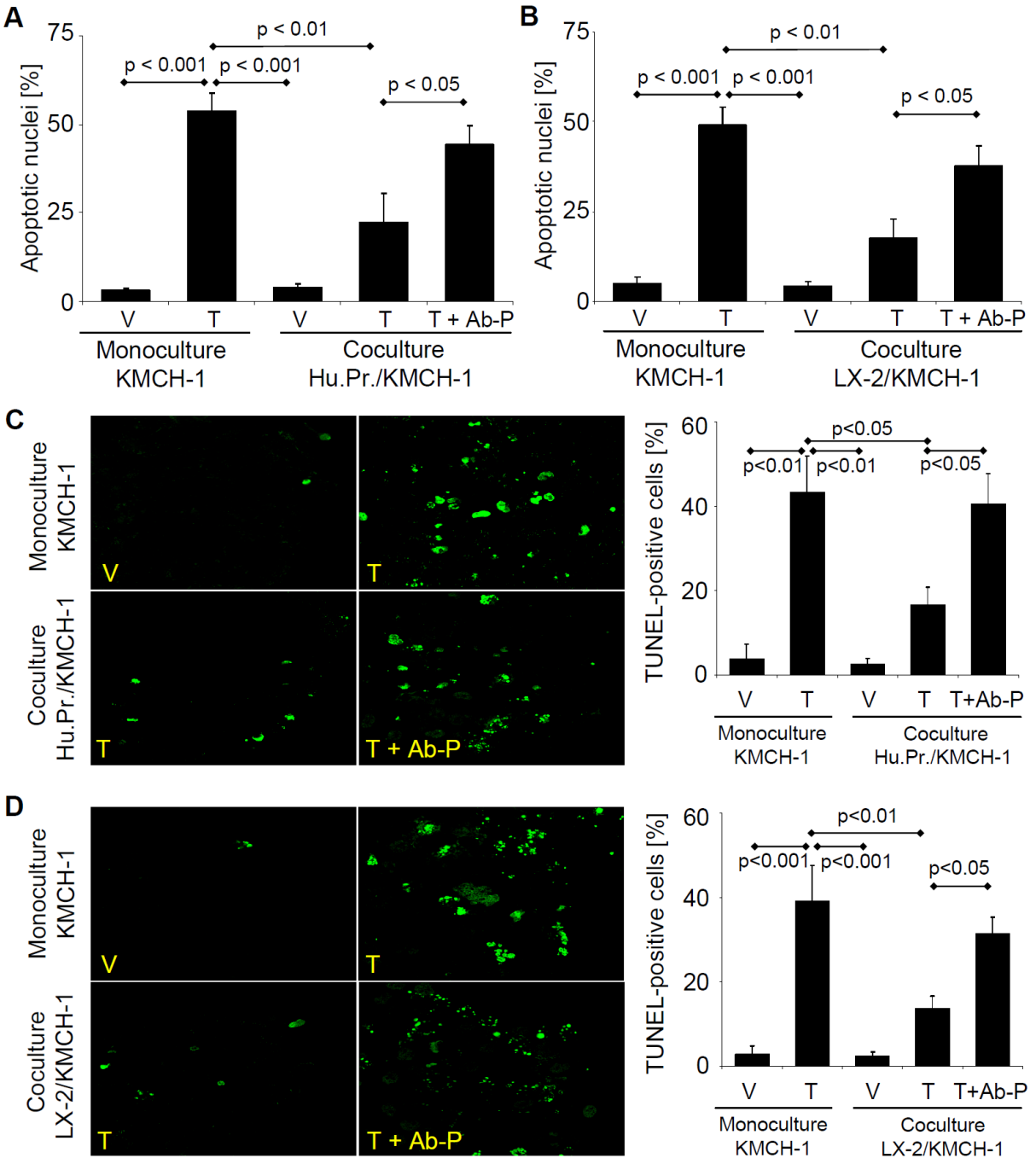

Figure 7. PDGF-BB promotes resistance to TRAIL cytotoxicity. KMCH-1 cells were plated alone (monoculture) or together with PDGF-BB-secreting human primary HSCs (Hu.Pr.; A and C) or LX-2 (B and D) cells in a transwell insert co-culture system (KMCH-1 cells in the bottom and human primary HSCs or LX-2 cells in the top wells; 1:1 ratio) for 6 days. Cells were treated as indicated with vehicle (V), rhTRAIL (T; 10ng/mL for 6 hrs on day 6) or rhTRAIL plus anti-human PDGF-BB antiserum (T + AB-P; rhTRAIL: 10ng/mL for 6 hrs on day 6; anti-human PDGF-BB antiserum: 10µg/mL for 24 hrs on day 5). After rhTRAIL treatment for 6 hrs, KMCH-1 cells were analyzed for apoptotic nuclear morphology by DAPI-staining (A and B) and for DNA fragmentation by TUNEL-staining (C and D) with quantitation of apoptotic nuclei by fluorescence microscopy. Mean ± s.e.m. (n=5). (C and D left) Representative fluorescent photomicrographs of TUNEL-positive KMCH-1 cells are depicted.

by a caspase-3/-7 activity assay (Figure 8A lower). Exogenous PDGF-BB protected KMCH-1 cells from TRAIL-induced apoptosis (Figure 8). In contrast, cyclopamine, an inhibitor of SMO

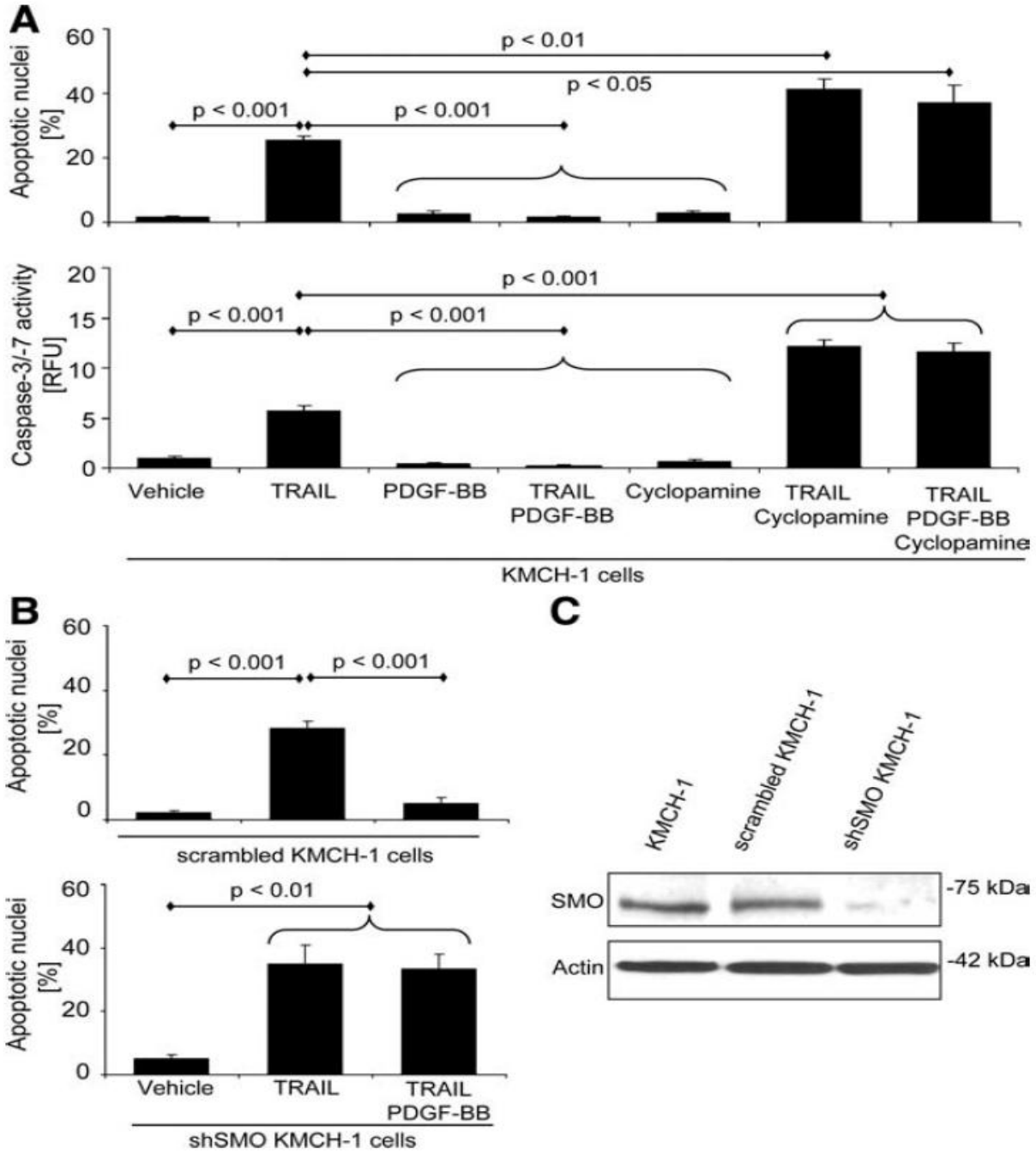

Figure 8. Cytoprotection by PDGF-BB is dependent on Hh signaling. (A) First, KMCH-1 cells (serum-starved for 2 days) were treated with vehicle or PDGF-BB (200 ng/mL) for 8 hrs. PDGF-BB was retained in the culture media, and the cells were then treated with rhTRAIL (5 ng/mL), cyclopamine (a Hh [SMO] inhibitor; 5 μM) or TRAIL plus cyclopamine (5 ng/mL; 5 μM) for additional 6 hrs. (B) Similar experiments (same PDGF-BB and TRAIL treatment) were performed with shSMO KMCH-1 instead of cyclopamine-treated KMCH-1 cells (lower) and stable scrambled KMCH-1 instead of normal KMCH-1 cells (controls, upper). (C) Stable knockdown of SMO only in shSMO KMCH-1 cells was confirmed by immunoblot analysis. Apoptosis was measured by DAPI-staining with quantitation of apoptotic nuclei by fluorescence microscopy (A upper and B; mean ± s.e.m.; n=3) or fluorescent analysis of caspase-3/-7 activity (A lower; mean ± s.e.m.; n=6; RFU, relative fluorescence unit).

(the transducer of Hh signaling) [97] sensitized KMCH-1 cells to TRAIL-induced apoptosis (Fig. Figure 8A). Moreover, cyclopamine completely abrogated PDGF-BB inhibition of

TRAIL-induced apoptosis (Figure 8A). Likewise, shSMO KMCH-1 cells also underwent TRAIL-mediated apoptosis despite exogenous PDGF-BB treatment (Figure 8B lower; compare with stable scrambled KMCH-1 cells Figure 8B upper). Taken together, these observations suggest that PDGF-BB-mediated protection from TRAIL-induced apoptosis is dependent upon an intact Hh signaling pathway.

PDGF-BB induces translocation of SMO to the plasma membrane. We next sought to explore how PDGF-BB stimulates Hh signaling in order to promote CCA cell survival. Initially, we analyzed the direct effect of PDGF-BB on mRNA expression of the Hh signaling ligands *SHH*, *IHH* and *DHH* as well as *PTCH1*, *SMO*, and *GLI1-3* by quantitative RT-PCR (Figure 9A). PDGF-BB did not significantly alter mRNA expression of the three Hh ligands nor that of *PTCH1*, *SMO*, or *GLI1-3* in KMCH-1 and HuCCT-1 cells.

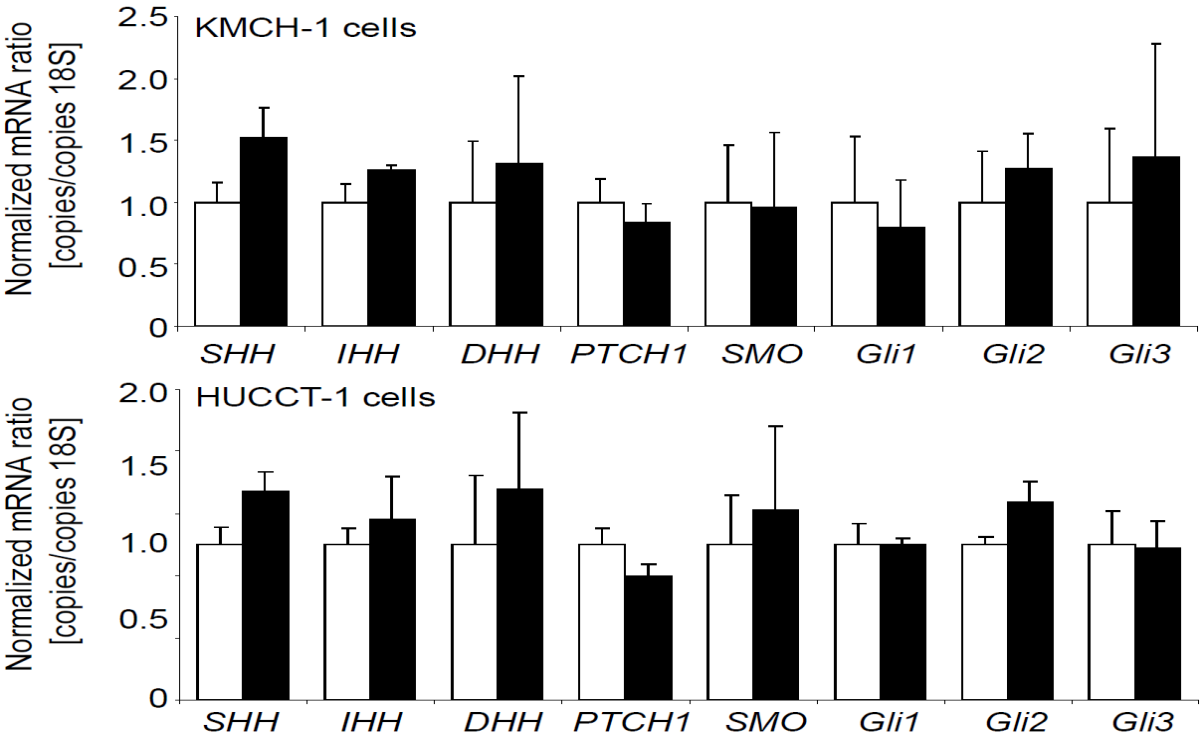

Figure 9. PDGF-BB has no effect on mRNA expression of members of the Hh signaling pathway. (A) The two human CCA cell lines (serum-starved for 2 days) KMCH-1 (upper) and HuCCT-1 (lower) were treated with vehicle or PDGF-BB (500 ng/mL) for 8 hrs followed by quantitative RT-PCR analysis for mRNA expression of the Hh signaling mediators sonic (*SHH*), indian (*IHH*), and desert hedgehog (*DHH*) as well as patched-1 (*PTCH1*), smoothened (*SMO*), and glioma-associated oncogenes (*GLI*) 1-3. 18S ribosomal RNA was used to normalize expression. Mean ± s.e.m. (n=3).

Because translocation of SMO from intracellular vesicles to the plasma membrane results in its activation during Hh signaling, [64] we next examined the cellular localization of SMO upon PDGF-BB treatment by immunocytochemistry (Figure 10A). PDGF-BB significantly induced translocation of SMO from intracellular compartments to the plasma membrane (Arrows; Figure 10A, middle). This process appears to be PKA-dependent as it was effectively attenuated by the PKA inhibitor H-89. Similar results were obtained when we employed KMCH-1 cells transiently transfected with a plasmid expressing GFP-tagged human SMO and analyzed GFP-SMO localized at the plasma membrane by TIRF microscopy [68] (Figure 10B). As a further indicator for Hh signaling activation, we examined the effect of PDGF-BB on GLI2 nuclear translocation in KMCH-1 cells by immunoblot analysis (Figure 10C). PDGF-BB treatment increased GLI2 abundance in nuclear protein extracts, an effect that again was attenuated by the PKA inhibitor H-89. Consistent with these results, KMCH-1 cells transiently transfected with a GLI reporter construct displayed GLI activation upon PDGF-BB treatment. The SMO inhibitor cyclopamine effectively blocked PDGF-BB-mediated GLI activation (Figure 10D upper). Likewise, stable scrambled KMCH cells also displayed PDGF-BB-induced GLI activation, whereas no PDGF-BB effect was observed in shSMO KMCH-1 cells (Figure 10D lower). Thus, PDGF-BB appears to promote Hh signaling-dependent cytoprotection by inducing PKA-mediated SMO trafficking to the plasma membrane.

To further characterize the PDGF-BB-stimulated, SMO-dependent gene regulation, we finally also identified 67 target genes to be commonly up-regulated (50 genes) or down-regulated (17 genes) by both SHH and PDGF-BB in a cyclopamine-inhibitable manner in KMCH-1 cells via an Affymetrix U133 Plus 2.0 GeneChip analysis (Table 6).

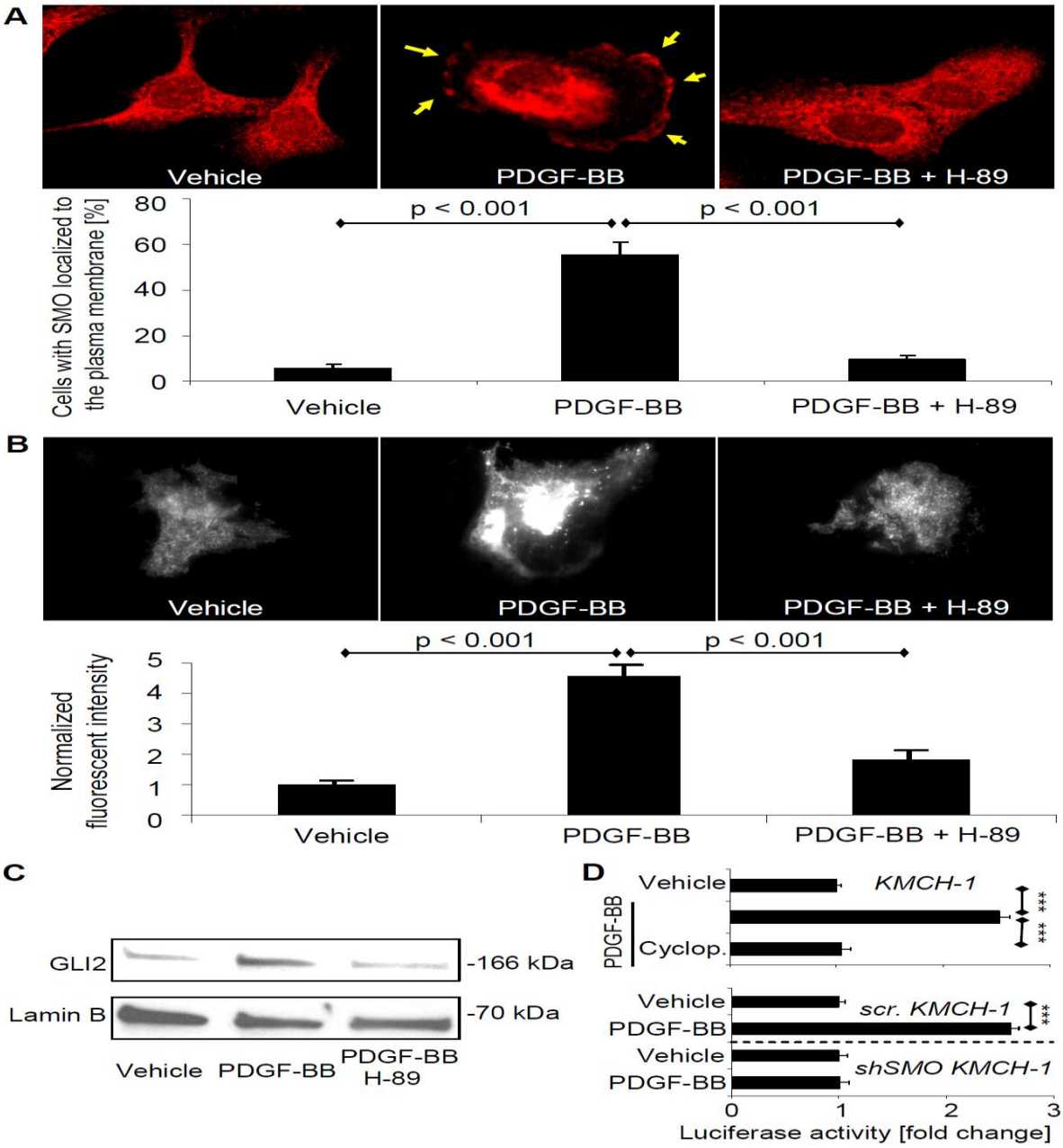

Figure 10. PDGF-BB induces SMO trafficking to the plasma membrane resulting in GLI2 nuclear translocation and transcriptional activation of a GLI reporter gene. (A) HuCCT-1 cells were treated with vehicle, PDGF-BB (200 ng/mL) or PDGF-BB plus the PKA inhibitor H-89 (5 μM) for 2 hrs. SMO cellular localization was analyzed by immunocytochemistry. Note that PDGF-BB induces translocation of SMO from intracellular compartments (left) to the plasma membrane (yellow arrows, middle), an effect that is inhibited by the PKA inhibitor H-89 (right). Cells with membranes positive for SMO immunocytochemistry were counted in each of these conditions. Mean ± s.e.m. (n=7). (B) KMCH-1 cells were transiently transfected with a plasmid expressing GFP-tagged human SMO (GFP-SMO; 48h) and then treated with vehicle or PDGF-BB (200 ng/mL) with and without H-89 (5 μM) for 2 hrs. GFP-SMO localized at the plasma membrane was analyzed by TIRF microscopy and the fluorescent intensity quantified using image analysis software. Mean ± s.e.m. (n=20). (C) GLI2 nuclear translocation in KMCH-1 cells was assessed by immunoblot analysis after treating the cells with vehicle or PDGF-BB (200 ng/mL) with and without H-89 (5 μM) for 8 hrs. Lamin B was used as loading control for the nuclear protein extracts. (D) KMCH-1 cells (normal, stable scrambled [scr.], or shSMO) were transiently transfected (24 hrs) with a reporter construct containing eight consecutive consensus GLI-binding sites (8x-GLI) and co-transfected with pRL-CMV. Cells were then treated as indicated with vehicle or PDGF-BB (200 ng/mL) with and without cyclopamine (5 μM) for 24 hrs. Both firefly and Renilla luciferase activities were quantified and data (firefly/Renilla luciferase activity) are expressed as fold increase over vehicle-treated cells transfected with the 8x-GLI/pRL-CMV reporter constructs. Mean ± s.e.m. (n=3; ***p<0.001).

DOI:10.14753/SE.2016.1969

Gene Symbol	Gene Name	GenBank Accession No.
	Up-regulated†	
C7orf40	Chromosome 7 open reading frame 40	AI937446
CARD10	Caspase recruitment domain family, member 10	AY028896
CCL2	Chemokine (C-C motif) ligand 2	S69738
CYR61	Cysteine-rich, angiogenic inducer, 61	AF003114
DKK1	Dickkopf homolog 1 (*Xenopus laevis*)	NM_012242
ENC1	Ectodermal-neural cortex (with BTB-like domain)	NM_003633
EPHA2	EPH receptor A2	NM_004431
F3	Coagulation factor III (thromboplastin, tissue factor)	NM_001993
GPATCH4	G patch domain containing 4	BE794289
HAS3	Hyaluronan synthase 3	AF232772
HBEGF	Heparin-binding EGF-like growth factor	NM_001945
HEATR1	HEAT repeat containing 1	NM_018072
ISG20L2	Interferon-stimulated exonuclease gene 20 kDa-like 2	AW294587
JAG1	Jagged 1 (Alagille syndrome)	U77914
LAMB3	Laminin, beta 3	L25541
LUC7L	LUC7-like (*Saccharomyces cerevisiae*)	BE049621
LYAR	Ly1 antibody reactive homolog (mouse)	AW958593
LYAR	Ly1 antibody reactive homolog (mouse)	AL136750
MAT2A	Methionine adenosyltransferase II, alpha	BC001686
METAP2	Methionyl aminopeptidase 2	AW003997
MKI67IP	MKI67 (FHA domain) interacting nucleolar phosphoprotein	AL577809
MORC4	MORC family CW-type zinc finger 4	NM_024657
MRPS2	Mitochondrial ribosomal protein S2	NM_016034
NOB1	NIN1/RPN12 binding protein 1 homolog (*S. cerevisiae*)	BC000050
NOC3L	Nucleolar complex associated 3 homolog (*S. cerevisiae*)	NM_022451
NSUN2	NOL1/NOP2/Sun domain family, member 2	BC001041
NUP35	Nucleoporin 35 kDa	AL529634
PFKFB3	6-phosphofructo-2-kinase/fructose-2,6-biphosphatase 3	NM_004566
PLK2	Polo-like kinase 2 (*Drosophila*)	NM_006622
PNN	Pinin, desmosome-associated protein	BF508848
PNPT1	Polyribonucleotide nucleotidyltransferase 1	AI967971
POLR1E	Polymerase (RNA) I polypeptide E, 53 kDa	NM_022490
POP1	Processing of precursor 1, ribonuclease P/MRP subunit (*S. cerevisiae*)	D31765
PRKCH	Protein kinase C, eta	NM_024064
PUS3	Pseudouridylate synthase 3	NM_031307
PWP2	PWP2 periodic tryptophan protein homolog (yeast)	U56085
RBM34	RNA-binding motif protein 34	AA887480
RND3	Rho family GTPase 3	BG054844
RRAD	Ras-related associated with diabetes	NM_004165
SERPINE1	Serpin peptidase inhibitor, clade E (nexin, plasminogen activator inhibitor type 1), member 1	AL574210
SLC25A32	Solute carrier family 25, member 32	NM_030780
SLC41A1	Solute carrier family 41, member 1	AW439816
SNHG7	Small nucleolar RNA host gene 7 (nonprotein coding)	AL533103
SYTL2	Synaptotagmin-like 2	AB046817
TGFB2	Transforming growth factor, beta 2	M19154
UTP14A	UTP14, U3 small nucleolar ribonucleoprotein, homolog A (yeast)	BC001149
VEGFC	Vascular endothelial growth factor C	U58111
WDR73	WD repeat domain 73	AF161382
ZNF239	Zinc finger protein 239	NM_005674
ZYX	Zyxin	BC002323
	Down-regulated†	
BNIP3L	BCL2/adenovirus E1B 19 kDa interacting protein 3-like	AL132665
CCNG1	Cyclin G1	BC000196
CCNG2	Cyclin G2	AW134535
ELMOD2	ELMO/CED-12 domain containing 2	BG477315
IFIT2	Interferon-induced protein with tetratricopeptide repeats 2	AA131041
INSIG1	Insulin-induced gene 1	BG292233
LMO4	LIM domain only 4	BC003600
LQK1	Hypothetical LOC642946	N51468
MEGF9	Multiple EGF-like domains 9	W68084
NBR1	Neighbor of BRCA1 gene 1	NM_005899
NHSL1	NHS-like 1	AA503387
PCMTD1	Protein-L-isoaspartate (D-aspartate) O-methyltransferase domain containing 1	AA453163
SCD	Stearoyl-CoA desaturase (delta-9-desaturase)	AB032261
SCD	Stearoyl-CoA desaturase (delta-9-desaturase)	AF132203
TCEAL8	Transcription elongation factor A (SII)-like 8	AI743979
TMEM135	Transmembrane protein 135	AK000684
TP53INP1	Tumor protein p53-inducible nuclear protein 1	AW341649

Table 6. Gene targets regulated by both SHH and PDGF-BB in a cyclopamine-inhibitable manner in KMCH-1 CCA cells (alphabetical order). Affymetrix U133 Plus 2.0 GeneChip analysis was performed. Genes were considered to be up-regulated when they (1) displayed significant up-regulation ($P < 0.05$, compared with the control group) upon SHH (single treatment), as well as PDGF-BB (single treatment) stimulation, and (2) displayed significant downregulation ($P < 0.05$, compared with the SHH and PDGF-BB groups, respectively) upon the addition of Hh inhibitor cyclopamine to the SHH as well as to the PDGF-BB treatment. Down-regulated genes were regulated vice versa to (1) and (2).

Figure 11. BDEneu cells express Hh signaling pathway effectors. mRNA expression levels of the Hh signaling pathway members sonic (*SHH*), indian (*IHH*), and desert hedgehog (*DHH*) as well as patched-1 (*PTCH1*), smoothened (*SMO*) and the transcription factors glioma-associated oncogene (GLI) 1, 2, and 3 were assessed by qualitative RT-PCR analysis in the ErbB-2/neu transformed malignant rat cholangiocyte cell line BDEneu (employed in the *in vivo* CCA model). 18S ribosomal RNA expression is shown in the last column (bold).

Hh signaling inhibition is tumor suppressive in vivo. To determine if the pro-apoptotic *in vitro*-effect of Hh signaling inhibition by cyclopamine observed in co-cultures is translatable to an *in vivo* model, we employed a syngeneic rat orthotopic CCA model (BDEneu malignant cells injected into the liver of male Fischer 344 rats). Like human CCA, the BDEneu cells also express TRAIL *in vivo*.[84-86] We confirmed that BDEneu cells express mRNA of members of the Hh signaling pathway, i.e. *SHH*, *IHH*, *DHH*, *PTCH1*, *SMO*, and *GLI 1-3* (Figure 11). This rodent model of CCA also duplicates the desmoplasia characteristic of the human disease with numerous α-SMA-positive MFBs present in the stromal tumor microenvironment (Figure 12A). We confirmed that the tumor samples (including MFBs and CCA cells) in this *in vivo* model also richly expresses mRNA for PDGF-BB and its cognate receptor PDGFR-β as compared non-tumor liver tissue (Figure 12B). Moreover, PDGFR-β immunoreactivity was identified in CCA cells (Figure 12C), whereas PDGF-BB expression was apparent in the MFBs and at the margin of CCA glands (Figure 12D). Thus, this preclinical, rodent model of CCA mimics the characteristic features observed in human CCA tissue and cell lines.

Next, we examined the potential therapeutic effects of the hedgehog signaling inhibitor cyclopamine in this *in vivo* model of CCA. In cyclopamine-treated animals, CCA cell apoptosis was increased as compared to controls. Apoptosis of CCA cells was confirmed by demonstrating colocalization of TUNEL-positive cells with cells displaying CK7 (a biliary epithelial cell marker expressed by CCA cells; Figure 12E). Consistent with the pro-apoptotic effects of cyclopamine in this model, cyclopamine also had an effect on tumor size. Indeed, tumor weight, and tumor/liver as well as tumor/body weight ratios were significantly decreased in cyclopamine-treated rats (Figure 13A and B). In addition, animals treated with

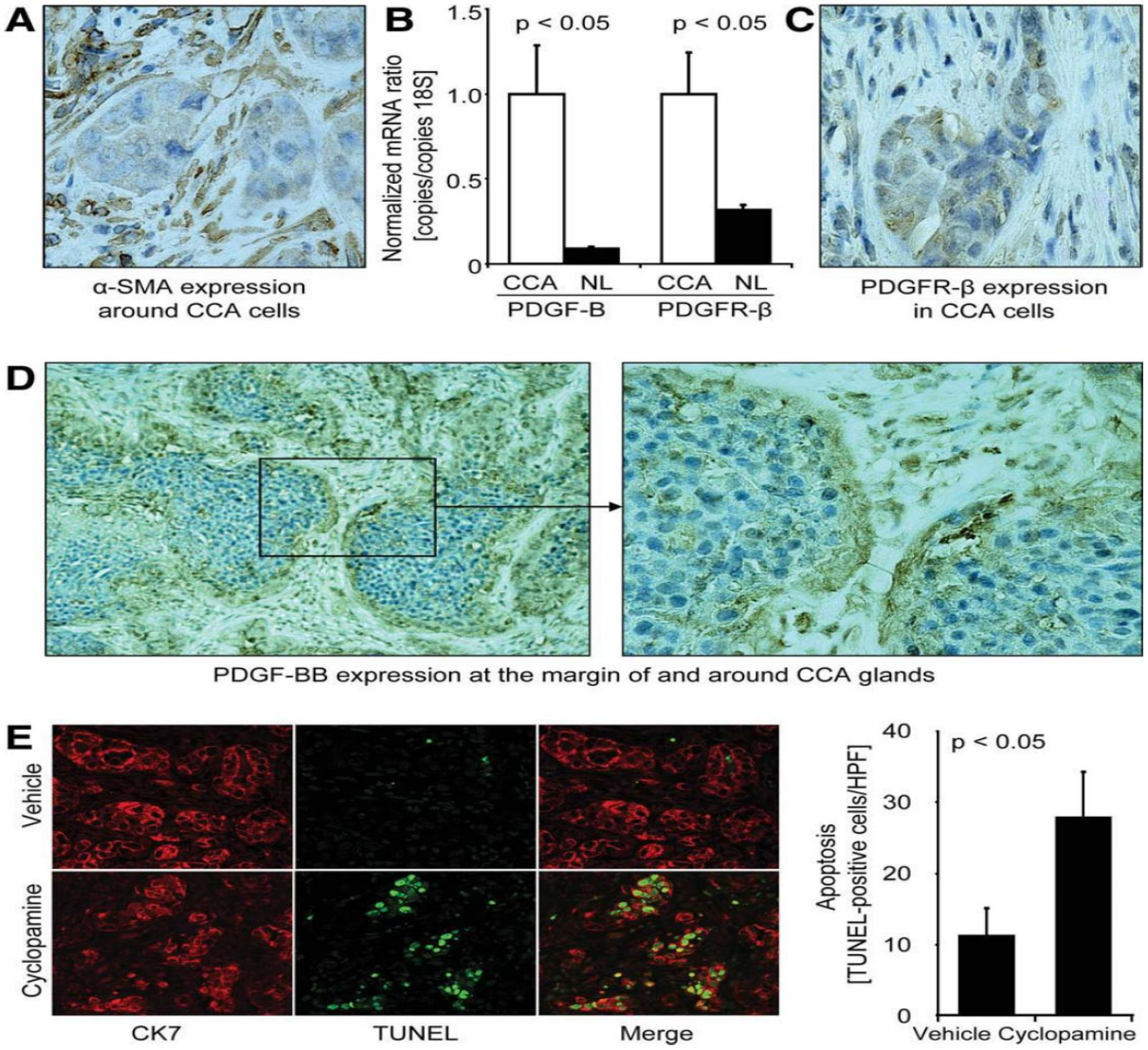

Figure 12. Hh signaling inhibition promotes apoptosis in PDGFR-β-expressing CCA cells *in vivo*. A syngeneic rat orthotopic model of CCA (BDEneu cells; Fischer 344 rats) was employed for this examination. (A-D) The rodent CCA model recapitulates cellular expression patterns of α-SMA, PDGF-BB, and PDGFR-β observed in human CCA. (A) α-SMA protein expression (brown) in tumors of untreated tumor-bearing rats was examined by immunohistochemistry (counterstaining with Mayers' Hematoxylin; photomicrograph was taken in 600x magnification). (B) CCA and normal liver specimens of untreated tumor-bearing rats (14 days after tumor cell implantation into the left lateral liver lobe) were analyzed for mRNA expression of PDGF-B and PDGFR-β by quantitative RT-PCR. Mean ± s.e.m. (n=3). (C) PDGFR-β protein expression (brown) in tumors of untreated tumor-bearing rats was examined by immunohistochemistry (counterstaining with Mayers' Hematoxylin; photomicrograph was taken in 600x magnification). PDGFR-β-positive CCA cell nests are surrounded by a paucicellular stromal matrix (counterstaining with Mayers' Hematoxylin; photomicrograph was taken in 200x magnification and the inset is further magnified electronically). (D) PDGF-BB immunoreactivity (brown) was similarly analyzed and the most intense signal was observed in stromal cells and the tumor-stromal interface. (E) Apoptosis of CCA cells was assessed in tumor tissues by TUNEL staining (green) and the identity of cells determined by co-staining via immunohistochemistry for CK7 (a CCA marker; red) Animals were treated with vehicle (upper) or cyclopamine (lower; 2.5 mg/kg BW intraperitoneally daily for one week; 1st injection: 7th post-operative day, 7th injection: 13th post-operative day). Quantitation of TUNEL- and CK7-positive cells (expressed as number per HPF) 14 days after CCA cell implantation demonstrated that in cyclopamine-treated animals CCA cell apoptosis was increased as compared to controls (bar graph). Mean ± s.e.m. (n=10). HPF, high power field.

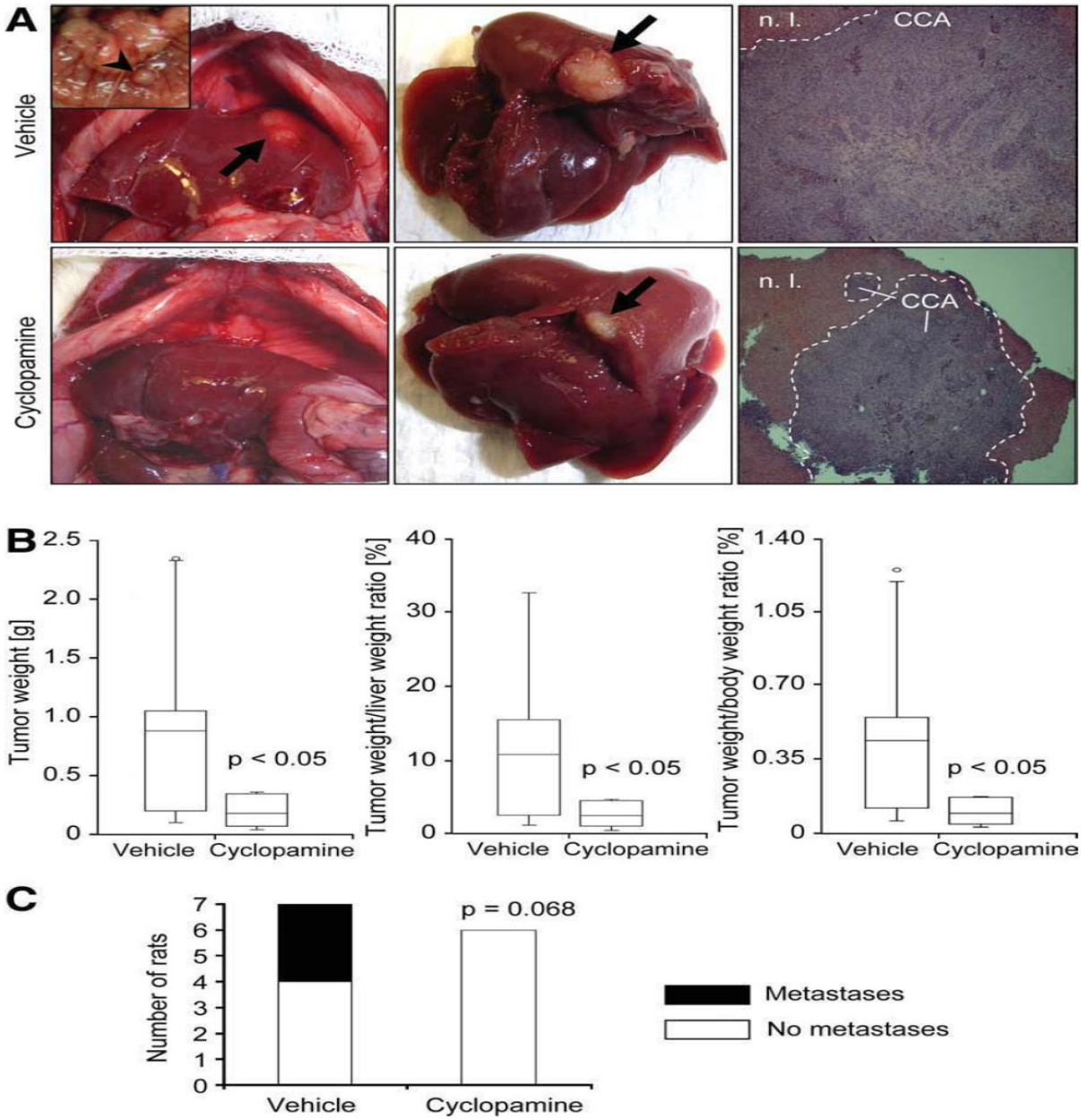

Figure 13. Hh signaling inhibition reduces tumor growth and metastasis *in vivo*. A syngeneic rat orthotopic model of CCA (BDEneu cells; Fischer 344 rats) was employed for this examination. In cyclopamine- (2.5 mg/kg BW intraperitoneally daily for one week; 1st injection: 7th post-operative day, 7th injection: 13th post-operative day) or vehicle-treated tumor-bearing rats (n=7 rats/group) tumor/liver/body weight and extrahepatic metastasis were assessed 14 days after tumor cell implantation into the left lateral liver lobe. (A) Depicted are representative abdominal cavities (left), explanted livers (middle), and hematoxylin/eosin sections (right) of vehicle- (upper) and cyclopamine-treated (lower) rats (HE staining; photomicrographs was taken in 40x magnification). Arrows indicate the liver tumors, while the arrowhead (insert in the upper left photomicrograph) displays a representative example of extrahepatic metastasis (peritoneum). N.l., normal liver; CCA, cholangiocarcinoma. (B) Changes in tumor weight as well as tumor/liver and tumor/body weight ratios are depicted as box-and-whisker plots showing lowest value, 25th percentile, median, 75th percentile, highest value, and in some cases outliers. (C) The stacked column plot indicates the numbers of animals with and without metastases for vehicle- and cyclopamine-treated groups ($p = 0.068$ by χ^2 test).

cyclopamine displayed no extrahepatic metastases whereas 43% of vehicle-treated animals had extrahepatic metastases, predominantly occurring in the greater omentum and peritoneum (Figure 13C, inset Figure 13A left upper). Moreoover, direct targeting of PDGF-BB signaling with imatinib mesylate was comparably effective in reducing tumor growth (Figure 14A-C) and metastasis (Figure 14D).

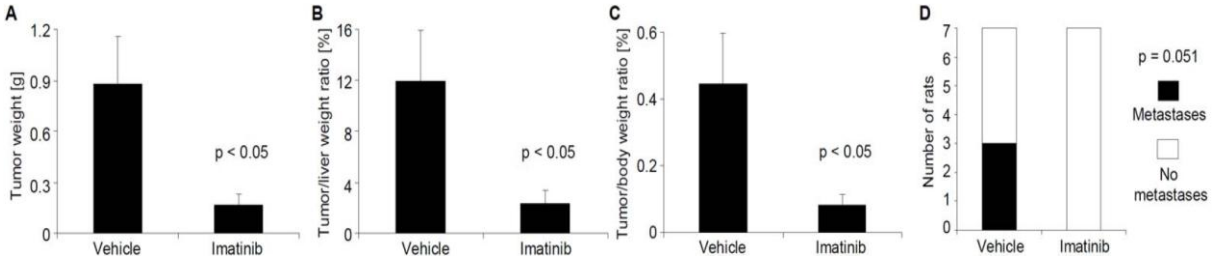

Figure 14. Imatinib administration reduces tumor growth and metastasis *in vivo*. A syngeneic rat orthotopic model of CCA (BDEneu cells; Fischer 344 rats) was employed. In imatinib (30 mg/kg BW intraperitoneally daily for one week;1st injection: 7th post-operative day, 7th injection: 13th post-operative day)- or vehicle-treated tumor-bearing rats tumor/liver/body weight and extrahepatic metastasis were assessed 14 days after tumor cell implantation into the left lateral liver lobe. (A-C) Changes in tumor weight (A), tumor/liver (B) and tumor/body (C) weight ratios are depicted as bar graphs. Mean ± s.e.m., n=7. (D) The stacked column plot indicates the numbers of animals with and without metastases for vehicle- and imatinib-treated groups ($p = 0.051$ by χ^2 test).

In aggregate, these data suggest that targeting the PDGFR-β/Hh signaling axis (e.g., with cyclopamine or imatinib mesylate) promotes CCA cell apoptosis and decreases tumor growth in an *in vivo* rodent model of CCA. Thus, these mechanistic treatment approaches might be a suitable adjuvant therapy to optimize the Mayo LTx protocol for CCA patients.

5.2.2 Polo-like kinase 2 is a mediator of hedgehog survival signaling

PLK1, PLK2 and PLK3 are prominently expressed in human CCA. Initially, we examined the expression of PLK1, PLK2 and PLK3 (due to their structural and functional divergences from other PLK family members, PLK4 and PLK5 were excluded from this study[73, 74]) in 50 CCA samples (25 intrahepatic and 25 extrahepatic CCA) by immunohistochemistry (Fig. 1). PLK1, PLK2 and PLK3 immunoreactive cells were present in the preponderance of the intrahepatic and extrahepatic CCA specimens (Figure 15A). Histological grading revealed that in extrahepatic and intrahepatic CCA samples, PLK2 was slightly less expressed than PLK1, whereas more cells stained positive for PLK2 than for PLK3 (Fig. 1B, Suppl. Fig. 1). PLK1, PLK2 and

DOI:10.14753/SE.2016.1969

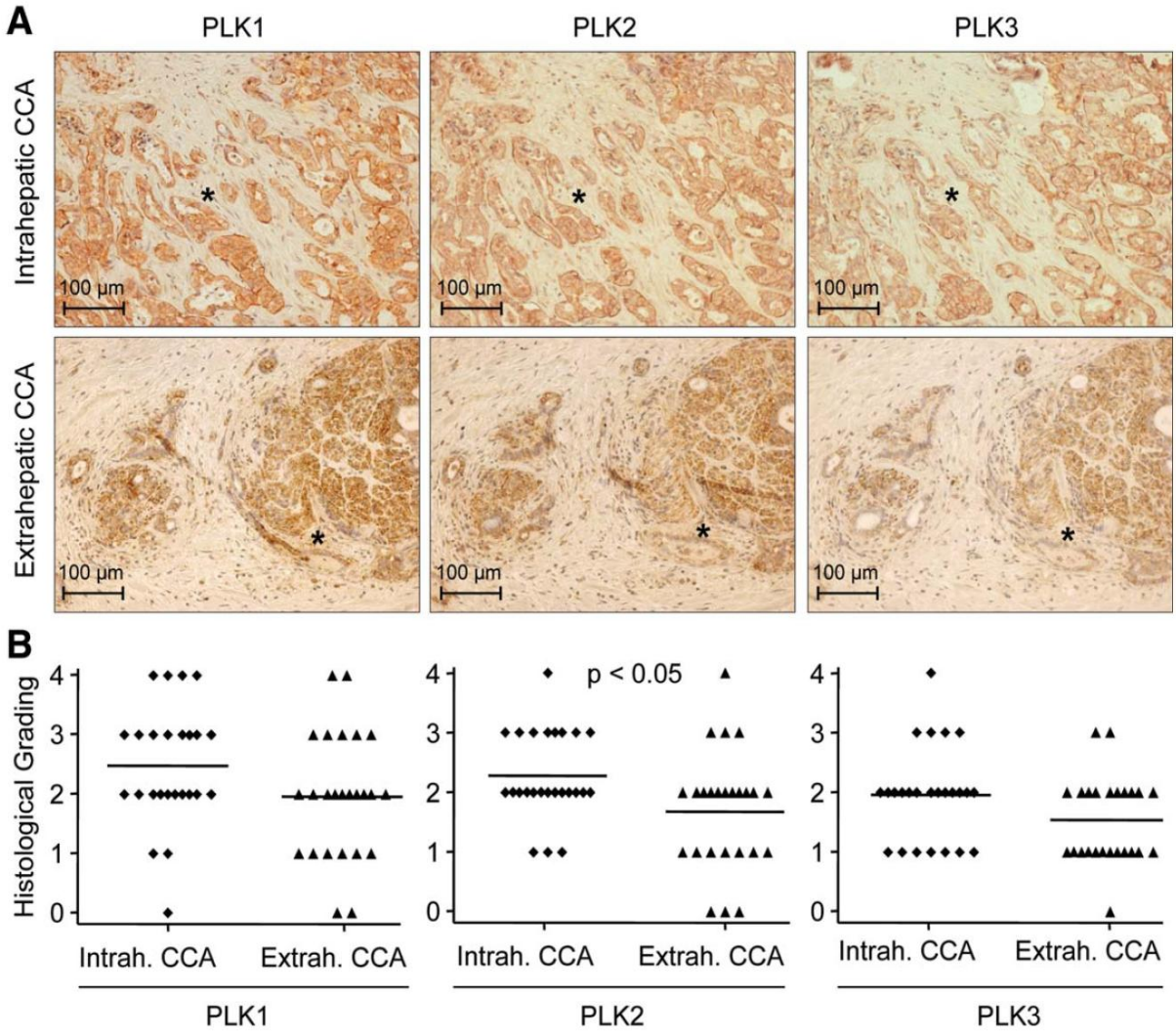

Figure 15. PLK proteins are abundantly expressed in human CCA. (A) PLK1 (left), PLK2 (middle) and PLK3 (right) expression in 25 intrahepatic (upper) and 25 extrahepatic (lower) human CCA samples was examined by immunohistochemistry. Photomicrographs were taken in 200x magnification. The asterisks indicate similar positions within the tumors as PLK immunohistochemistry was performed on neighboring slides. Note that predominantly tumorous glands but also some stromal cells exhibit PLK immunoreactivity (brown). Counterstaining was performed with hematoxylin (blue). (B) PLK1/2/3 protein expression quantitation of intrahapatic and extrahepatic CCA samples by histological grading (grade 0 = no protein expression, grade 4 = high protein expression).

PLK3 expression was more pronounced in intrahepatic as compared to extrahepatic CCA and for PLK2 expression this difference was statistically significant (Figure 15B). In intrahepatic and extrahepatic CCA, predominantly cancer cells/glands stained positive for PLK proteins; however, some stromal cells within the tumor microenvironment also displayed PLK1, PLK2 and PLK3 immunoreactivity. Thus, PLK1, PLK2 and PLK3 are abundantly expressed in the majority of human CCA specimens.

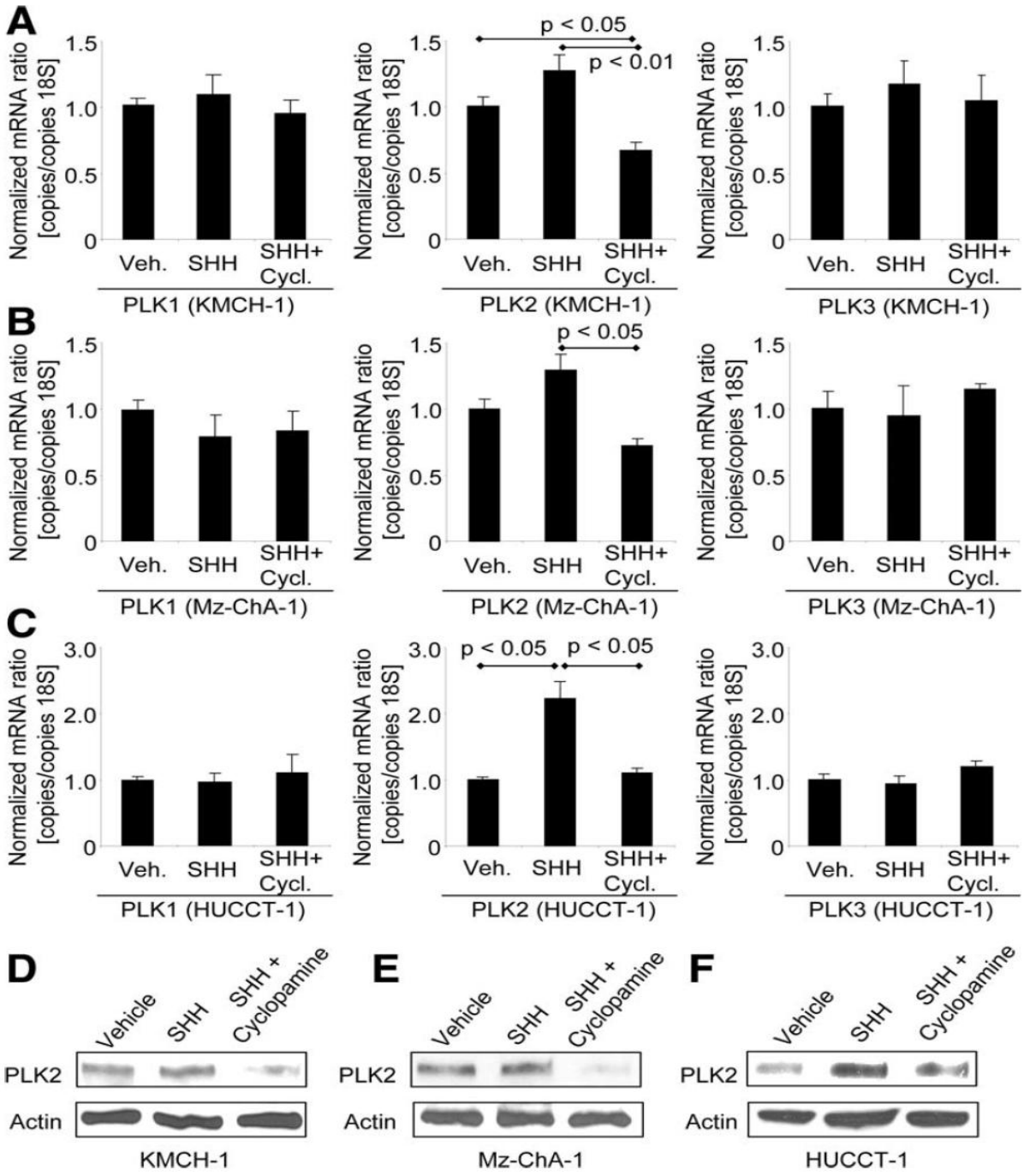

Figure 16. Hh signaling inhibition reduces PLK2 expression in CCA cells. Cells were treated as indicated in serum-free medium with vehicle or rhSHH (500 ng/ml, 4 hrs) in the presence or absence of Hh signaling inhibitor cyclopamine (10 μM, 4 hrs). (A-C) Quantitative RT-PCR analysis for PLK1/2/3 mRNA expression was performed in the human CCA cell lines KMCH-1 (A), Mz-ChA-1 (B) and HUCCT-1 (C). Mean ± s.e.m., n=3. (D-E) Treatment of KMCH-1 (D), Mz-ChA-1 (E) and HUCCT-1 (F) cells was followed by immunoblot analysis for PLK2 protein expression (actin = loading control).

PLK2 is regulated by hedgehog signaling in human CCA cells. Having confirmed an abundant expression of PLK 1, 2, and 3 proteins in human CCA, we next examined whether PLK signaling can be regulated by the Hh survival pathway as implicated by our prior genome-wide mRNA expression analysis in KMCH-1 CCA cells (Table 6). Consistent with this study,

inhibition of Hh signaling with cyclopamine (an inhibitor of the Hh mediator smoothened) reduced PLK2 but not PLK1 or PLK3 mRNA expression as compared to SHH only-treated CCA cells (Figure 16A [KMCH-1 cells], Figure 16B [Mz-ChA-1 cells] and Figure 16C [HUCCT-1 cells]). This observation was confirmed on the protein level by immunoblot analysis for PLK2 protein expression in similarly treated CCA cells (Figure 16D [KMCH-1 cells], Figure 16E [Mz-ChA-1 cells] Figure 16F [HUCCT-1 cells]). Consistent with these findings, more specific Hh signaling inhibition with SHH neutralizing antibody 5E1 or the small molecule smoothened inhibitor GDC-0449 also reduced PLK2 protein expression as compared to SHH only-treated KMCH-1, MzChA-1 and HUCCT-1 cells (Figure 17). Thus, PLK2, but not PLK1 or PLK3, appears to be positively regulated by Hh signaling.

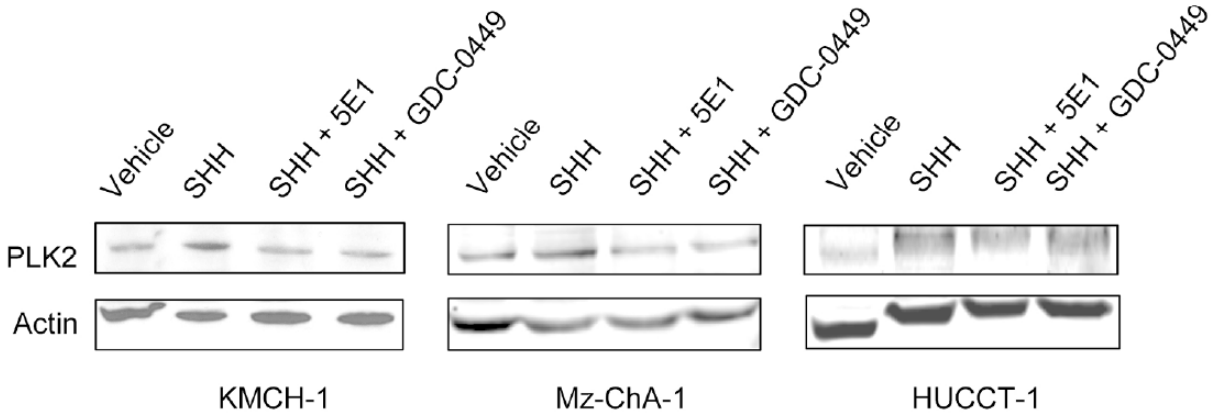

Figure 17. Protein expression of PLK2 is reduced upon various Hh inhibition approaches. Cells were treated as indicated in serum-free medium with vehicle or rhSHH (500 ng/ml, 4 hrs) plusminus SHH neutralizing antibody 5E1 (10 µg/ml, 4 hrs) or smoothened inhibitor GDC-0449 (20 µM, 4 hrs). Treatment of KMCH-1 (left), Mz-ChA-1 (middle) and HUCCT-1 (right) cells was followed by immunoblot analysis for PLK2 protein expression (actin = loading control).

To further investigate how Hh signaling promotes PLK2 expression, we examined whether the hedgehog transcription factors GLI1, GLI2, and/or GLI3 bind to the PLK2 promoter. After identification of two putative GLI binding sites (site I and II) within the PLK2 promoter region containing two mismatches compared to the consensus sequence GACCACCCA [98]

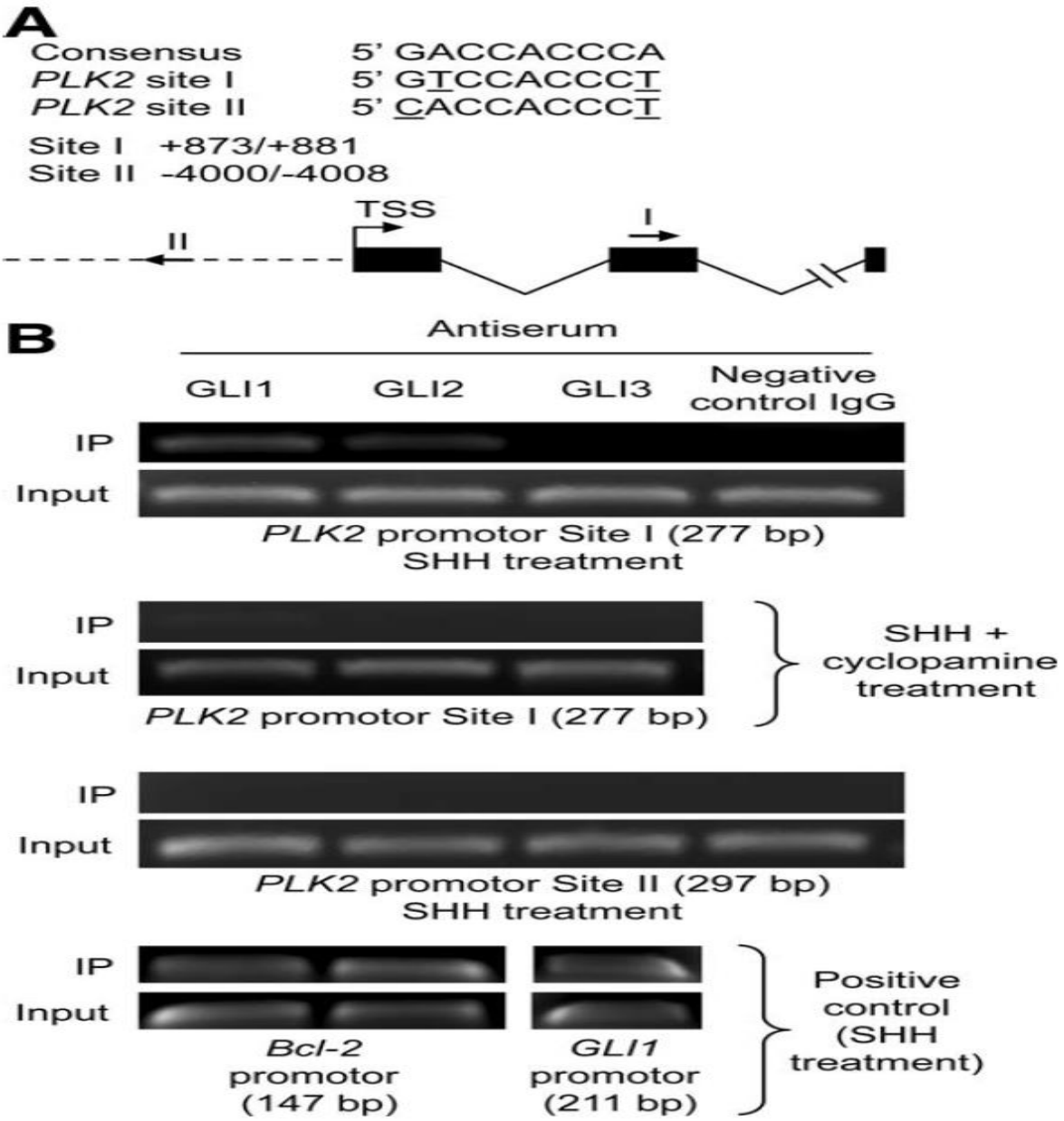

Figure 18: GLI1 and GLI2 bind to a predicted GLI-binding site in the PLK2 promoter region. (A) Two putative GLI binding sites that contain two mismatches compared to the consensus sequence were identified in the PLK2 promoter region. Nucleotide positions were counted from the transcription start site (TSS). Positions and directions of both potential binding sites are illustrated by arrows (I and II). (B) KMCH-1 cells treated with rhSHH (500 ng/ml, 5 hrs) plusminus cyclopamine (10μM, 5 hrs) were employed for this study. Chromatin immunoprecipitation (ChIP) using antiserum to GLI1, GLI2, GLI3, or a sheep negative control IgG was performed, followed by PCR using primers flanking site I (277 bp) or site II (297) within the PLK2 promoter region. As positive controls, ChIP was performed using primers flanking the Bcl-2 promoter GLI-binding sites (GLI1 and GLI2; 147 bp), or primers flanking the GLI3 binding site within the GLI1 promoter (211 bp).

(Figure 18A), we performed a chromatin immunoprecipitation assay in SHH-stimulated KMCH-1 cells (with or without cyclopamine) employing antibodies to GLI1, GLI2, and GLI3. Indeed, binding of GLI1 and GLI2 was exclusively observed in SHH only-treated cells

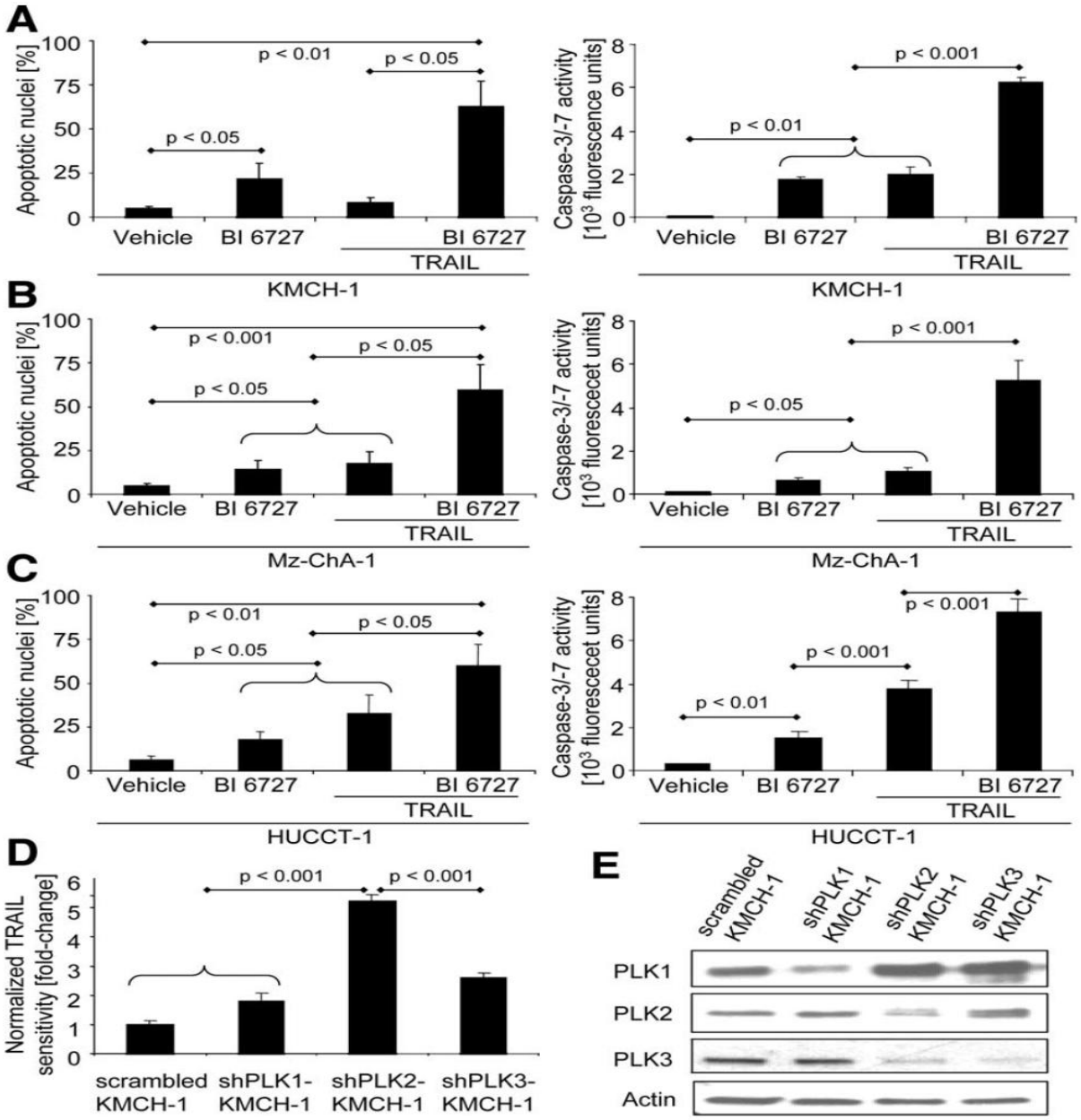

Figure 19: PLK2 inhibition is pro-apoptotic in CCA cells. (A-C) KMCH-1 (A), Mz-ChA-1 (B) and HUCCT-1 (C) cells were treated as indicated with vehicle, PLK inhibitor BI 6727 (200 nM, 24 hrs), rhTRAIL (2.5 ng/mL, 8 hrs), or BI 6727 (200 nM, 24 hrs) plus rhTRAIL (2.5 ng/mL, 8 hrs). Apoptosis was measured by DAPI staining with quantitation of apoptotic nuclei by fluorescence microscopy (left; mean ± s.e.m.; n=3) or fluorescent analysis of caspase-3/-7 activity (right; mean ± s.e.m.; n=5). (D) Stable scrambled, shPLK1-, shPLK2- and shPLK3-KMCH-1 cells were treated with vehicle or rhTRAIL (2.5 ng/mL, 8 hrs) and apoptosis was measured by DAPI staining with quantitation of apoptotic nuclei by fluorescence microscopy. Sensitivity to TRAIL (apoptosis ratio TRAIL- vs. vehicle-treated cells) was normalized to stable scrambled KMCH cells (A; mean ± s.e.m.; n=3). (E) PLK1/2/3 expression/knockdown in stable scrambled, shPLK1-, shPLK2- and shPLK3-KMCH-1 cells was assessed by immunoblot analysis (actin = loading control). Note that stable PLK3 knockdown also affects PLK2 expression.

using primers that amplify site I (277 bp; Figure 18B first and second panel) but not site II (297 bp; Figure 18B third panel). A control IgG did not yield a product additionally demonstrating specificity of the antisera used. As a positive control, we employed the Bcl-2 promoter which contains well recognized GLI1/2 binding sites [99] and the GLI1 promotor which contains well recognized GLI3 binding sites [100]. These studies identified the expected occupation by GLI1 and GLI2 (Bcl-2 promoter, 147 bp) as well as GLI3 (GLI1 promoter 211 bp; Figure 18B forth panel). Taken together, these data suggest that hedgehog signaling may directly regulate PLK2 expression by binding of the GLI1 and GLI2 transcription factors to the PLK2 promoter.

PLK2 inhibition is pro-apoptotic in CCA cells. Next, we examined whether inhibition of Hh target gene PLK2 with the potent PLK inhibitor BI 6727 (volasertib) promotes (TRAIL-induced) apoptosis in CCA cells. As measured by either cell morphology (Figure 19A-C left) or biochemically (Figure 19A-C right), BI 6727 and especially BI 6727 plus TRAIL significantly induced apoptosis in KMCH-1 (Figure 19A), Mz-ChA-1 (Figure 19B) as well as HUCCT-1 (Figure 19C) cells. As BI 6727 not only inhibits PLK2 but also PLK1 and PLK3,[81] we selectively silenced PLK1, PLK2, or PLK3 in KMCH-1 cells by an shRNA technique to more specifically investigate the effect of PLK inhibition on CCA cell apoptosis (Figure 19D; knockdown of PLKs was confirmed by immunoblot analysis [Figure 19E]). Stable knockdown of PLK2 sensitized KMCH-1 to TRAIL-induced apoptosis as compared to control KMCH-1 cells (Figure 19D). Knocking down PLK1 and PLK3 also was also pro-apoptotic; however, this effect was significantly less pronounced (Figure 19D). Thus, PLK2 can mediate Hh cytoprotection against TRAIL-induced apoptosis in CCA cells.

Pro-apoptotic effects of PLK2 inhibition are mediated by Mcl-1 degradation. We next sought to investigate the mechanism whereby PLK2 inhibition exerts its pro-apoptotic effects. Because cell cycle enzymes can regulate Mcl-1 expression [101] and Mcl-1 as well as Bcl-2 are downregulated by PLK inhibition in osteosarcoma and esophageal carcinoma cells,[76, 77] we

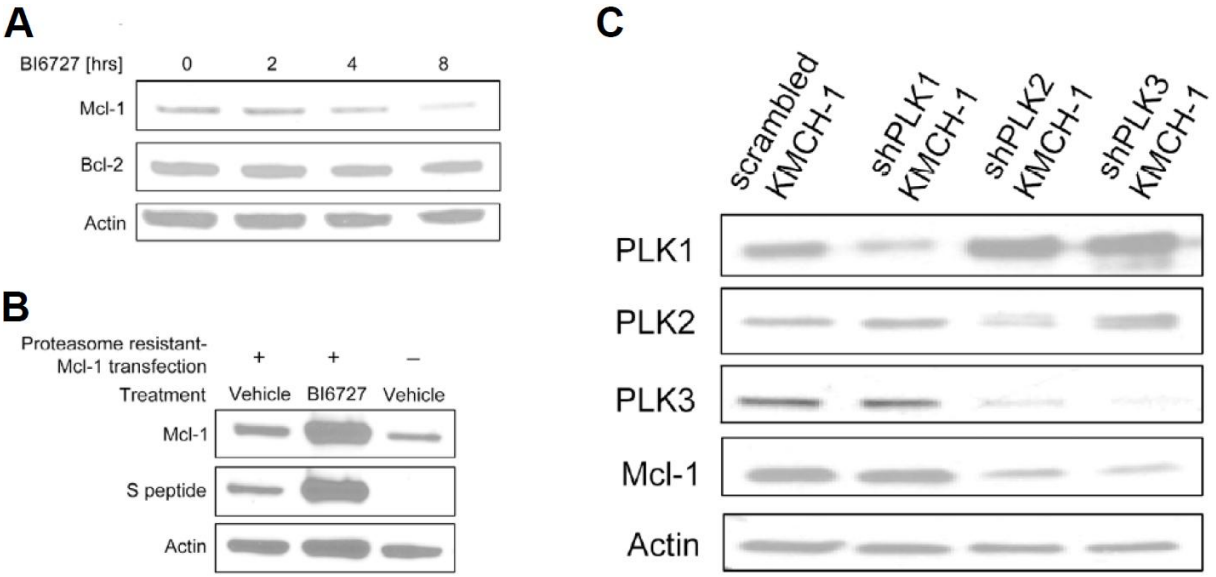

Figure 20. PLK inhibition induces proteasomal degradation of Mcl-1 but not Bcl-2. (A) KMCH-1 cells were treated with vehicle or 200 nM BI 6727 for the indicated time intervals followed by immunoblot analysis for Mcl-1 and Bcl-2 protein expression (actin = loading control). (B) PLK inhibition increases the protein levels of a proteasome resistant Mcl-1 mutant. Initially, KMCH-1 cells were either transfected (FuGENE HD, Promega, Madison, WI) with an enhanced green fluorescent protein (GFP) expressing construct alone (pEGFP-N1; Clontech, Mountain View, CA) or with the GFP construct plus the vector expressing a S peptide-tagged mutated human Mcl-1 at a 1:2 ratio (transfected cells were identified by expression of GFP). The human Mcl-1 mutant is resistant to proteasomal degradation due to sequential mutagenesis of the established Mcl-1 ubiquitination sites (amino acids 5, 40, 136, 194, and 197) from lysine to arginine. Subsequently, cells were treated as indicated with vehicle or BI 6727 (200 nM, 24 hrs) followed by immunoblot analysis for Mcl-1 and S peptide protein expression. Note that GFP-only transfected KMCH-1 cells only express the wild-type Mcl-1 but not the S peptide (actin = loading control). (C) PLK2 knockdown reduces Mcl-1 protein expression. Mcl-1 expression and PLK 1/2/3 expression/knockdown in stable scrambled, shPLK1-, shPLK2- and shPLK3-KMCH-1 cells was assessed by immunoblot analysis (actin = loading control). Note that stable PLK3 knockdown also affects PLK2 expression giving an explanation for the reduced Mcl-1 protein expression also seen in shPLK3-KMCH-1 cells.

explored the effect of PLK inhibition on cellular Mcl-1 and Bcl-2 protein levels. Indeed, BI 6727 administration rapidly decreased Mcl-1 (but not Bcl-2) protein levels in KMCH-1 cells (Figure 20A). To assess if decreased Mcl-1 protein levels are due to proteasomal degradation, we employed the potent proteasome inhibitor MG-132 or transfected KMCH-1 cells with a proteasome-resistant Mcl-1 mutant. Mcl-1 downregulation by BI 6727 is likely mediated by proteasomal degradation as MG-132 (Figure 21A [KMCH-1 cells], Figure 21B [Mz-ChA-1 cells] and Figure 21C [HUCCT-1 cells]) or transfection with the proteasome-resistant Mcl-1 mutant (Figure 20B) completely abrogated this effect. Moreover, inhibition of proteasomal degradation in the presence of BI 6727 increased Mcl-1 protein levels as compared to vehicle-controls (Figure 21A and B as well as Figure 20B) suggesting Mcl-1

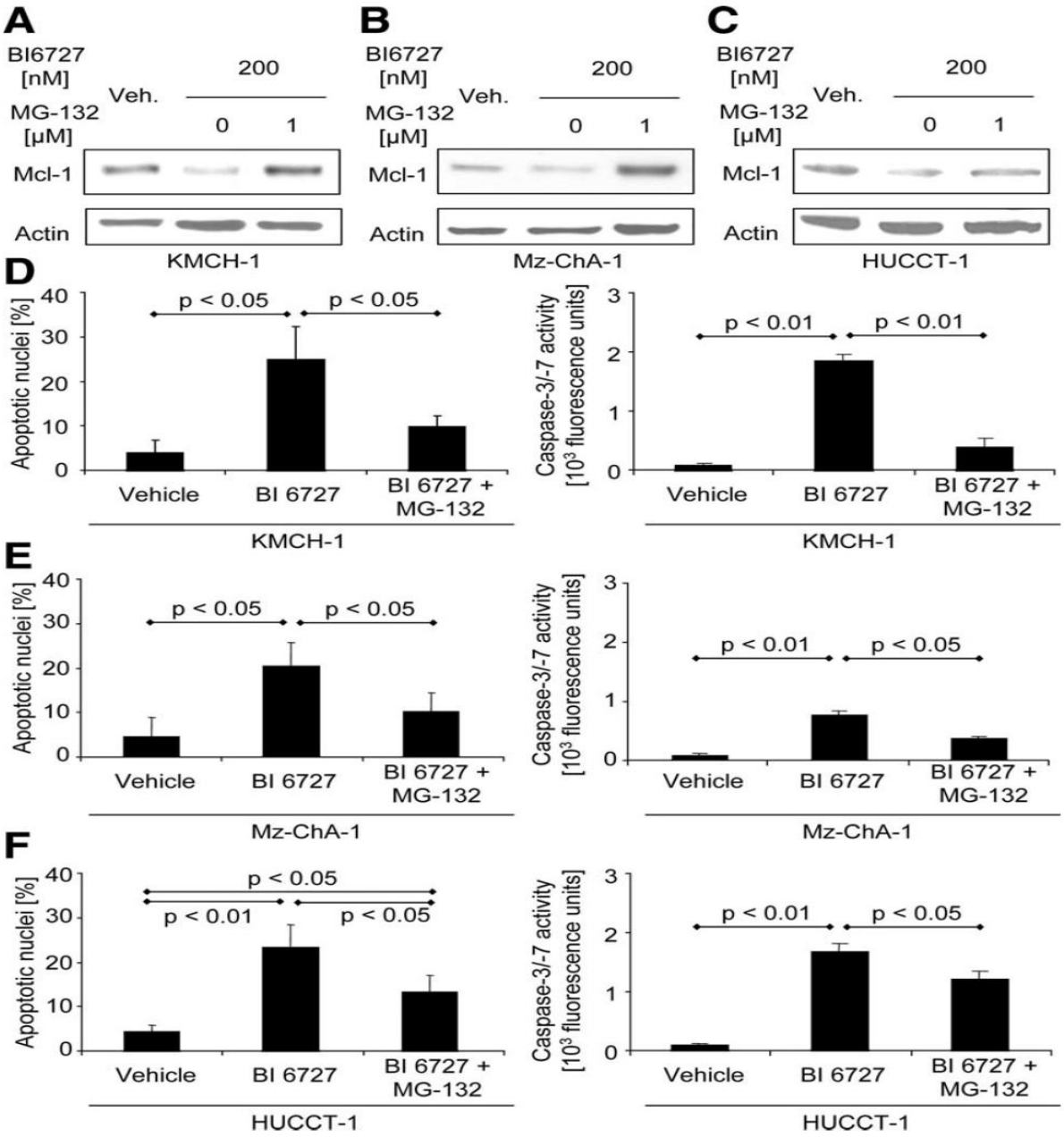

Figure 21. Pro-apoptotic effects of PLK2 inhibition are mediated by Mcl-1 degradation. (A-C) KMCH-1 (A), Mz-ChA-1 (B) and HUCCT-1 (C) cells were treated as indicated with vehicle or BI 6727 (200 nM, 24hrs) in the absence or presence of the potent proteasome inhibitor MG-132 (1 μM, 24 hrs) followed by immunoblot analysis for Mcl-1 protein expression (actin = loading control). (D-F) KMCH-1 (D), Mz-ChA-1 (E) and HUCCT-1 (F) cells were treated as indicated with vehicle or BI 6727 (200 nM, 24 hrs) in the absence or presence of MG-132 (1 μM, 24 hrs). Apoptosis was measured by DAPI staining with quantitation of apoptotic nuclei by fluorescence microscopy (left; mean ± s.e.m.; n=3) or fluorescent analysis of caspase-3/-7 activity (right; mean ± s.e.m.; n=5).

upregulation is an initial protective cell response to BI 6727 (which in BI 6727 only-treated cells is overwhelmed by proteasomal Mcl-1 degradation). Accordingly, BI 6727-treated KMCH-1 cells display a compensatory upregulation of Mcl-1 mRNA levels (Figure 22A). Consistent with these observations, MG-132 also blocked BI 6727-induced apoptosis in KMCH-1

DOI:10.14753/SE.2016.1969

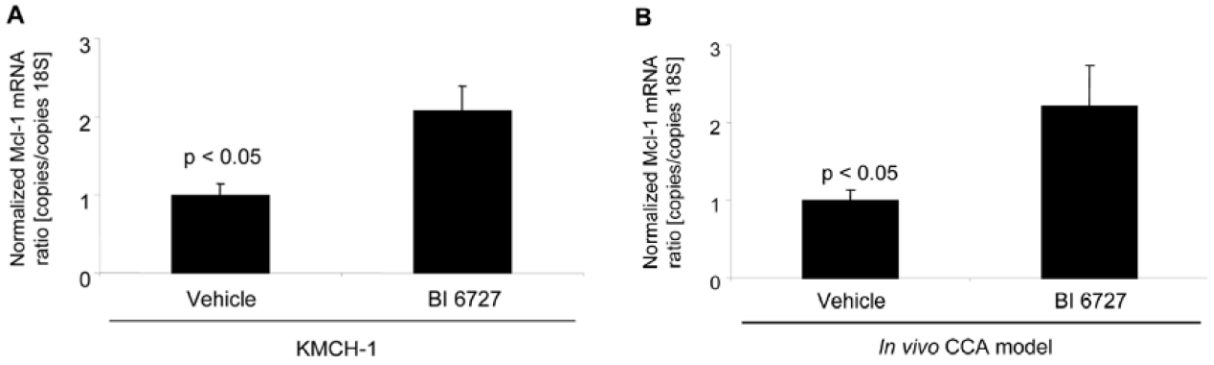

Figure 22. PLK inhibition increases Mcl-1 mRNA expression *in vitro* and *in vivo*. (A) KMCH-1 cells were treated as indicated with vehicle or BI 6727 (200 nM, 24 hrs) followed by quantitative RT-PCR analysis for Mcl-1 mRNA expression. Mean ± s.e.m., n=3. (B) A syngeneic rat orthotopic CCA model (BDEneu cells; Fischer 344 rats) was employed for this study. CCA specimens of BI 6727 (3 injections of 10 mg/kg BW intraperitoneally every other day; 1st injection: 7th post-operative day, 3rd injection: 11th post-operative day)- or vehicle-treated rats were analyzed for Mcl-1 mRNA expression by quantitative RT-PCR. Mean ± s.e.m., n=9.

(Figure 21D), Mz-ChA-1 (Figure 21E) and HUCCT-1 (Figure 21F), cells as assessed morphologically (Figure 21D-F left) or biochemically (Figure 21D-F right). Moreover, stable knockdown of PLK2 by shRNA technique also reduced Mcl-1 protein levels as displayed by immunoblot analysis (Figure 20C). These data suggest that PLK2 inhibition reduces Mcl-1 protein levels in a post-translational manner by proteasomal degradation thereby promoting apoptosis.

PLK inhibition promotes CCA cell apoptosis and is tumor suppressive in vivo. To determine if the pro-apoptotic *in vitro* effect of PLK signaling inhibition by BI 6727 also is translatable to an *in vivo* model, weagain employed the syngeneic rat orthotopic CCA model (BDEneu malignant cells injected into the liver of male Fischer 344 rats).[43, 69, 85, 86] First, we sought to further validate this model by assessing mRNA expression of PLK1-3 in CCA specimens as

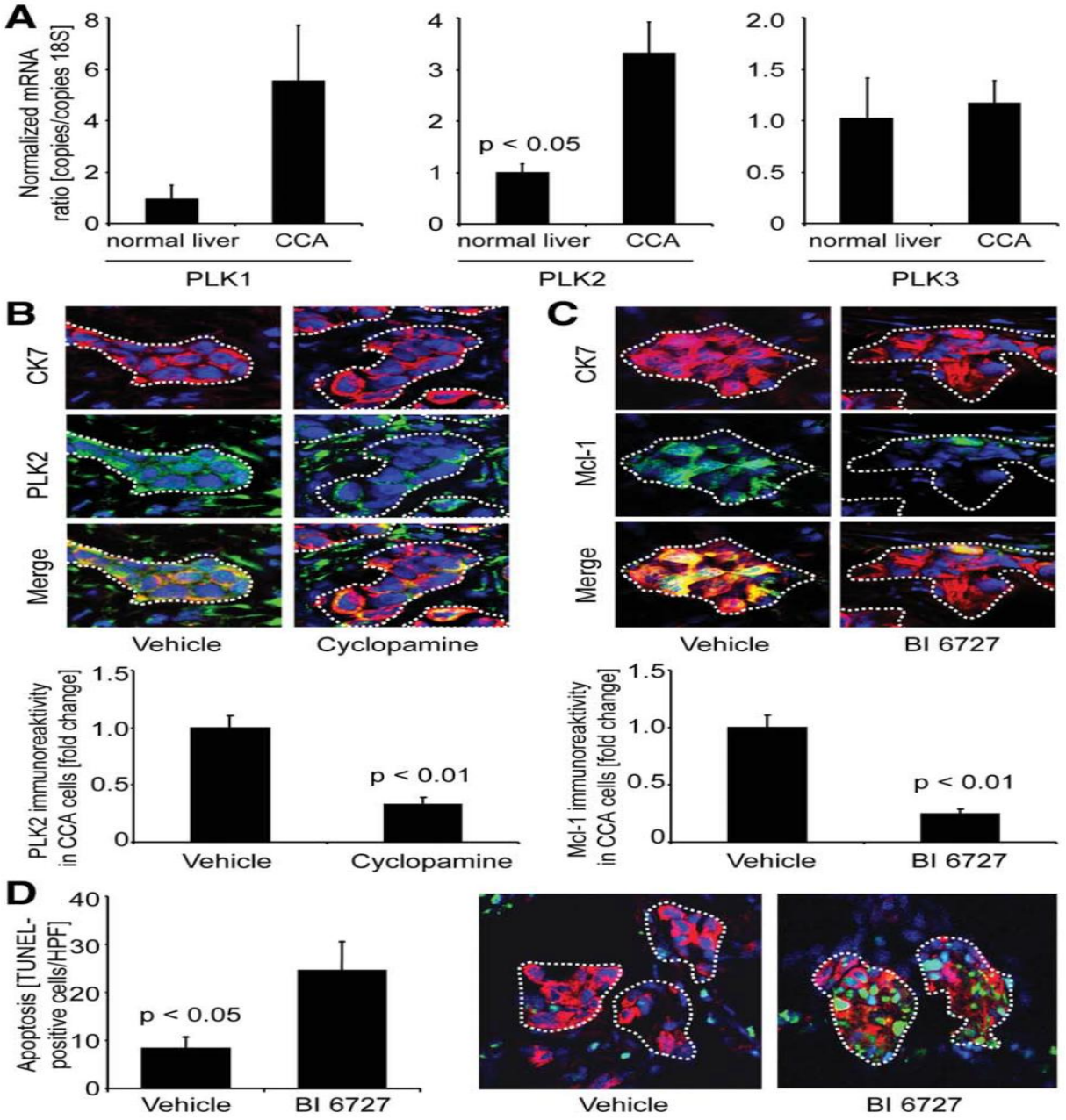

Figure 23 Effects of Hh and PLK inhibition are recapitulated *in vivo.* The syngeneic rat orthotopic CCA model (BDEneu cells; Fischer 344 rats) was employed for this study. (A) CCA and normal liver specimens of untreated rats were analyzed for mRNA expression of PLK1 (left), PLK2 (middle) and PLK3 (right) by quantitative RT-PCR. Mean ± s.e.m., n=3. (B) CCA specimens of cyclopamine (2.5 mg/kg BW intraperitoneally daily for one week; 1st injection: 7th post-operative day, 7th injection: 13th post-operative day)- or vehicle-treated rats were analyzed for PLK2 (green) expression of tumor cells (identified via co-staining for CCA cell marker cytokeratin 7 [CK7]; red) by immunofluorescence microscopy. Merged images depict colocalized CK7/PLK2 protein expression in yellow (green-red overlay). PLK2 immunoreactivity in CCA cells was quantitated using the software ImageJ 1.44o (B lower; mean ± s.e.m., n=7). (C) CCA specimens of BI 6727 (3 injections of 10mg/kg BW intraperitoneally every other day; 1st injection: 7th post-operative day, 3rd injection: 11th post-operative day)- or vehicle-treated rats were analyzed for Mcl-1 (green) expression of CCA cells (similar CK7 co-staining and quantitation [mean ± s.e.m., n=9] as in B). (D) Apoptotic nuclei were assessed in CCA samples of vehicle (left photomicrograph)- and BI 6727 (right photomicrograph)-treated rats by TUNEL staining (green) and the identity of TUNEL-positive cells confirmed by CK7 co-staining (red). Quantitation of TUNEL-positive cells (expressed as number per high power field [HPF], D left) demonstrates that in BI 6727-treated animals, CCA cell apoptosis was increased as compared to controls (mean ± s.e.m., n=9). In all photomicrographs nuclei are counterstained with DAPI (blue) and CCA glands within the tumor stroma are illustrated by white dotted lines.

compared to normal rat liver tissue via quantitative RT-PCR. PLK2 mRNA levels in CCA were significantly higher as compared to normal rat livers (Figure 23A). On the protein level, PLK2, similar to the human disease (Figure 15), was abundantly expressed in tumorous glands (identified by cytokeratin 7 [CK7] co-staining; CK7 is a biliary epithelial cell marker expressed by CCA cells) and also by occasional stromal cells within the tumor microenvironment (Figure 23B). Administration of Hh inhibitor cyclopamine significantly decreased PLK2 expression in tumorous glands (dotted lines) but not stromal cells in this *in vivo* CCA model (Figure 23B middle photomicrographs and bar graph). Also consistent with our *in vitro* observations, treatment with PLK inhibitor BI 6727 *in vivo* reduced Mcl-1 protein expression in CCA cells (Figure 23C middle photomicrographs and bar graph). PLK2 mRNA levels were also increased in CCA specimens of BI 6727-treated rats as compared to controls (Figure 22B). Finally, CCA cell apoptosis was increased in animals treated with BI 6727 as compared to vehicle-treated rats (Figure 23D; CCA cell apoptosis was confirmed by demonstrating colocalization of TUNEL-positive cell nests with tumorous glands displaying CK7). Thus, this preclinical rodent model of CCA recapitulates characteristic features observed in human CCA tissue and *in vitro* studies including the pro-apoptotic effect of PLK inhibition on CCA cells.

Consistent with the pro-apoptotic effects of PLK2 observed in the CCA *in vivo* model, PLK2 was also effective in reducing tumor size and metastasis (Figure 24A-F). Indeed, tumor weight and tumor/liver weight ratios were significantly decreased in BI 6727-treated rats (Figure 24A-E). Additionally, 100% of the rats treated with BI 6727 displayed no extrahepatic metastases, whereas only 56% of the vehicle-treated animals were free of metastases (four out of nine animals in this group showed tumors predominantly occurring in the greater omentum and peritoneum; Figure 24A [lower right photomicrograph] and F). Taken together, these data suggest that BI 6727 decreases tumor growth as well as metastasis in an *in vivo* rodent model of CCA. Thus, this mechanistic treatment strategy might also be an eligible accompanying therapy to optimize the Mayo LTx protocol for CCA patients.

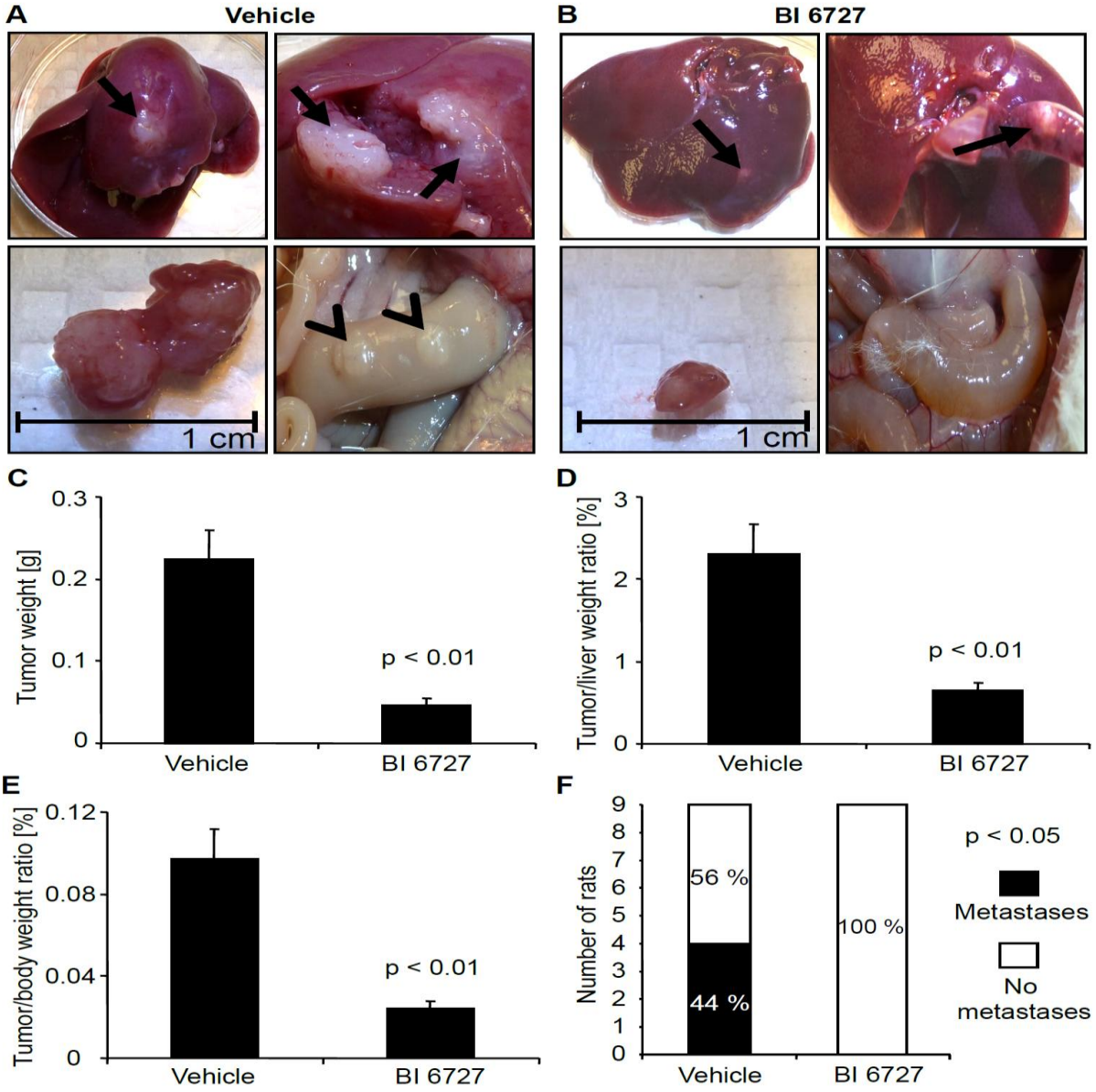

Figure 24. **PLK inhibition is tumor suppressive *in vivo***. The syngeneic rat orthotopic model of CCA (BDEneu cells; Fischer 344 rats) was employed for this study. In BI 6727 (3 injections of 10mg/kg BW intraperitoneally every other day; 1st injection: 7th post-operative day, 3rd injection: 11th post-operative day)- or vehicle-treated rats tumor/liver/body weight and extrahepatic metastasis were assessed 13 days after tumor cell implantation into the left lateral liver lobe. (A and B) Representative photomicrographs display explanted livers (left upper), gross pathological tumor appearance within the livers (right upper), extirpated tumors with scale (left lower), and the abdominal cavity (right lower) of vehicle (A)- or BI 6727 (B)-treated rats (arrows indicate liver tumors and arrowheads extrahepatic metastases). (C-E) Changes in tumor weight (C), tumor/liver weight ratios (D), and tumor/body weight ratios (E) are depicted as bar graphs. Mean ± s.e.m., n=9. (F) The stacked column plot indicates the numbers of animals with and without extrahepatic metastases for the vehicle- and BI 6727-treated group ($p < 0.05$ by χ^2 test).

DOI:10.14753/SE.2016.1969

6 DISCUSSION

6.1 General Optimization Approaches For Liver Transplantation

6.1.1 Preservation solution/chloride study

The present *in vivo* study performed with a chloride-poor and a chloride-containing variant of a new HTK-based preservation solution suggests that beneficial effects of chloride-containing media on the endothelium/microcirculation overbalances chloride-dependent cold storage injury of hepatocytes.

The new preservation solution. Taking into account new findings on the mechanisms of initial preservation injury triggered by hypoxia,[5, 6, 8, 102-106] hypothermia,[7, 9, 10, 18, 19, 21, 107-110] preservation solution toxicity,[11, 12] and inflammatory processes,[7, 13, 14] a new HTK-based preservation solution was developed.[15] The amino acids glycine and alanine were incorporated into the new solution in order to attenuate hypoxic cell injury, in which increased intracellular sodium plays a crucial role.[5, 103-106] Previous studies have shown that glycine provides protection from hypoxic injury by preventing the formation of nonspecific leaks for small ions including sodium.[106] In addition, several studies demonstrated that Kupffer cell activation triggered by organ manipulation can be inhibited by glycine.[111-113] Alanine, structurally related to glycine, seems to exert similar inhibitory effects on intracellular sodium accumulation induced by hypoxia.[106] It has been shown to inhibit hypoxic injury to isolated hepatocytes [106, 114] and to improve recovery of the liver exposed to cold ischemia and reperfusion.[115]

In previous *in vitro* experiments we showed that histidine (serving as buffer; pK_a = 6.2 at 20 °C) can be toxic due to an iron-dependent formation of reactive oxygen species.[12] Therefore, histidine, the only buffer in HTK solution, was partly (in confines given by charge) replaced by the nearly non-toxic *N*-acetylhistidine, which possesses comparable buffering power (pK_a = 7.2 at 20 °C). Aspartate was added to the new solution together with α-ketoglutarate to allow replenishment of the citric acid cycle (after transamination) and to improve energy state [116], arginine serves as substrate for NO synthase, thus counteracting postischemic sinusoidal constriction.[117-119] Enhanced NO levels also can improve bile production[120] and decrease necrotic as well as apoptotic cell death.[121] Since mannitol might permeate the membrane of hepatocytes causing cell swelling[122, 123] it was replaced by sucrose.

In this composition, the new preservation solution was already shown to attenuate preservation injury to isolated perfused rat livers compared to HTK.[15] In order to obtain a chloride-

containing variant of the new solution for the present study (with 34.04 mmol/l to be the highest possible chloride concentration without altering inorganic cation concentrations or further decreasing organic anions), additional slight modifications − mainly affecting the concentrations of *N*-acetylhistidine (partly anionic), histidine (partly cationic) and sucrose − became necessary for reasons of charge and osmolarity. In the future it is planned to supplement the new base solution with iron chelators, which should inhibit cold-induced cell injury and further attenuate histidine toxicity (transplant studies testing the new preservation solution with the iron chelators deferoxamine and LK 614, which proved beneficial in isolated perfused organs,[124-126] are currently under way); however, here, we intended to optimize the base solution and did not yet add iron chelators.

Chloride and cold-induced injury in vitro. The effects of extracellular chloride on cold-induced injury are dissimilar in cultures with different cell types. Isolated hepatocytes from Wistar rats suffer cold storage injury in cell culture media/preservation solutions that contain chloride at concentrations above 40 to 50 mmol/l due to an entity preliminarily characterized by us as iron-*in*dependent cold-induced injury.[22] How physiological extracellular chloride concentrations contribute to cell death of hepatocytes under hypothermic conditions is currently unclear. A likely explanation can be adverse effects of chloride on cellular pH regulation. Influences on apoptotic processes may represent another possibility, since two studies suggested extracellular chloride to promote apoptosis via interference with a receptor-mediated pore formation[127] and the early intrinsic apoptotic pathway,[128] respectively.
In contrast to that, cold-stored porcine aortic endothelial cells, and endothelium of intact porcine aortic segments benefit from chloride-containing preservation solutions as shown by improved cell survival rates.[23, 24] Again, the mechanism of action is currently unclear.

Chloride and hypoxic injury in vitro. The impact of chloride on hypoxic cell injury has been discussed controversially. In the pathogenesis of hypoxic injury to hepatocytes, rising cytosolic sodium concentrations play a crucial role[5, 103-106] – a process that can be inhibited by the amino acid glycine.[106, 129] Carini et al. proposed that the protective effect of glycine results from inhibition of glycine-sensitive ligand-gated chloride channels and concluded that chloride influx might be coupled with intracellular sodium accumulation.[129] In their experiments chloride-poor media attenuated intracellular sodium accumulation and improved cell viability.
In contrast to that, a study of Frank et al. demonstrated glycine to be even protective in a chloride-free medium while a chloride-free medium itself did not inhibit hypoxic injury at all.[106]

This apparent discrepancy may be due to the usage of cultured hepatocytes in the latter study, while Carini et al. performed their experiments with isolated hepatocytes in suspension; the use of a cell suspension may, for instance, result in a more pronounced hypoxia-induced acidification leading to better antagonization of an injurious alkalinization by chloride-free conditions.[130] Frank et al. suggested sodium influx and hypoxic cell injury to be chloride-independent and rather to be related to the formation of nonspecific ion leaks.[106]

Chloride and preservation injury in vivo. With the chloride-containing preservation solution, sinusoidal perfusion rates as well as blood flow velocities in sinusoids and postsinusoidal venules were significantly improved after LTx. This is consistent with our *in vitro* data demonstrating beneficial effects of chloride on endothelial cell survival.[23] It can be speculated whether the improved microcirculation and the tendency of vasodilation seen in postsinusoidal venules with chloride is due to a less impaired endothelial dysfunction leading to increased NO levels and/or a better NO response since increased NO formation is sufficient to improve hepatic tissue blood flow after reperfusion as shown by laser flowmetry.[118]

It is not necessarily a contradiction that previous *in vitro* experiments found cold-stored rat hepatocytes to be harmed by extracellular chloride,[22] but here a slight decrease of serum transaminase and LDH activities in rats after LTx with the chloride-containing solution was observed (Fig. 3A). First, the injurious effects of chloride become evident mainly at chloride concentrations exceeding 40-50 mmol/l.[22] Moreover, the beneficial effect of chloride on hepatocytes in transplanted rat livers is possibly a consequence of the clearly improved microcirculation following reperfusion. Thus, chloride-containing media might be advantageous for hepatocytes due to an indirect effect *in vivo*.

As a consequence of both, the direct advantageous effect of chloride on the endothelium and the possibly indirect beneficial effect of chloride on parenchymal cells, bile flow − a reliable indicator of energy-dependent liver function[131, 132] − and survival were shown to be improved. It must be emphasized that survival represents the study criterion with the highest medical relevance and therefore was tested in three different series. In these series the broad range of potential clinical situations was reflected by LTx protocols with different combinations of cold ischemic and warm ischemic injury as well as surgical trauma and genetic background/immunological influences. In all experimental series, survival rates after LTx with the chloride-containing variant of the new solution were increased. At first view, these results might appear counterintuitive as UW solution (or Viaspan), which greatly improved liver preservation in comparison to the chloride-containing (15 mM chloride) Euro-Collins solution[133] and which appears to yield results largely equivalent to HTK solution,[134, 135] provides

good liver preservation despite the absence of chloride. This good preservation, however, might also be due to the other components of UW solution that largely differ from these other two solutions. That in one study with a modified, *sodium-rich* UW solution an injurious effect of chloride was observed[136] is also not necessarily contradictory with regards to the known role of a sodium influx in hypoxic injury (see above), that might be accompanied by a chloride influx. Thus, the effects of chloride might differ in sodium-rich vs. sodium-poor preservation solutions. Whether also the *potassium-rich* UW solution or other preservation solutions would become more protective for the endothelium with the incorporation of chloride remains to be established.

The data shown here suggest that chloride concentrations in HTK-based (and possibly also other) preservation solutions for LTx should not be too low (in confines given by toxicity for hepatocytes) in order to provide protection to endothelial cells since these cells are likely to be more sensitive to cold-induced injury than hepatocytes. This is in accordance with various studies describing a comparably higher loss of non-parenchymal cell viability after cold storage/reperfusion as assessed by nuclear trypan blue uptake, LDH release, electron microscopy, and TUNEL assay.[3, 137-141] One reason for the higher susceptibility of endothelial cells to cold-induced injury may be their reduced antioxidant status in comparison with hepatocytes.[142, 143]

As already mentioned above, the addition of iron chelators can be expected to further improve protection from cold-induced cell injury and to further inhibit histidine toxicity.[7, 12, 18, 19] Studies comparing the new (chloride-containing) solution supplemented with the well-known iron chelator deferoxamine and the new, more membrane-permeable iron chelator LK 614 [126] to HTK solution have shown further improvement in rat liver preservation[126] and attenuation of lipid peroxidation, serum liver enzyme activities and histological damage in isolated perfused marginal livers from non-heart beating rat donors.[124] Similarly, this solution ameliorated liver injury after hypothermic machine preservation of marginal rat liver grafts when compared to HTK solution.[125] Finally, the modified HTK-based preservation solution tested here is non-toxic, [15] and its physical characteristics as well as its use are similar to traditional HTK solution (e.g. it can be used without flush-out, unpublished results).

6.1.2 Erythropoietin study

In this *in vivo* study, we demonstrated that EPO treatment induces a proliferative response in hepatocytes resulting in an increased LBWR before and especially after pLTx. This is

associated with an increased overall survival. The underlying mechanisms of these beneficial effects include an increased expression of the pro-regenerative mediator *c-jun* as well as the blockage of apoptotic pathways by upregulation of the anti-apoptotic gene Bcl-X_L.

In our preconditioning experiments we have demonstrated that EPO treatment can raise the LBWR and Ki-67-proliferation index of normal (donor) livers. Still, one of the major concerns in using exogenous mitogens is that the preoperative stimulus during preconditioning results in suppression of regeneration after surgery. Data from Malik et al. and our group, however, suggest that the DNA synthetic response of the hepatocytes is not changed after treatment with the mitogen tri-iodothyronine.[28, 144] These results indicate that a larger remnant size and the resulting reduced volume deficit after PH caused by exogenous stimuli does not inevitably result in a diminished stimulation of regeneration. In addition, EPO did not impair the regenerative response after surgery, since rats that were treated with additional EPO perioperatively showed an increased remnant liver mass and a higher Ki-67 proliferation index after pLTx. The dose of EPO used in our experiment was not much higher than employed in clinical practice (i.e., only 10 times higher than doses applied in bone marrow transplants).

Unexpectedly, EPO-treatment did not significantly improve laboratory parameters after pLTx. In contrast, Sepodes et al. could demonstrate an advantageous effect of EPO-preconditioning on serum parameters in their ischemia-reperfusion experiments, possibly by reducing the oxidative stress and caspase-3 activation, suggesting the subsequent reduction of apoptosis.[145] Despite the lack of positive effects on laboratory parameters, preconditioning with EPO significantly improved overall survival following pLTx.

Malik et al. demonstrated a beneficial effect of exogenously administered tri-iodothyronine on the regenerative response of the liver following PH.[146] The authors suggest a synergistic effect of two distinct liver growth pathways: direct hyperplasia and compensatory regeneration. In our experiments, 24 h following pLTx, EPO mediated amplifications of regeneration pathways including *c-jun* signaling seems to be more likely. C-*jun* is an important mediator of the EPO signaling transduction cascade.[147, 148] During liver regeneration *c-jun* may be activated by EGF- and HGF-dependent signaling cascades.[149] Together with the *c-fos* gene, which is induced via TNF-α, NF-κB, IL-6 and STAT 3, [150] it forms the AP-1 complex. C-*jun then* seems to exert its proliferative effects by regulating the cell cycle via p53/p21-, cyclin D1- and PCNA-dependent pathways. [151-154]. The importance of c-jun for cells to exit from p53-imposed growth arrest

already was described by Shaulian et al.[153] Moreover, the role of *c-jun* for liver regeneration after PH and during perinatal/postnatal liver development is not only of theoretical nature since various knock-out experiments could reveal detrimental consequences if this gene is lacking.[149, 155]

In a model of cardiac injury, Calvillo et al. reported that EPO prevents the majority of cells from apoptosis.[156] We therefore investigated whether EPO can protect hepatocytes from apoptosis 24h after pLTx and were able to show that EPO-treated animals exhibit a lower proportion of apoptotic cells. In addition, the anti-apoptotic gene Bcl-X_L was significantly upregulated. Further findings concerning EPO and apoptosis have been reported for the central nervous system, suggesting a specific anti-apoptotic effect of EPO in non-hematopoietic cells.[157, 158]. Moreover, it has been demonstrated that EPO reduces cell death in cultured human proximal tubular cells, too.[159]

Interestingly, *c-jun* is also involved in the complex regulation of apoptosis. Jacobs-Helber et al. reported that *c-jun* has the potential to hamper erythroid cells from entering apoptosis.[147] In further knock-out experiments and studies with mice models of HCC it was demonstrated that this anti-apoptotic effect is partially mediated by crosstalk with NF-κB signaling as well as by antagonizing p53 activity [154, 160, 161]. However, *c-jun* is part of pro-apoptotic pathways as well.[162]

Although EPO has also been described as a proangiogenetic factor, [32, 33] there was no evidence for such an effect in our experiments. Administration of EPO also had no impact on the hematocrit level within the first 48h, implying that its beneficial effects are not mediated by this component. Interestingly, despite several injections with high EPO doses, EPO-receptor mRNA was not considerably downregulated suggesting that there was no development of an early tolerance in our model.

By stimulating cell proliferation and downregulating apoptotic pathways, EPO may also have a procancerogenic potential, especially in the setting of its clinical use in oncologic patients (e.g., LTx due to HCC or CCA). It remains to be determined whether short-term therapy before and after surgery would have such an effect. Therefore, further studies have to be carried out in order to investigate this important aspect more precisely. However, EPO is already widely used for the prevention and treatment of anemia resulting from cancer chemotherapy and recent studies show that at least in leukemia and breast cancer EPO fails to stimulate a cancerous proliferation.[163]

DOI:10.14753/SE.2016.1969

6.2 Optimization Of Liver Transplantation For Cholangiocarcinoma

6.2.1 Myofibroblast-derived PDGF-BB/hedgehog signaling study

The results of this study provide new mechanistic insights regarding cytoprotective MFB-to-tumor cell paracrine signaling in CCA. These data indicate that MFB-derived PDGF-BB (1) protects CCA cells from TRAIL-induced cell death *in vitro*; (2) exerts this cytoprotection in a Hh signaling-dependent manner by inducing cAMP/PKA-mediated SMO trafficking to the plasma membrane resulting in GLI2 nuclear translocation and GLI transcriptional activity; (3) and appears to act similarly in a rodent *in vivo*-model of CCA, where PDGF-BB/Hh signaling inhibition by imatinib mesylate or cyclopamine promotes CCA cell apoptosis and is tumor suppressive. These findings are illustrated in Figure 25 and discussed in greater detail below.

In this study, we explored a role for PDGF-BB as a MFB-derived survival factor for CCA cells. Indeed, in coculture experiments, MFB cytoprotection against TRAIL-induced apoptosis was abrogated by neutralizing antisera to PDGF-BB suggesting MFB-derived PDGF-BB is a potent anti-TRAIL survival factor for CCA cells. Although many cancer cells may not express PDGF receptors,[96] our data indicate CCA cells express PDGFR-β and respond to PDGF-BB by activating this receptor (phosphorylation). These observations suggest the existence of a distinctive paracrine survival signaling pathway between MFB and CCA cells.

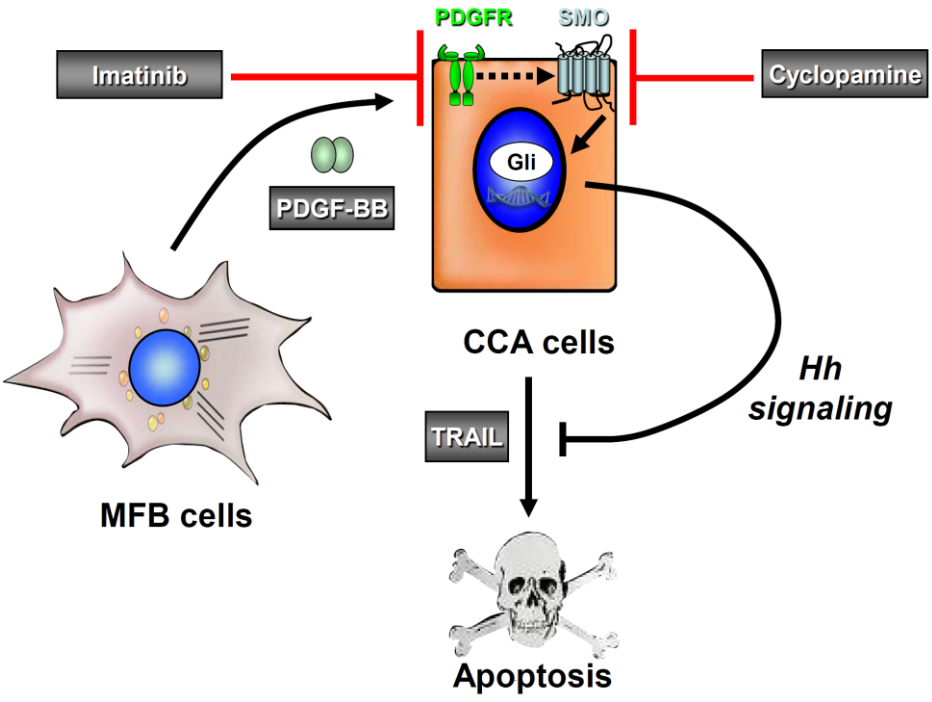

Figure 25. Schematic diagram illustrating the role of platelet-derived growth factor (PDGF)-BB in promoting apoptosis resistance in cholangiocarcinoma (CCA) cells. PDGF-BB, mainly secreted by myofibroblasts (MBFs), promotes hedgehog (Hh) signaling by inducing trafficking of Hh signaling mediator smoothened (SMO) to the plasma membrane with subsequent glioma-associated oncogene (GLI) activation resulting in apoptosis resistance. PDGF-BB/Hh signaling inhibitors such as imatinib mesylate/cyclopamine block Hh survival signaling and, thus, promote apoptosis in CCA cells. TRAIL; tumor necrosis factor-related apoptosis-inducing ligand.

Coactivation networks are being increasingly recognized in cancer biology.[164] We had previously implicated a major role for Hh-signaling directed survival signals against TRAIL cytotoxicity of CCA cells *in vitro*. [67, 68] Also, others have suggested PDGF-BB increases Hh ligand generation in immature bile ductular cells.[58] Given this information, we posited that a PDGF-BB and Hh signaling co-activation network could contribute to survival signaling in CCA cells. Somewhat surprisingly, we found that PDGF-BB does not induce Hh ligand expression. [57, 58] Instead, PDGF-BB appears to increase Hh signaling by promoting SMO trafficking to the plasma membrane (an event known to increase SMO activation [64]). Moreover, these processes were blocked by H89 (an inhibitor of the cAMP-regulated kinase PKA), suggesting that PDGF-BB-induced SMO trafficking is PKA-mediated. We note that the role of PKA in the Hh pathway is complex and likely depends upon the cell type and cellular context. For example, although PKA has been reported to promote Hh signaling at the level of SMO, it may act as a negative regulator by promoting the cleavage of GLI proteins into their repressor forms. [64] However, in CCA cells treated with PDGF-BB, PKA does not repress PDGF-BB-mediated GLI transcriptional activity as we observed activation of a GLI reporter gene assay, and common gene expression between SHH and PDGF-BB stimulation in a cyclopamine-inhibitable manner.

Because receptor tyrosine kinases - as opposed to G-protein coupled receptors - do not directly stimulate adenylate cyclase (the enzyme generating cAMP), the mechanism by which PDGFR-β signaling enhances PKA activity in CCA cells will require further elucidation. A plausible mechanism would be the PDGF-BB/mitogen-activated protein kinase (MAPK)/prostaglandin E2/cAMP axis described in arterial smooth muscle cells. [165]

The SMO inhibitor, cyclopamine, and the PDGFR inhibitor, imatinib mesylate, also achieved suppression of CCA tumor growth in a preclinical rodent model of CCA as single agents. The orthotopic rodent model of CCA employed in these studies reflects a similar molecular signature and TRAIL expression as human CCA, [85, 86] exhibits a tumor microenvironment rich

in activated α-SMA-secreting MFBs, and also recapitulates the cellular expression patterns of PDGF-BB and PDGFR-β found in many human CCA samples.

Berman *et al.* also reported cyclopamine suppresses digestive tract tumors including CCA *in vivo* (in a xenograft tumor model).[61] Herein, we expand this observation and provide evidence of functional interactions between tumor microenvironment and CCA cells. Moreover, we demonstrate that Hh signaling inhibition increases apoptosis of CCA cells *in vivo*. The mechanism by which cyclopamine induces apoptosis *in vivo* likely involves TRAIL expression in the tumor tissue, because cyclopamine does not increase apoptosis of monocultured CCA cells in the absence of TRAIL. Hh signaling has also been implicated in altering the tumor microenvironment.[166] For example, Hh inhibitors increase the efficiency of cytotoxic chemotherapy in rodent models of pancreatic cancer by modulating the microenvironment of the cancer.[54] In contrast to those studies, we did not observe a decrease in α-SMA positive MFBs in cyclopamine treated tumors (data not shown). Moreover, the importance of Hh signaling in cancer cells as opposed to stromal cells has recently been emphasized. [167] Our observations are most consistent with a direct effect of cyclopamine on the tumor cells *in vivo*, although we cannot fully exclude a non-cytotoxic effect of cyclopamine on MFB function.

6.2.2 Hedgehog signaling/Polo-like kinase 2 study

This study provides new mechanistic insights regarding a Hh and PLK signaling co-activation network in CCA. These data indicate that (1) Hh signaling directly regulates PLK2 mRNA and protein expression; (2) PLK2 promotes Mcl-1 stabilization providing resistance to cell death by TRAIL; and (3) PLK inhibition is tumor suppressive in an orthotopic syngeneic rodent *in vivo* CCA model. These findings are illustrated in Figure 26 and discussed in greater detail below.

In the prior study, we reported that MFB-to-cancer cell paracrine signaling imparts survival signals for CCA by co-activation of the Hh signaling pathway. Indeed, Hh signaling inhibition by cyclopamine increased the susceptibility of CCA cells to apoptotic stimuli. Moreover, a microarray mRNA expression analysis also suggested Hh signaling positively regulates cell cycle enzyme PLK2 in CCA cells (Table 6). Therefore, we further examined PLK2 regulation by Hh signaling and explored whether targeting of PLK2 signaling would be similarly effective in restoring CCA cell susceptibility to TRAIL-induced apoptosis. As cancer cells frequently develop resistance to smoothened inhibitors, [168, 169] blocking PLK2 may

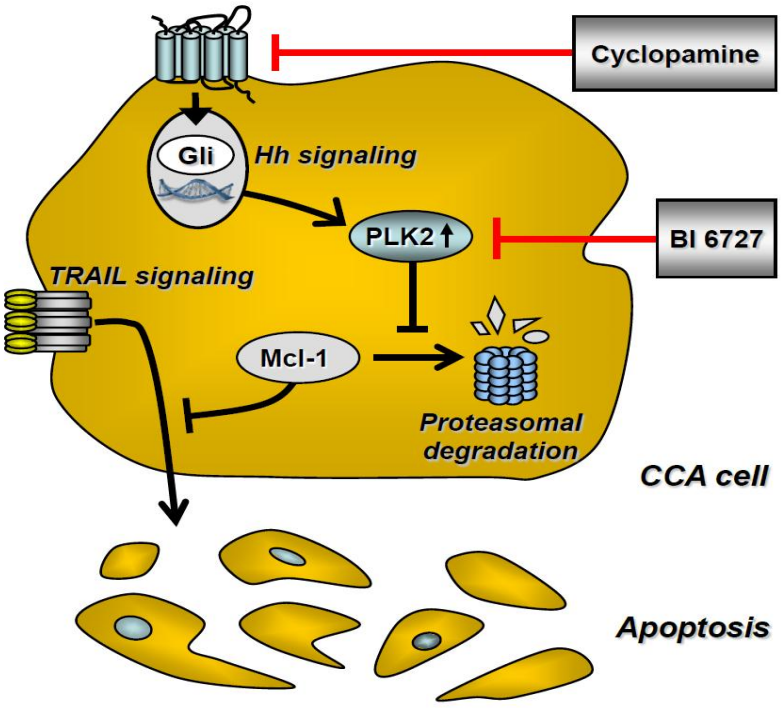

Figure 26. Schematic diagram illustrating the role of Hh and PLK2 signaling in promoting CCA cell resistance to endogenous TRAIL cytotoxicity via stabilization of anti-apoptotic Mcl-1. Hedgehog (Hh)/Smoothened or (Polo-like kinase) PLK inhibitors such as cyclopamine or BI 6727 block Hh/PLK2 survival signaling and, thus, promote apoptosis in CCA cells. GLI, glioma-associated oncogene; Mcl-1, myeloid cell leukemia-1; TRAIL; tumor necrosis factor-related apoptosis-inducing ligand.

be a promising new therapeutic approach for targeting this cancer survival pathway downstream of smoothened. *In vitro*, PLK2 was found to be directly regulated by the Hh pathway. PLK2 cytoprotection against TRAIL-induced apoptosis was abrogated in the presence of PLK inhibitor BI 6727 or when PLK2 was selectively knocked down in KMCH-1 cells. Moreover, PLK2-mediated cytoprotection was, at least in part, due to stabilization of Mcl-1, a crucial survival factor for CCA.[78-80] These observations suggest that PLK2 represents an important link between Hh survival signaling and Mcl-1 protein expression in CCA cells. Thus, PLK inhibition might be a promising strategy for the multimodal treatment of CCA including the Mayo LTx protocol.

The effect of PLK inhibition on CCA cell viability has also been investigated in a single prior study.[170] In their *in vitro* study, Thrum et al. reported that PLK inhibition reduces CCA cell proliferation. Herein, we expand the effects of PLK inhibition by demonstrating that it also is pro-apoptotic *in vitro* and *in vivo.* Moreover, we demonstrate that selective PLK2 inhibition has a more pronounced pro-apoptotic effect than selective PLK1 or PLK3 inhibition in CCA cells. Other than PLK2 or PLK3, PLK1 has been intensively studied and is also a potential target for anti cancer therapy in other cell types.[74] The roles of PLK2 and PLK3 are less well understood and studies in haematologic diseases assume PLK2 and PLK3 act as tumor suppressors through their interactions with p53 signaling.[74, 171] Consistent with these observations PLK 2 and PLK3 are minimally expressed in various human tumors.[172] In CCA cells, however, PLK2 (and perhaps PLK3) appears to have a cytoprotective function, which likely explanes their abundant expression in human and rodent CCA specimens. Like MET, NF-κB, β-Cantenin, Jnk, Shp 2 and Stat3, PLK2 (and PLK3), thus, might belong to the emerging group of molecules that seem to have conflicting tumor-suppressive and oncogenic roles in carcinogenesis depending on tumor type and state of tumor development.[173]

The orthotopic, syngeneic rodent CCA model used in the present study recapitulates the molecular signature and TRAIL expression of human CCA as discussed above. It also provides a syngeneic tumor microenvironment avoiding problems of immunocompromise and tumor-stromal incompatibilities problematic in human xenograft models and mimics the cellular expression patterns of PLK2 found in the human disease. Moreover, the BDEneu CCA cells injected into the rat livers express all relevant Hh signaling pathway factors as shown before (Figure 11). In the prior study employing this *in vivo* model, Hh signaling inhibition with smoothened inhibitor cyclopamine was reported to induce CCA cell death and inhibit tumor

growth. In the present study, we extend these prior observations by demonstrating that Hh inhibition also reduces PLK2 protein expression *in vivo*. In addition, we show that PLK inhibition leads to a decrease in Mcl-1 protein expression in CCA cells also resulting in CCA cell apoptosis and reduced tumor growth *in vivo*. Our *in vitro* observations are most consistent with the pro-apoptotic and tumor-suppressive *in vivo* effects of BI 6727 mainly being mediated by PLK2 inhibition; however, at this point we cannot completely exclude a contribution of PLK1 and PLK3 inhibition to the effects seen in BI 6727-treated animals.

DOI:10.14753/SE.2016.1969

7 CONCLUSIONS

The observations from the studies presented suggest that:

1. *In vivo* beneficial effects of chloride-containing preservation solutions on the endothelium/microcirculation exceed chloride-dependent hepatocyte injury occurring during cold storage. Therefore, HTK-based and possibly other preservation solutions for liver (and vessel) grafts should contain chloride.
2. Erythropoietin treatment significantly improves liver regeneration and survival after pLTx, in part, by upregulation of pro-regenerative mediator *c-jun* as well as the anti-apoptotic gene Bcl-X_L. Thus, EPO application may represent a promising adjuvant strategy to optimize the clinical outcome especially after sLTx and LDLT.
3. MFB-derived PDGF-BB protects CCA cells from TRAIL cytotoxicity by a Hh signaling–dependent process. Targeting PDGFR-β and/or Hh signaling sensitizes these tumor cells to apoptotic cell death. Therefore, these results might have therapeutical implications for the pretreatment of patients awaiting LTx for CCA.
4. PLK2 appears to be a pivotal mediator of Hh survival signaling in CCA cells. Targeting the Hh/PLK signaling co-activation network also sensitizes CCA cells to apoptosis. Thus, besides Hh inhibitors, PLK inhibitors might be of therapeutic value for the multimodal treatment of human CCA including the Mayo LTx protocol.

DOI:10.14753/SE.2016.1969

8 SUMMARY

INTRODUCTION. Liver transplantation (LTx) is a viable treatment option of end-stage liver diseases including neoplasms like cholangiocellular carcinoma (CCA). However, various new insights regarding preservation injury, regeneration and apoptosis mechanisms of normal hepatocytes and CCA tumor cells are not considered by established LTx procedures yet. OBJECTIVES. The present studies aimed to develop different adjuvant mechanistic therapies suitable for LTx optimization in general terms and regarding the multimodal LTx concept of the Mayo protocol for CCA patients. METHODS. We tested a new preservation solution with different chloride concentrations, erythropoietin (EPO) as well as platelet-derived growth factor (PDGF)-BB, hedgehog (Hh), or polo-like kinase (PLK)2 inhibitors for these purposes. We employed a full size and partial (30%, pLTx) rat LTx model as well as a syngeneic rat orthotopic CCA model in addition to human CCA samples as well as the human CCA cell lines KMCH-1/HUCCT-1/Mz-CHA-1 and human myofibroblastic (MFB) LX-2 cells for these studies. RESULTS. The new chloride-containing preservation solution improved rat overall survival by beneficial effects on microcirculation in sinusoids and postsinusoidal venules. EPO increased liver growth in unresected (donor) and pLTx recipient rats. Moreover, apoptosis clearly was reduced in pLTX liver grafts accompanied by longer recipient overall survival rates. The EPO effects, in part, were mediated by upregulation of the pro-regenerative *c-jun* and the anti-apoptotic Bcl-X_L gene. In the CCA-specific studies, targeting PDGF-BB or Hh signaling rendered CCA cells sensitive to apoptosis due to blockage of a Hh-dependent and MFB-derived protective effect of PDGF-BB. Additionally, PLK2 was identified as an important mediator of Hh survival signalling and PLK inhibition also proved to be pro-apoptotic. CONCLUSIONS. The present findings might be of therapeutic value for LTx procedures in general as well as the multimodal Mayo LTx protocol for CCA patients.

DOI:10.14753/SE.2016.1969

9 ÖSSZEFOGLALÓ

BEVEZETÉS. A májátültetés (LTx) ma már világszerte elfogadott eljárás a végállapotú májbetegségek, többek között a hepatocellularis carcinoma és szelektált esetekben a cholangiocelluláris carcinoma (CCA) kezelésére. Általánosan megfigyelhető új tendencia, hogy egyre több kiterjesztett kritériummal bíró májgraft (ECD-extended criteria donor) kerül beültetésre a donorok életkorának eltolódása miatt. A máj prezervációs ártalmai ezáltal új jelentőséggel bírnak és a beültetést követő iszkémiás-reperfúziós károsodás további kutatása is kiemelt fontosságú. Emiatt is időszerű, hogy a prezervációs károsodással kapcsolatos ismeretanyagokat átértékeljük és új elemekkel egészítsük ki. A daganatos beteségek miatt végzett májátültetések köre is bővül. Ide tartoznak az irreszekábilis cholangiocelluláris carcinoma szelektált esetei, ahol a pár évvel korábban bevezetett Mayo-protokoll átértékelése és kibővítése is aktuális. CÉLKITŰZÉSEK. A jelen tanulmány célja az eddig alkalmazott máj graft prezervációs eljárások vizsgálata, elemzése és új elemekkel történő kiegészítése. Továbbá olyan új lehetőségek kidolgozása, melyek hozzásegíthetnek a májátültetés további fejlődéséhez és sikerességéhez a multimodális Mayo protokoll szerint kezelt CCA betegeknél. MÓDSZEREK. Megvizsgáltunk egy új prezervációs oldatot eltérő klorid koncentrációval, elemeztük az eritropoetin, a „platelet-derived growth factor” (PDGF)-BB, a „hedgehog” (Hh)és a „poli-like kinase” (PLK)2 hatását a máj graft működésére. A vizsgálatokat teljes és szegmentum májátültetéssel járó, valamint szingeneikus orthotopikus patkány CCA állatkísérletes májtranszplantációs modellek segítségével végeztük el. Továbbá a humán CCA sejtvonalból származó, valamint KMCH-1/HUCCT-1/Mz/CHA-1 és és MFB LX-2 sejteket is vizsgáltunk in vitro. EREDMÉNYEK. Az új klorid-koncentrációjú prezervációs oldat jótékony hatással volt a mikrocirkulációra a sinusoidokban és post-sinusoid venulákban javította a patkányok túlélését a májtranszplantációt követően. Az EPO használata serkentette a máj növekedését, mind a donorban a májreszekciót követően, mind a májszegment transzplantáción átesett patkányokban. Az EPO hatásai részben a pro-regeneratív c-jun mediátor, részben a BcL-X_L anti-apoptikus gén serkentésével magyarázhatóak. CCA vizsgálatainkkal igazoltuk, hogy a célzott PDGFR-Beta és/vagy Hh jelátvitel kezelés elősegítheti a tumor-sejtek apoptózisát, az MFB-irányított PDGF-BB protektív hatás, és egy Hh jelátvitel-dependens folyamat gátlása révén. Ezeken felül a PLK2-nek kiemelkedő szerepe lehet a CCA sejtekben Hh túlélésért felelős jelátvitelében pro-apoptikus hatásai révén. KÖVETKEZTETÉS. Az eredményeink jelentősen hozzájárulhatnak a májgraftok prezervációs károsodásának csökkentéséhez és új adatokkal szolgálnak a parciális májátültetést követő májregeneráció pontosabb megismeréséhez. Továbbá a tanulmányban feltárt új utak és mechanizmusok elősegíthetik a cholangiocarcinoma miatt végzett májátültetés indikációjának kiszélesítését és az eredmények javítását.

10 BIBLIOGRAPHY

1. De Vreede I, Steers JL, Burch PA, Rosen CB, Gunderson LL, Haddock MG, Burgart L, Gores GJ. (2000) Prolonged disease-free survival after orthotopic liver transplantation plus adjuvant chemoirradiation for cholangiocarcinoma. Liver Transpl, 6:309-16.
2. Briceno J, Marchal T, Padillo J, Solorzano G, Pera C. (2002) Influence of marginal donors on liver preservation injury. Transplantation, 74:522-6.
3. Lemasters JJ, Thurman RG. (1997) Reperfusion injury after liver preservation for transplantation. Annu Rev Pharmacol Toxicol, 37:327-38.
4. Mittler J, Pascher A, Neuhaus P, Pratschke J. (2008) The utility of extended criteria donor organs in severely ill liver transplant recipients. Transplantation, 86:895-6.
5. Fuckert O, Rauen U, De Groot H. (2000) A role for sodium in hypoxic but not in hypothermic injury to hepatocytes and LLC-PK1 cells. Transplantation, 70:723-30.
6. Kohli V, Gao W, Camargo CA, Jr., Clavien PA. (1997) Calpain is a mediator of preservation-reperfusion injury in rat liver transplantation. Proc Natl Acad Sci U S A, 94:9354-9.
7. Rauen U, de Groot H. (2004) New insights into the cellular and molecular mechanisms of cold storage injury. J Investig Med, 52:299-309.
8. Rosser BG, Gores GJ. (1995) Liver cell necrosis: cellular mechanisms and clinical implications. Gastroenterology, 108:252-75.
9. Kerkweg U, Li T, de Groot H, Rauen U. (2002) Cold-induced apoptosis of rat liver cells in University of Wisconsin solution: the central role of chelatable iron. Hepatology, 35:560-7.
10. Salahudeen AK. (2004) Cold ischemic injury of transplanted kidneys: new insights from experimental studies. Am J Physiol Renal Physiol, 287:F181-7.
11. Currin RT, Thurman RG, Lemasters JJ. (1991) Carolina rinse solution protects adenosine triphosphate-depleted hepatocytes against lethal cell injury. Transplant Proc, 23:645-7.
12. Rauen U, Klempt S, de Groot H. (2007) Histidine-induced injury to cultured liver cells, effects of histidine derivatives and of iron chelators. Cell Mol Life Sci, 64:192-205.
13. Clavien PA, Harvey PR, Strasberg SM. (1992) Preservation and reperfusion injuries in liver allografts. An overview and synthesis of current studies. Transplantation, 53:957-78.
14. Jaeschke H. (1996) Preservation injury: mechanisms, prevention and consequences. J Hepatol, 25:774-80.

15. Bahde R, Palmes D, Gemsa O, Minin E, Stratmann U, de Groot H, Rauen U, Spiegel HU. (2008) Attenuated cold storage injury of rat livers using a modified HTK solution. J Surg Res, 146:49-56.
16. Bartels-Stringer M, Kramers C, Wetzels JF, Russel FG, Groot H, Rauen U. (2003) Hypothermia causes a marked injury to rat proximal tubular cells that is aggravated by all currently used preservation solutions. Cryobiology, 47:82-91.
17. Rauen U, Kerkweg U, Wusteman MC, de Groot H. (2006) Cold-induced injury to porcine corneal endothelial cells and its mediation by chelatable iron: implications for corneal preservation. Cornea, 25:68-77.
18. Rauen U, Petrat F, Li T, De Groot H. (2000) Hypothermia injury/cold-induced apoptosis--evidence of an increase in chelatable iron causing oxidative injury in spite of low O2-/H2O2 formation. FASEB J, 14:1953-64.
19. Rauen U, Polzar B, Stephan H, Mannherz HG, de Groot H. (1999) Cold-induced apoptosis in cultured hepatocytes and liver endothelial cells: mediation by reactive oxygen species. Faseb J, 13:155-68.
20. Huang H, Salahudeen AK. (2002) Cold induces catalytic iron release of cytochrome P-450 origin: a critical step in cold storage-induced renal injury. Am J Transplant, 2:631-9.
21. Rauen U, Kerkweg U, Weisheit D, Petrat F, Sustmann R, de Groot H. (2003) Cold-induced apoptosis of hepatocytes: mitochondrial permeability transition triggered by nonmitochondrial chelatable iron. Free Radic Biol Med, 35:1664-78.
22. Rauen U, Kerkweg U, de Groot H. (2007) Iron-dependent vs. iron-independent cold-induced injury to cultured rat hepatocytes: a comparative study in physiological media and organ preservation solutions. Cryobiology, 54:77-86.
23. Wille T, de Groot H, Rauen U. (2008) Improvement of the cold storage of blood vessels with a vascular preservation solution. Study in porcine aortic segments. J Vasc Surg, 47:422-31.
24. Wille T. (2010; Medical Faculty of the University Duisburg-Essen, Germany) Optimierung der kalten Lagerung von Blutgefäßen. Dissertation
25. Broelsch CE, Whitington PF, Emond JC, Heffron TG, Thistlethwaite JR, Stevens L, Piper J, Whitington SH, Lichtor JL. (1991) Liver transplantation in children from living related donors. Surgical techniques and results. Ann Surg, 214:428-37; discussion 437-9.
26. Lo CM, Fan ST, Liu CL, Chan JK, Lam BK, Lau GK, Wei WI, Wong J. (1999) Minimum graft size for successful living donor liver transplantation. Transplantation, 68:1112-6.

27. Valentin-Gamazo C, Malago M, Karliova M, Lutz JT, Frilling A, Nadalin S, Testa G, Ruehm SG, Erim Y, Paul A, Lang H, Gerken G, Broelsch CE. (2004) Experience after the evaluation of 700 potential donors for living donor liver transplantation in a single center. Liver Transpl, 10:1087-96.
28. Bockhorn M, Frilling A, Benko T, Best J, Sheu SY, Trippler M, Schlaak JF, Broelsch CE. (2007) Tri-Iodothyronine as a Stimulator of Liver Regeneration after Partial and Subtotal Hepatectomy. Eur Surg Res, 39:58-63.
29. Bockhorn M, Goralski M, Prokofiev D, Dammann P, Grunewald P, Trippler M, Biglarnia A, Kamler M, Niehues EM, Frilling A, Broelsch CE, Schlaak JF. (2007) VEGF is Important for Early Liver Regeneration After Partial Hepatectomy. J Surg Res.
30. Erslev AJ. (1991) Erythropoietin. N Engl J Med, 324:1339-44.
31. Krantz SB. (1991) Erythropoietin. Blood, 77:419-34.
32. Jaquet K, Krause K, Tawakol-Khodai M, Geidel S, Kuck KH. (2002) Erythropoietin and VEGF exhibit equal angiogenic potential. Microvasc Res, 64:326-33.
33. Ribatti D, Vacca A, Roccaro AM, Crivellato E, Presta M. (2003) Erythropoietin as an angiogenic factor. Eur J Clin Invest, 33:891-6.
34. Tan CC, Eckardt KU, Ratcliffe PJ. (1991) Organ distribution of erythropoietin messenger RNA in normal and uremic rats. Kidney Int, 40:69-76.
35. Naughton BA, Kaplan SM, Roy M, Burdowski AJ, Gordon AS, Piliero SJ. (1977) Hepatic regeneration and erythropoietin production in the rat. Science, 196:301-2.
36. Dornfest BS, Naughton BA, Kolks GA, Liu P, Piliero SJ, Gordon AS. (1981) Recovery of an erythropoietin inducing factor from the regenerating rat liver. Ann Clin Lab Sci, 11:37-46.
37. Gordon AS, Naughton BA. (1980) Mechanisms of extrarenal erythropoietin (Ep) production. Exp Hematol, 8 Suppl 8:14-28.
38. Naughton BA, Birnbach DJ, Liu P, Kolks GA, Tung MZ, Piliero JA, Piliero SJ, Gordon AS. (1979) Reticuloendothelial system (RES) hyperfunction and erythropoietin (Ep) production in the regenerating liver. J Surg Oncol, 12:227-42.
39. Naughton GK, Naughton BA, Gordon AS. (1985) Erythropoietin production by macrophages in the regenerating liver. J Surg Oncol, 30:184-97.
40. Paul P, Rothmann SA, McMahon JT, Gordon AS. (1984) Erythropoietin secretion by isolated rat Kupffer cells. Exp Hematol, 12:825-30.

41. Naughton BA, Kolks GA, Arce JM, Liu P, Gamba-Vitalo C, Piliero SJ, Gordon AS. (1979) The regenerating liver: a site of erythropoiesis in the adult Long-Evans rat. Am J Anat, 156:159-67.
42. de Groen PC, Gores GJ, LaRusso NF, Gunderson LL, Nagorney DM. (1999) Biliary tract cancers. N Engl J Med, 341:1368-78.
43. Fingas CD, Katsounas A, Kahraman A, Siffert W, Jochum C, Gerken G, Nuckel H, Canbay A. (2010) Prognostic assessment of three single-nucleotide polymorphisms (GNB3 825C>T, BCL2-938C>A, MCL1-386C>G) in extrahepatic cholangiocarcinoma. Cancer Invest, 28:472-8.
44. Roberts SK, Ludwig J, Larusso NF. (1997) The pathobiology of biliary epithelia. Gastroenterology, 112:269-79.
45. Blechacz B, Gores GJ. (2008) Cholangiocarcinoma: advances in pathogenesis, diagnosis, and treatment. Hepatology, 48:308-21.
46. Ishimura N, Isomoto H, Bronk SF, Gores GJ. (2006) Trail induces cell migration and invasion in apoptosis-resistant cholangiocarcinoma cells. Am J Physiol Gastrointest Liver Physiol, 290:G129-36.
47. Kuperwasser C, Chavarria T, Wu M, Magrane G, Gray JW, Carey L, Richardson A, Weinberg RA. (2004) Reconstruction of functionally normal and malignant human breast tissues in mice. Proc Natl Acad Sci U S A, 101:4966-71.
48. Olumi AF, Grossfeld GD, Hayward SW, Carroll PR, Tlsty TD, Cunha GR. (1999) Carcinoma-associated fibroblasts direct tumor progression of initiated human prostatic epithelium. Cancer Res, 59:5002-11.
49. Rasanen K, Vaheri A. (2010) Activation of fibroblasts in cancer stroma. Exp Cell Res.
50. Dranoff JA, Wells RG. (2010) Portal fibroblasts: Underappreciated mediators of biliary fibrosis. Hepatology, 51:1438-44.
51. Wells RG. (2010) The epithelial-to-mesenchymal transition in liver fibrosis: here today, gone tomorrow? Hepatology, 51:737-40.
52. Erez N, Truitt M, Olson P, Arron ST, Hanahan D. (2010) Cancer-Associated Fibroblasts Are Activated in Incipient Neoplasia to Orchestrate Tumor-Promoting Inflammation in an NF-kappaB-Dependent Manner. Cancer Cell, 17:135-47.
53. Kalluri R, Zeisberg M. (2006) Fibroblasts in cancer. Nat Rev Cancer, 6:392-401.
54. Olive KP, Jacobetz MA, Davidson CJ, Gopinathan A, McIntyre D, Honess D, Madhu B, Goldgraben MA, Caldwell ME, Allard D, Frese KK, Denicola G, Feig C, Combs C, Winter SP, Ireland-Zecchini H, Reichelt S, Howat WJ, Chang A, Dhara M, Wang L,

Ruckert F, Grutzmann R, Pilarsky C, Izeradjene K, Hingorani SR, Huang P, Davies SE, Plunkett W, Egorin M, Hruban RH, Whitebread N, McGovern K, Adams J, Iacobuzio-Donahue C, Griffiths J, Tuveson DA. (2009) Inhibition of Hedgehog signaling enhances delivery of chemotherapy in a mouse model of pancreatic cancer. Science, 324:1457-61.

55. Chuaysri C, Thuwajit P, Paupairoj A, Chau-In S, Suthiphongchai T, Thuwajit C. (2009) Alpha-smooth muscle actin-positive fibroblasts promote biliary cell proliferation and correlate with poor survival in cholangiocarcinoma. Oncol Rep, 21:957-69.
56. Okabe H, Beppu T, Hayashi H, Horino K, Masuda T, Komori H, Ishikawa S, Watanabe M, Takamori H, Iyama K, Baba H. (2009) Hepatic stellate cells may relate to progression of intrahepatic cholangiocarcinoma. Ann Surg Oncol, 16:2555-64.
57. Omenetti A, Yang L, Li YX, McCall SJ, Jung Y, Sicklick JK, Huang J, Choi S, Suzuki A, Diehl AM. (2007) Hedgehog-mediated mesenchymal-epithelial interactions modulate hepatic response to bile duct ligation. Lab Invest, 87:499-514.
58. Omenetti A, Popov Y, Jung Y, Choi SS, Witek RP, Yang L, Brown KD, Schuppan D, Diehl AM. (2008) The hedgehog pathway regulates remodelling responses to biliary obstruction in rats. Gut, 57:1275-82.
59. Friedman SL. (2008) Hepatic stellate cells: protean, multifunctional, and enigmatic cells of the liver. Physiol Rev, 88:125-72.
60. Deming PB, Campbell SL, Baldor LC, Howe AK. (2008) Protein kinase A regulates 3-phosphatidylinositide dynamics during platelet-derived growth factor-induced membrane ruffling and chemotaxis. J Biol Chem, 283:35199-211.
61. Berman DM, Karhadkar SS, Maitra A, Montes De Oca R, Gerstenblith MR, Briggs K, Parker AR, Shimada Y, Eshleman JR, Watkins DN, Beachy PA. (2003) Widespread requirement for Hedgehog ligand stimulation in growth of digestive tract tumours. Nature, 425:846-51.
62. Saqui-Salces M, Merchant JL. (2010) Hedgehog signaling and gastrointestinal cancer. Biochim Biophys Acta, 1803:786-95.
63. Walterhouse DO, Yoon JW, Iannaccone PM. (1999) Developmental pathways: Sonic hedgehog-Patched-GLI. Environ Health Perspect, 107:167-71.
64. Milenkovic L, Scott MP. (2010) Not lost in space: trafficking in the hedgehog signaling pathway. Sci Signal, 3:pe14.
65. Yang Y, Lin X. (2010) Hedgehog signaling uses lipid metabolism to tune smoothened activation. Dev Cell, 19:3-4.

66. Yavari A, Nagaraj R, Owusu-Ansah E, Folick A, Ngo K, Hillman T, Call G, Rohatgi R, Scott MP, Banerjee U. (2010) Role of lipid metabolism in smoothened derepression in hedgehog signaling. Dev Cell, 19:54-65.
67. Kurita S, Mott JL, Almada LL, Bronk SF, Werneburg NW, Sun SY, Roberts LR, Fernandez-Zapico ME, Gores GJ. (2010) GLI3-dependent repression of DR4 mediates hedgehog antagonism of TRAIL-induced apoptosis. Oncogene, 29:4848-58.
68. Hirasaki S, Koide N, Ujike K, Shinji T, Tsuji T. (2001) Expression of Nov, CYR61 and CTGF genes in human hepatocellular carcinoma. Hepatology Research, 19:294-305.
69. Fingas CD, Bronk SF, Werneburg NW, Mott JL, Guicciardi ME, Cazanave SC, Mertens JC, Sirica AE, Gores GJ. (2011) Myofibroblast-derived PDGF-BB promotes hedgehog survival signaling in cholangiocarcinoma cells. Hepatology, 54:2076-88.
70. Kurita S, Mott JL, Cazanave SC, Fingas CD, Guicciardi ME, Bronk SF, Roberts LR, Fernandez-Zapico ME, Gores GJ. (2011) Hedgehog Inhibition Promotes a Switch from Type II to Type I Cell Death Receptor Signaling in Cancer Cells. PLoS One, 6:e18330.
71. El Khatib M, Kalnytska A, Palagani V, Kossatz U, Manns MP, Malek NP, Wilkens L, Plentz RR. (2013) Inhibition of hedgehog signaling attenuates carcinogenesis in vitro and increases necrosis of cholangiocellular carcinoma. Hepatology, 57:1035-45.
72. Barr FA, Sillje HH, Nigg EA. (2004) Polo-like kinases and the orchestration of cell division. Nat Rev Mol Cell Biol, 5:429-40.
73. de Carcer G, Manning G, Malumbres M. (2011) From Plk1 to Plk5: functional evolution of polo-like kinases. Cell Cycle, 10:2255-62.
74. Strebhardt K. (2010) Multifaceted polo-like kinases: drug targets and antitargets for cancer therapy. Nat Rev Drug Discov, 9:643-60.
75. Schoffski P. (2009) Polo-like kinase (PLK) inhibitors in preclinical and early clinical development in oncology. Oncologist, 14:559-70.
76. Feng YB, Lin DC, Shi ZZ, Wang XC, Shen XM, Zhang Y, Du XL, Luo ML, Xu X, Han YL, Cai Y, Zhang ZQ, Zhan QM, Wang MR. (2009) Overexpression of PLK1 is associated with poor survival by inhibiting apoptosis via enhancement of survivin level in esophageal squamous cell carcinoma. Int J Cancer, 124:578-88.
77. Liu X, Choy E, Harmon D, Yang S, Yang C, Mankin H, Hornicek FJ, Duan Z. (2011) Inhibition of polo-like kinase 1 leads to the suppression of osteosarcoma cell growth in vitro and in vivo. Anticancer Drugs, 22:444-53.

78. Isomoto H, Kobayashi S, Werneburg NW, Bronk SF, Guicciardi ME, Frank DA, Gores GJ. (2005) Interleukin 6 upregulates myeloid cell leukemia-1 expression through a STAT3 pathway in cholangiocarcinoma cells. Hepatology, 42:1329-38.
79. Okaro AC, Deery AR, Hutchins RR, Davidson BR. (2001) The expression of antiapoptotic proteins Bcl-2, Bcl-X(L), and Mcl-1 in benign, dysplastic, and malignant biliary epithelium. J Clin Pathol, 54:927-32.
80. Taniai M, Grambihler A, Higuchi H, Werneburg N, Bronk SF, Farrugia DJ, Kaufmann SH, Gores GJ. (2004) Mcl-1 mediates tumor necrosis factor-related apoptosis-inducing ligand resistance in human cholangiocarcinoma cells. Cancer Res, 64:3517-24.
81. Rudolph D, Steegmaier M, Hoffmann M, Grauert M, Baum A, Quant J, Haslinger C, Garin-Chesa P, Adolf GR. (2009) BI 6727, a Polo-like kinase inhibitor with improved pharmacokinetic profile and broad antitumor activity. Clin Cancer Res, 15:3094-102.
82. Masuoka HC, Mott J, Bronk SF, Werneburg NW, Akazawa Y, Kaufmann SH, Gores GJ. (2009) Mcl-1 degradation during hepatocyte lipoapoptosis. J Biol Chem, 284:30039-48.
83. Anan A, Baskin-Bey ES, Bronk SF, Werneburg NW, Shah VH, Gores GJ. (2006) Proteasome inhibition induces hepatic stellate cell apoptosis. Hepatology, 43:335-44.
84. Blechacz BR, Smoot RL, Bronk SF, Werneburg NW, Sirica AE, Gores GJ. (2009) Sorafenib inhibits signal transducer and activator of transcription-3 signaling in cholangiocarcinoma cells by activating the phosphatase shatterproof 2. Hepatology, 50:1861-70.
85. Fingas CD, Blechacz BR, Smoot RL, Guicciardi ME, Mott J, Bronk SF, Werneburg NW, Sirica AE, Gores GJ. (2010) A smac mimetic reduces TNF related apoptosis inducing ligand (TRAIL)-induced invasion and metastasis of cholangiocarcinoma cells. Hepatology, 52:550-61.
86. Sirica AE, Zhang Z, Lai GH, Asano T, Shen XN, Ward DJ, Mahatme A, Dewitt JL. (2008) A novel "patient-like" model of cholangiocarcinoma progression based on bile duct inoculation of tumorigenic rat cholangiocyte cell lines. Hepatology, 47:1178-1190.
87. Anthuber M, Farkas S, Rihl M, Menger MD, Schildberg FW, Jauch KW, Messmer K. (1997) Angiotensin-converting enzyme inhibition by enalapril: a novel approach to reduce ischemia/reperfusion damage after experimental liver transplantation. Hepatology, 25:648-51.
88. Steyer JA, Almers W. (2001) A real-time view of life within 100 nm of the plasma membrane. Nat Rev Mol Cell Biol, 2:268-75.

89. Malhi H, Barreyro FJ, Isomoto H, Bronk SF, Gores GJ. (2007) Free fatty acids sensitise hepatocytes to TRAIL mediated cytotoxicity. Gut, 56:1124-31.
90. Isomoto H, Mott JL, Kobayashi S, Werneburg NW, Bronk SF, Haan S, Gores GJ. (2007) Sustained IL-6/STAT-3 signaling in cholangiocarcinoma cells due to SOCS-3 epigenetic silencing. Gastroenterology, 132:384-96.
91. Schlaak JF, Hilkens CM, Costa-Pereira AP, Strobl B, Aberger F, Frischauf AM, Kerr IM. (2002) Cell-type and donor-specific transcriptional responses to interferon-alpha. Use of customized gene arrays. J Biol Chem, 277:49428-37.
92. Sasaki H, Hui C, Nakafuku M, Kondoh H. (1997) A binding site for Gli proteins is essential for HNF-3beta floor plate enhancer activity in transgenics and can respond to Shh in vitro. Development, 124:1313-22.
93. Kamada N, Calne RY. (1979) Orthotopic liver transplantation in the rat. Technique using cuff for portal vein anastomosis and biliary drainage. Transplantation, 28:47-50.
94. van den Brink GR, Bleuming SA, Hardwick JC, Schepman BL, Offerhaus GJ, Keller JJ, Nielsen C, Gaffield W, van Deventer SJ, Roberts DJ, Peppelenbosch MP. (2004) Indian Hedgehog is an antagonist of Wnt signaling in colonic epithelial cell differentiation. Nat Genet, 36:277-82.
95. van den Brink GR, Hardwick JC, Tytgat GN, Brink MA, Ten Kate FJ, Van Deventer SJ, Peppelenbosch MP. (2001) Sonic hedgehog regulates gastric gland morphogenesis in man and mouse. Gastroenterology, 121:317-28.
96. Andrae J, Gallini R, Betsholtz C. (2008) Role of platelet-derived growth factors in physiology and medicine. Genes Dev, 22:1276-312.
97. Taipale J, Chen JK, Cooper MK, Wang B, Mann RK, Milenkovic L, Scott MP, Beachy PA. (2000) Effects of oncogenic mutations in Smoothened and Patched can be reversed by cyclopamine. Nature, 406:1005-9.
98. Hallikas O, Palin K, Sinjushina N, Rautiainen R, Partanen J, Ukkonen E, Taipale J. (2006) Genome-wide prediction of mammalian enhancers based on analysis of transcription-factor binding affinity. Cell, 124:47-59.
99. Regl G, Kasper M, Schnidar H, Eichberger T, Neill GW, Philpott MP, Esterbauer H, Hauser-Kronberger C, Frischauf AM, Aberger F. (2004) Activation of the BCL2 promoter in response to Hedgehog/GLI signal transduction is predominantly mediated by GLI2. Cancer Res, 64:7724-31.

100. Hu MC, Mo R, Bhella S, Wilson CW, Chuang PT, Hui CC, Rosenblum ND. (2006) GLI3-dependent transcriptional repression of Gli1, Gli2 and kidney patterning genes disrupts renal morphogenesis. Development, 133:569-78.
101. Kobayashi S, Lee SH, Meng XW, Mott JL, Bronk SF, Werneburg NW, Craig RW, Kaufmann SH, Gores GJ. (2007) Serine 64 phosphorylation enhances the antiapoptotic function of Mcl-1. J Biol Chem, 282:18407-17.
102. Brecht M, Brecht C, De Groot H. (1992) Late steady increase in cytosolic Ca2+ preceding hypoxic injury in hepatocytes. Biochem J, 283 (Pt 2):399-402.
103. Carini R, Autelli R, Bellomo G, Dianzani MU, Albano E. (1995) Sodium-mediated cell swelling is associated with irreversible damage in isolated hepatocytes exposed to hypoxia or mitochondrial toxins. Biochem Biophys Res Commun, 206:180-5.
104. Carini R, Bellomo G, Benedetti A, Fulceri R, Gamberucci A, Parola M, Dianzani MU, Albano E. (1995) Alteration of Na+ homeostasis as a critical step in the development of irreversible hepatocyte injury after adenosine triphosphate depletion. Hepatology, 21:1089-98.
105. Carini R, De Cesaris MG, Splendore R, Bagnati M, Bellomo G, Albano E. (2000) Alterations of Na(+) homeostasis in hepatocyte reoxygenation injury. Biochim Biophys Acta, 1500:297-305.
106. Frank A, Rauen U, de Groot H. (2000) Protection by glycine against hypoxic injury of rat hepatocytes: inhibition of ion fluxes through nonspecific leaks. J Hepatol, 32:58-66.
107. Rauen U, de Groot H. (1998) Cold-induced release of reactive oxygen species as a decisive mediator of hypothermia injury to cultured liver cells. Free Radic Biol Med, 24:1316-23.
108. Schroder C, Heintz A, Pexa A, Rauen U, Deussen A. (2007) Preclinical evaluation of coronary vascular function after cardioplegia with HTK and different antioxidant additives. Eur J Cardiothorac Surg, 31:821-6.
109. Vairetti M, Ferrigno A, Bertone R, Richelmi P, Berte F, Freitas I. (2005) Apoptosis vs. necrosis: glutathione-mediated cell death during rewarming of rat hepatocytes. Biochim Biophys Acta, 1740:367-74.
110. Vairetti M, Griffini P, Pietrocola G, Richelmi P, Freitas I. (2001) Cold-induced apoptosis in isolated rat hepatocytes: protective role of glutathione. Free Radic Biol Med, 31:954-61.

111. Schemmer P, Bradford BU, Rose ML, Bunzendahl H, Raleigh JA, Lemasters JJ, Thurman RG. (1999) Intravenous glycine improves survival in rat liver transplantation. Am J Physiol, 276:G924-32.
112. Schemmer P, Bunzendahl H, Klar E, Thurman RG. (2000) Reperfusion injury is dramatically increased by gentle liver manipulation during harvest. Transpl Int, 13 Suppl 1:S525-7.
113. Schemmer P, Enomoto N, Bradford BU, Bunzendahl H, Raleigh JA, Lemasters JJ, Thurman RG. (2001) Activated Kupffer cells cause a hypermetabolic state after gentle in situ manipulation of liver in rats. Am J Physiol Gastrointest Liver Physiol, 280:G1076-82.
114. Brecht M, de Groot H. (1994) Protection from hypoxic injury in cultured hepatocytes by glycine, alanine, and serine. Amino Acids, 6:25-35.
115. Arnault I, Bao YM, Dimicoli JL, Lemoine A, Sebagh M, Adam R. (2002) Combined effects of fasting and alanine on liver function recovery after cold ischemia. Transpl Int, 15:89-95.
116. Weinberg JM, Venkatachalam MA, Roeser NF, Nissim I. (2000) Mitochondrial dysfunction during hypoxia/reoxygenation and its correction by anaerobic metabolism of citric acid cycle intermediates. Proc Natl Acad Sci U S A, 97:2826-31.
117. Clemens MG. (1999) Nitric oxide in liver injury. Hepatology, 30:1-5.
118. Shiraishi M, Hiroyasu S, Nagahama M, Miyaguni T, Higa T, Tomori H, Okuhama Y, Kusano T, Muto Y. (1997) Role of exogenous L-arginine in hepatic ischemia-reperfusion injury. J Surg Res, 69:429-34.
119. Wang Y, Mathews WR, Guido DM, Farhood A, Jaeschke H. (1995) Inhibition of nitric oxide synthesis aggravates reperfusion injury after hepatic ischemia and endotoxemia. Shock, 4:282-8.
120. Rodriguez JV, Guibert EE, Quintana A, Scandizzi A, Almada L. (1999) Role of sodium nitroprusside in the improvement of rat liver preservation in University of Wisconsin solution: A study in the isolated perfused liver model. J Surg Res, 87:201-8.
121. Yagnik GP, Takahashi Y, Tsoulfas G, Reid K, Murase N, Geller DA. (2002) Blockade of the L-arginine/NO synthase pathway worsens hepatic apoptosis and liver transplant preservation injury. Hepatology, 36:573-81.
122. El-Wahsh M. (2007) Liver graft preservation: an overview. Hepatobiliary Pancreat Dis Int, 6:12-6.

123. Sumimoto R, Kamada N, Jamieson NV, Fukuda Y, Dohi K. (1991) A comparison of a new solution combining histidine and lactobionate with UW solution and eurocollins for rat liver preservation. Transplantation, 51:589-93.
124. Stegemann J, Hirner A, Rauen U, Minor T. (2009) Gaseous oxygen persufflation or oxygenated machine perfusion with Custodiol-N for long-term preservation of ischemic rat livers? Cryobiology, 58:45-51.
125. Stegemann J, Hirner A, Rauen U, Minor T. (2010) Use of a new modified HTK solution for machine preservation of marginal liver grafts. J Surg Res, 160:155-62.
126. Wu S, Wohlschlaeger J, de Groot H, Rauen U. (2009) Evaluation of a modified HTK solution containing the new iron chelator LK 614 in an isolated rat liver perfusion model. J Invest Surg, 22:340-7.
127. Tsukimoto M, Harada H, Ikari A, Takagi K. (2005) Involvement of chloride in apoptotic cell death induced by activation of ATP-sensitive P2X7 purinoceptor. J Biol Chem, 280:2653-8.
128. Heimlich G, Cidlowski JA. (2006) Selective role of intracellular chloride in the regulation of the intrinsic but not extrinsic pathway of apoptosis in Jurkat T-cells. J Biol Chem, 281:2232-41.
129. Carini R, Bellomo G, Grazia De Cesaris M, Albano E. (1997) Glycine protects against hepatocyte killing by KCN or hypoxia by preventing intracellular Na+ overload in the rat. Hepatology, 26:107-12.
130. Benedetti A, Strazzabosco M, Corasanti JG, Haddad P, Graf J, Boyer JL. (1991) Cl(-)-HCO3- exchanger in isolated rat hepatocytes: role in regulation of intracellular pH. Am J Physiol, 261:G512-22.
131. Bowers BA, Branum GD, Rotolo FS, Watters CR, Meyers WC. (1987) Bile flow--an index of ischemic injury. J Surg Res, 42:565-9.
132. Sumimoto K, Inagaki K, Yamada K, Kawasaki T, Dohi K. (1988) Reliable indices for the determination of viability of grafted liver immediately after orthotopic transplantation. Bile flow rate and cellular adenosine triphosphate level. Transplantation, 46:506-9.
133. Todo S, Nery J, Yanaga K, Podesta L, Gordon RD, Starzl TE. (1989) Extended preservation of human liver grafts with UW solution. Jama, 261:711-4.
134. Feng L, Zhao N, Yao X, Sun X, Du L, Diao X, Li S, Li Y. (2007) Histidine-tryptophan-ketoglutarate solution vs. University of Wisconsin solution for liver transplantation: a systematic review. Liver Transpl, 13:1125-36.

135. Mangus RS, Fridell JA, Vianna RM, Milgrom MA, Chestovich P, Chihara RK, Tector AJ. (2008) Comparison of histidine-tryptophan-ketoglutarate solution and University of Wisconsin solution in extended criteria liver donors. Liver Transpl, 14:365-73.
136. Sumimoto R, Jamieson NV, Kamada N. (1990) Examination of the role of the impermeants lactobionate and raffinose in a modified UW solution. Transplantation, 50:573-6.
137. Caldwell-Kenkel JC, Currin RT, Tanaka Y, Thurman RG, Lemasters JJ. (1989) Reperfusion injury to endothelial cells following cold ischemic storage of rat livers. Hepatology, 10:292-9.
138. Caldwell-Kenkel JC, Currin RT, Tanaka Y, Thurman RG, Lemasters JJ. (1991) Kupffer cell activation and endothelial cell damage after storage of rat livers: effects of reperfusion. Hepatology, 13:83-95.
139. Caldwell-Kenkel JC, Thurman RG, Lemasters JJ. (1988) Selective loss of nonparenchymal cell viability after cold ischemic storage of rat livers. Transplantation, 45:834-7.
140. Gao W, Bentley RC, Madden JF, Clavien PA. (1998) Apoptosis of sinusoidal endothelial cells is a critical mechanism of preservation injury in rat liver transplantation. Hepatology, 27:1652-60.
141. Marzi I, Zhong Z, Lemasters JJ, Thurman RG. (1989) Evidence that graft survival is not related to parenchymal cell viability in rat liver transplantation. The importance of nonparenchymal cells. Transplantation, 48:463-8.
142. DeLeve LD, Wang X, Kuhlenkamp JF, Kaplowitz N. (1996) Toxicity of azathioprine and monocrotaline in murine sinusoidal endothelial cells and hepatocytes: the role of glutathione and relevance to hepatic venoocclusive disease. Hepatology, 23:589-99.
143. Hamer I, Wattiaux R, Wattiaux-De Coninck S. (1995) Deleterious effects of xanthine oxidase on rat liver endothelial cells after ischemia/reperfusion. Biochim Biophys Acta, 1269:145-52.
144. Malik R, Habib M, Tootle R, Hodgson H. (2005) Exogenous thyroid hormone induces liver enlargement, whilst maintaining regenerative potential--a study relevant to donor preconditioning. Am J Transplant, 5:1801-7.
145. Sepodes B, Maio R, Pinto R, Sharples E, Oliveira P, McDonald M, Yaqoob M, Thiemermann C, Mota-Filipe H. (2006) Recombinant human erythropoietin protects the liver from hepatic ischemia-reperfusion injury in the rat. Transpl Int, 19:919-26.

146. Malik R, Mellor N, Selden C, Hodgson H. (2003) Triiodothyronine enhances the regenerative capacity of the liver following partial hepatectomy. Hepatology, 37:79-86.
147. Jacobs-Helber SM, Wickrema A, Birrer MJ, Sawyer ST. (1998) AP1 regulation of proliferation and initiation of apoptosis in erythropoietin-dependent erythroid cells. Mol Cell Biol, 18:3699-707.
148. Seong SR, Lee JW, Lee YK, Kim TI, Son DJ, Moon DC, Yun YW, Yoon do Y, Hong JT. (2006) Stimulation of cell growth by erythropoietin in RAW264.7 cells: association with AP-1 activation. Arch Pharm Res, 29:218-23.
149. Behrens A, Sibilia M, David JP, Mohle-Steinlein U, Tronche F, Schutz G, Wagner EF. (2002) Impaired postnatal hepatocyte proliferation and liver regeneration in mice lacking c-jun in the liver. Embo J, 21:1782-90.
150. Fausto N, Campbell JS, Riehle KJ. (2006) Liver regeneration. Hepatology, 43:S45-53.
151. Bakiri L, Lallemand D, Bossy-Wetzel E, Yaniv M. (2000) Cell cycle-dependent variations in c-Jun and JunB phosphorylation: a role in the control of cyclin D1 expression. Embo J, 19:2056-68.
152. Liu YC, Chang HW, Lai YC, Ding ST, Ho JL. (1998) Serum responsiveness of the rat PCNA promoter involves the proximal ATF and AP-1 sites. FEBS Lett, 441:200-4.
153. Shaulian E, Schreiber M, Piu F, Beeche M, Wagner EF, Karin M. (2000) The mammalian UV response: c-Jun induction is required for exit from p53-imposed growth arrest. Cell, 103:897-907.
154. Wisdom R, Johnson RS, Moore C. (1999) c-Jun regulates cell cycle progression and apoptosis by distinct mechanisms. Embo J, 18:188-97.
155. Hilberg F, Aguzzi A, Howells N, Wagner EF. (1993) c-jun is essential for normal mouse development and hepatogenesis. Nature, 365:179-81.
156. Calvillo L, Latini R, Kajstura J, Leri A, Anversa P, Ghezzi P, Salio M, Cerami A, Brines M. (2003) Recombinant human erythropoietin protects the myocardium from ischemia-reperfusion injury and promotes beneficial remodeling. Proc Natl Acad Sci U S A, 100:4802-6.
157. Brines M, Grasso G, Fiordaliso F, Sfacteria A, Ghezzi P, Fratelli M, Latini R, Xie QW, Smart J, Su-Rick CJ, Pobre E, Diaz D, Gomez D, Hand C, Coleman T, Cerami A. (2004) Erythropoietin mediates tissue protection through an erythropoietin and common beta-subunit heteroreceptor. Proc Natl Acad Sci U S A, 101:14907-12.

158. Celik M, Gokmen N, Erbayraktar S, Akhisaroglu M, Konakc S, Ulukus C, Genc S, Genc K, Sagiroglu E, Cerami A, Brines M. (2002) Erythropoietin prevents motor neuron apoptosis and neurologic disability in experimental spinal cord ischemic injury. Proc Natl Acad Sci U S A, 99:2258-63.
159. Abdelrahman M, Sharples EJ, McDonald MC, Collin M, Patel NS, Yaqoob MM, Thiemermann C. (2004) Erythropoietin attenuates the tissue injury associated with hemorrhagic shock and myocardial ischemia. Shock, 22:63-9.
160. Eferl R, Ricci R, Kenner L, Zenz R, David JP, Rath M, Wagner EF. (2003) Liver tumor development. c-Jun antagonizes the proapoptotic activity of p53. Cell, 112:181-92.
161. Eferl R, Sibilia M, Hilberg F, Fuchsbichler A, Kufferath I, Guertl B, Zenz R, Wagner EF, Zatloukal K. (1999) Functions of c-Jun in liver and heart development. J Cell Biol, 145:1049-61.
162. Hu GH, Lu XS. (2005) Effect of normothermic liver ischemic preconditioning on the expression of apoptosis-regulating genes C-jun and Bcl-XL in rats. World J Gastroenterol, 11:2579-82.
163. Gewirtz DA, Di X, Walker TD, Sawyer ST. (2006) Erythropoietin fails to interfere with the antiproliferative and cytotoxic effects of antitumor drugs. Clin Cancer Res, 12:2232-8.
164. Xu AM, Huang PH. (2010) Receptor tyrosine kinase coactivation networks in cancer. Cancer Res, 70:3857-60.
165. Graves LM, Bornfeldt KE, Sidhu JS, Argast GM, Raines EW, Ross R, Leslie CC, Krebs EG. (1996) Platelet-derived growth factor stimulates protein kinase A through a mitogen-activated protein kinase-dependent pathway in human arterial smooth muscle cells. J Biol Chem, 271:505-11.
166. Yauch RL, Gould SE, Scales SJ, Tang T, Tian H, Ahn CP, Marshall D, Fu L, Januario T, Kallop D, Nannini-Pepe M, Kotkow K, Marsters JC, Rubin LL, de Sauvage FJ. (2008) A paracrine requirement for hedgehog signalling in cancer. Nature, 455:406-10.
167. Singh S, Wang Z, Liang Fei D, Black KE, Goetz JA, Tokhunts R, Giambelli C, Rodriguez-Blanco J, Long J, Lee E, Briegel KJ, Bejarano PA, Dmitrovsky E, Capobianco AJ, Robbins DJ. (2011) Hedgehog-Producing Cancer Cells Respond to and Require Autocrine Hedgehog Activity. Cancer Res, 71:4454-4463.
168. Metcalfe C, de Sauvage FJ. (2011) Hedgehog fights back: mechanisms of acquired resistance against Smoothened antagonists. Cancer Res, 71:5057-61.

169. Yauch RL, Dijkgraaf GJ, Alicke B, Januario T, Ahn CP, Holcomb T, Pujara K, Stinson J, Callahan CA, Tang T, Bazan JF, Kan Z, Seshagiri S, Hann CL, Gould SE, Low JA, Rudin CM, de Sauvage FJ. (2009) Smoothened mutation confers resistance to a Hedgehog pathway inhibitor in medulloblastoma. Science, 326:572-4.
170. Thrum S, Lorenz J, Mossner J, Wiedmann M. (2011) Polo-like kinase 1 inhibition as a new therapeutic modality in therapy of cholangiocarcinoma. Anticancer Res, 31:3289-99.
171. Coley HM, Hatzimichael E, Blagden S, McNeish I, Thompson A, Crook T, Syed N. (2012) Polo Like Kinase 2 Tumour Suppressor and cancer biomarker: new perspectives on drug sensitivity/resistance in ovarian cancer. Oncotarget, 3:78-83.
172. Winkles JA, Alberts GF. (2005) Differential regulation of polo-like kinase 1, 2, 3, and 4 gene expression in mammalian cells and tissues. Oncogene, 24:260-6.
173. Feng GS. (2012) Conflicting roles of molecules in hepatocarcinogenesis: paradigm or paradox. Cancer Cell, 21:150-4.

DOI:10.14753/SE.2016.1969

11 BIBLIOGRAPHY OF THE CANDIDATE'S PUBLICATIONS

11.1 Publications Related To The PhD Thesis

1. Bockhorn M, Fingas CD*, Rauen U, Canbay A, Sotiropoulos GC, Frey U, Sheu SY, Wohlschlager J, Broelsch CE, Schlaak JF. (2008) Erythropoietin treatment improves liver regeneration and survival in rat models of extended liver resection and living donor liver transplantation. Transplantation, 86:1578-85. (*joint 1st authorship)
2. Fingas CD, Wu S, Gu Y, Wohlschlaeger J, Scherag A, Dahmen U, Paul A, de Groot H, Rauen U. (2011) Assessment of a chloride-poor versus a chloride-containing version of a modified histidine-tryptophan-ketoglutarate solution in a rat liver transplantation model. Liver Transpl, 17:650-60.
3. Fingas CD, Bronk SF, Werneburg NW, Mott JL, Guicciardi ME, Cazanave SC, Mertens JC, Sirica AE, Gores GJ. (2011) Myofibroblast-derived PDGF-BB promotes hedgehog survival signaling in cholangiocarcinoma cells. Hepatology, 54:2076-88.
4. Fingas CD, Mertens JC, Razumilava N, Bronk SF, Sirica AE, Gores GJ. (2012) Targeting PDGFR-beta in Cholangiocarcinoma. Liver Int, 32:400-9.
5. Fingas CD, Mertens JC, Razumilava N, Sydor S, Bronk SF, Christensen JD, Rizvi SH, Canbay A, Treckmann JW, Paul A, Sirica AE, Gores GJ. (2013) Polo-like kinase 2 is a mediator of hedgehog survival signaling in cholangiocarcinoma. Hepatology, 58:1362-74.

11.2 Publications Not Related To The PhD Thesis

1. Bechmann LP, Zahn D, Gieseler RK, Fingas CD, Marquitan G, Jochum C, Gerken G, Friedman SL, Canbay A. (2009) Resveratrol amplifies profibrogenic effects of free fatty acids on human hepatic stellate cells. Hepatol Res, 39:601-8.
2. Bockhorn M, Sotiropoulos G, Neuhaus J, Sgourakis G, Sheu SY, Molmenti E, Fingas C, Trarbach T, Frilling A, Broelsch CE. (2009) Prognostic impact of intrahepatic lymphatic and microvascular involvement in cases of colorectal liver metastases. Int J Colorectal Dis, 24:845-50.
3. Cazanave SC, Mott JL, Bronk SF, Werneburg NW, Fingas CD, Meng XW, Finnberg N, El-Deiry WS, Kaufmann SH, Gores GJ. (2011) Death receptor 5 signaling promotes hepatocyte lipoapoptosis. J Biol Chem, 286:39336-48.
4. Dechene A, Jochum C, Fingas C, Paul A, Heider D, Syn WK, Gerken G, Canbay A, Zopf T. (2014) Endoscopic management is the treatment of choice for bile leaks after liver resection. Gastrointest Endosc, 80:626-633 e1.
5. Decking UK, Pai VM, Bennett E, Taylor JL, Fingas CD, Zanger K, Wen H, Balaban RS. (2004) High-resolution imaging reveals a limit in spatial resolution of blood flow measurements by microspheres. Am J Physiol Heart Circ Physiol, 287:H1132-40.
6. Fingas CD, Altinbas A, Schlattjan M, Beilfuss A, Sowa JP, Sydor S, Bechmann LP, Ertle J, Akkiz H, Herzer K, Paul A, Gerken G, Baba HA, Canbay A. (2013) Expression of apoptosis- and vitamin D pathway-related genes in hepatocellular carcinoma. Digestion, 87:176-81.
7. Fingas CD, Blechacz BR, Smoot RL, Guicciardi ME, Mott J, Bronk SF, Werneburg NW, Sirica AE, Gores GJ. (2010) A smac mimetic reduces TNF related apoptosis inducing ligand (TRAIL)-induced invasion and metastasis of cholangiocarcinoma cells. Hepatology, 52:550-61.
8. Fingas CD, Katsounas A, Kahraman A, Siffert W, Jochum C, Gerken G, Nuckel H, Canbay A. (2010) Prognostic assessment of three single-nucleotide polymorphisms (GNB3 825C>T, BCL2-938C>A, MCL1-386C>G) in extrahepatic cholangiocarcinoma. Cancer Invest, 28:472-8.
9. Flogel U, Laussmann T, Godecke A, Abanador N, Schafers M, Fingas CD, Metzger S, Levkau B, Jacoby C, Schrader J. (2005) Lack of myoglobin causes a switch in cardiac substrate selection. Circ Res, 96:e68-75.

10. Guicciardi ME, Mott JL, Bronk SF, Kurita S, Fingas CD, Gores GJ. (2011) Cellular inhibitor of apoptosis 1 (cIAP-1) degradation by caspase 8 during TNF-related apoptosis-inducing ligand (TRAIL)-induced apoptosis. Exp Cell Res, 317:107-16.
11. Herzer K, Fingas CD, Canbay A. (2012) Does ursodeoxycholic acid exert a protective effect on liver grafts in orthotopic liver transplantation? Digestion, 86:206-7.
12. Heuer M, Dreger NM, Cicinnati VR, Fingas C, Juntermanns B, Paul A, Kaiser GM. (2012) Tumor growth effects of rapamycin on human biliary tract cancer cells. Eur J Med Res, 17:20.
13. Juntermanns B, Grabellus F, Zhang H, Radunz S, Bernheim J, Fingas CD, Sauerwein W, Paul A, Kaiser GM. (2014) Vascular and nerval damage after intraoperative radiation therapy of the liver hilum in a large animal model. J Invest Surg, 27:163-8.
14. Kahraman A, Fingas CD, Syn WK, Gerken G, Canbay A. (2012) Role of stress-induced NKG2D ligands in liver diseases. Liver Int, 32:370-82.
15. Kahraman A, Schlattjan M, Kocabayoglu P, Yildiz-Meziletoglu S, Schlensak M, Fingas CD, Wedemeyer I, Marquitan G, Gieseler RK, Baba HA, Gerken G, Canbay A. (2010) Major histocompatibility complex class I-related chains A and B (MIC A/B): a novel role in nonalcoholic steatohepatitis. Hepatology, 51:92-102.
16. Kakisaka K, Cazanave SC, Fingas CD, Guicciardi ME, Bronk SF, Werneburg NW, Mott JL, Gores GJ. (2012) Mechanisms of lysophosphatidylcholine-induced hepatocyte lipoapoptosis. Am J Physiol Gastrointest Liver Physiol, 302:G77-84.
17. Kilicarslan A, Kahraman A, Akkiz H, Yildiz Menziletoglu S, Fingas CD, Gerken G, Canbay A. (2009) Apoptosis in selected liver diseases. Turk J Gastroenterol, 20:171-9.
18. Kurita S, Mott JL, Cazanave SC, Fingas CD, Guicciardi ME, Bronk SF, Roberts LR, Fernandez-Zapico ME, Gores GJ. (2011) Hedgehog inhibition promotes a switch from Type II to Type I cell death receptor signaling in cancer cells. PLoS One, 6:e18330.
19. Laussmann T, Janosi RA, Fingas CD, Schlieper GR, Schlack W, Schrader J, Decking UK. (2002) Myocardial proteome analysis reveals reduced NOS inhibition and enhanced glycolytic capacity in areas of low local blood flow. FASEB J, 16:628-30.
20. Mertens JC, Fingas CD, Christensen JD, Smoot RL, Bronk SF, Werneburg NW, Gustafson MP, Dietz AB, Roberts LR, Sirica AE, Gores GJ. (2013) Therapeutic effects of deleting cancer-associated fibroblasts in cholangiocarcinoma. Cancer Res, 73:897-907.

21. Razumilava N, Bronk SF, Smoot RL, Fingas CD, Werneburg NW, Roberts LR, Mott JL. (2012) miR-25 targets TNF-related apoptosis inducing ligand (TRAIL) death receptor-4 and promotes apoptosis resistance in cholangiocarcinoma. Hepatology, 55:465-75.

12 ACKNOWLEDGEMENTS

First of all, the superb supervision of Zoltan Mathé is gratefully acknowledged. I also want to thank U. Rauen/M. Bockhorn/A. Paul and G. Gores/A. Canbay for their pivotal help with the experiments performed at the Institute of Physiological Chemistry/Department of General, Visceral and Transplantation Surgery, University Hospital Essen, Germany as well as the Department of GI Research, Mayo Clinic, Rochester, Minnesota, USA, respectively.

The Affymetrix U133 Plus 2.0 GeneChip analysis was performed in collaboration with the Genomics Technology Center Core and Y. Li from the Division of Biomedical Statistics and Informatics (Mayo Clinic). The human primary myofibroblastic HSCs were kindly provided by V. H. Shah. U. Yaqoob helped with the immunoblotting for (phospho-)PDGFR-β. The pRK7 plasmid containing the human SMO sequence and the 8x-GLI reporter was a generous gift from M. Fernandez-Zapico. Imatinib mesylate/STI-571 was obtained from E. B. Leof. The mouse anti-S peptide antibody was provided by S. H. Kaufmann. Finally, the excellent secretarial and technical service of C. Hoover, L. Wingerter, and D. Möllmann is thankfully acknowledged.

The present studies were supported by the grants DFG FI 1630/3-1 (C. D. Fingas), IFORES D/107-114400 (C. D. Fingas). DFG KFO 117 (Clinical research group “Optimization of living donor liver transplantation”), and NIH DK59427 (G. Gores).